Development of A Dynamic Predictive Cruise Control System for Enhancing Eco-Driving in Urban Transport System

Nie, Zifei
九州大学総合理工学府環境エネルギー工学専攻

Development of A Dynamic Predictive Cruise Control for Enhancing Eco-Driving in Urban Transport System

Zifei Nie

Supervisor

Associate Professor. Hooman Farzaneh

August 2021

Energy and Environmental System Laboratory

Department of Energy and Environmental Engineering

Interdisciplinary Graduate School of Engineering Sciences

KYUSHU UNIVERSITY

Japan

Acknowledgment

The journey onto this thesis has been circuitous but scenic. Its consummation is by virtue to a great extent of the special people who questioned, endorsed, and carried on with me on the road.

Foremost, my deep gratitude goes to Professor. Hooman Farzaneh, who ushered me into the field outside the automobile into a fresh land that highly interests me, guided me through my master research, and imparted valuable experiences in scientific research. His steadfast and sedulous character for research work motivated me unceasingly engaged with my research exploration.

My appreciation also reaches out to my laboratory colleagues. Sajid Abrar's sensibly help, encouragement, genuine kindness and company have been especially valuable. Yuichiro Yoshida's enlightening mind and Hirotomo Kohno's approachable assistance also helped creating a positive atmosphere where to do research.

Abidingly, I am indebted to my parents, whose significance to me constantly deepens with age. And I am grateful to my beloved Tong, who is my champion and is always there with me in the hours when the lab lights were off.

Finally, to myself: thank you for doing your best in the past two years. Regardless of the research achievements, three rules have been engraved on your mind:
When you get the feeling that your work is OK, you have got killed another 'you' who can make it much better.
Your internal mediocrity is the moment when you lost the faith of being excellent.
Hard work is the most accessible way to preserve one's dignity.

Zifei Nie
2021.07

Abstract

The development of an energy and environmentally friendly driving strategy for the next generation automobile has been the focus of academia and industry. The design concept of the strategy is to adapt the velocity of the vehicles into the dynamic driving surroundings considering the factors such as real-time energy consumption, traffic flow, road infrastructure, speed limitations, trip time, etc., which entails multiple objectives optimization. Most current research, however, focuses only on the limited driving scenarios, e.g., car following scenario, velocity regulation according to "Green Wave" theory based on traffic lights information, or road curvature and road gradient, etc. To handle the eco-driving problem in daily synthetic traffic situations under mixed driving scenarios, a Predictive Cruise Control (PCC) system is firstly proposed and developed in this master research. After defining its control objectives, the thesis presented the PCC system architecture based on the Instantaneous Energy Consumption Model (IECM) and Model Predictive Control (MPC) algorithm.

To avoid solving complex optimization problems taking into account various objectives and system constraints, the PCC system is designed hierarchically into three typical driving scenarios, including car following scenario, signal anticipation scenario, and free driving scenario. A detailed Driving Scenario Switching Logic (DSSL) under the support of ITS is simultaneously formulated so that the PCC system can be automatically selected and triggered by different driving scenarios. As the foundation of developing the eco-driving algorithm, electric vehicle longitudinal dynamics model and inter-vehicle longitudinal dynamics model are proposed firstly. Taking the minimization of energy consumption of the electric vehicle during traveling as the main optimization objective, the artificial neural network-based instantaneous energy consumption model is then developed to evaluate the transient energy consumption level under different typical driving scenarios. For the car following scenario, a multi-objective optimization, including energy economy, driving safety and comfortability, considering the preceding vehicle is proposed based on a linear model predictive controller, which is converted into a quadratic programming problem and numerically solved. For the signal anticipation scenario, by tracking a reference velocity optimized by the Reference Velocity Planning (RPV) algorithm based on SPaT information, a nonlinear MPC problem is formulated with the objective of both following the optimal reference velocity and minimizing the energy consumption during traveling. For the free driving scenario, the energy consumption minimization considering road gradient information based on nonlinear MPC is presented. To reduce the error of model mismatch and external disturbance, the feedback correction method is introduced into the predictive inter-vehicle longitudinal dynamics model to enhance the system robustness of the closed-loop system to the model uncertainties.

The performances of the EV's PCC system are investigated by simulation experiments under three typical driving scenarios and a synthetic driving scenario. It is concluded that compared with conventional human driver's maneuver, the proposed PCC system can not only realize the driving safety and comfortability, but also harvest considerable energy saving rates in either car following scenario, signal anticipation scenario, or free driving scenario or the synthetic driving scenarios, which substantiates the robustness and system robustness of the developed PCC system for EV. For the car following scenario, signal anticipation scenario, and free driving scenario, the energy saving rates were realized by 16.7%, 15.6%, and 30.3%, respectively. Under the synthetic traffic situation under mixed driving scenarios, 19.97% cumulative energy savings was achieved by proposed PCC system.

Keywords:

Predictive cruise control; Economic (eco) driving; Model Predictive Control; Instantaneous energy consumption model; Driving assistance system

Contents

Chapter 1. Introduction 1
1.1. Research Background and Significance 1
1.2. Literature Review 3
1.2.1. Research Status of Safety Distance Car-following Strategies 3
1.2.2. Research Status of Vehicular Energy Consumption Model 6
1.2.3. Research Status of Vehicular Eco-Driving 9
1.2.4. Research Status of Eco-Driving Control Strategies 14
1.2.5. Summary of Research Status 16
1.3. What will be elucidated in this research 17
1.4. Technical Route 19
1.5. Summary of Chapter 1 19
Chapter 2. Eco-Driving Predictive Cruise Control System Architecture and Dynamics Modeling 20
2.1. Eco-Driving Predictive Cruise Control System Architecture 20
2.1.1. Predefined Assumption on ITS and CAVs 20
2.1.2. Predictive Cruise Control System Overall Scheme 22
2.2. System Dynamics Modeling 26
2.2.1. Vehicle Longitudinal Dynamics Modeling 27
2.2.2. Validation of Dynamic and Stability Performance 29
2.2.3. Safety Distance Modeling Based on Variable Time Headway Strategy 30
2.2.4. Stability Analysis of Safety Distance Model 31
2.2.5. Inter-Vehicle Longitudinal Dynamics Modeling and Discretization 32
2.2.6. Reference Velocity Planning Modeling Based on SPaT Information 33
2.3. Summary of Chapter 2 34
Chapter 3. Instantaneous Energy Consumption Model (IECM) 35
3.1. Analysis of IECM 35
3.2. Modeling Data Collection and Process 37
3.3. Artificial-Neural-Network-Based IECM 40
3.3.1. Establishment of Neural Network Structure 40
3.3.2. Feedback Training Algorithm 43
3.3.3. ANN-Based IECM Application Deployment 45
3.4. Validation of ANN-Based IECM 46
3.5. Summary of Chapter 3 48

Chapter 4. Predictive Cruise Control System for Eco-Driving Based on MPC 50
4.1. Eco-Driving System Based on MPC 50
4.1.1. MPC Theory 50
4.1.2. A Complete Example – Using MPC to Realize Velocity Tracking 53
4.1.3. Multi-Objective Optimization Considering Preceding Vehicle Based on LMPC 59
4.1.4. Energy Consumption Minimization Considering SPaT Information and Preceding Vehicle Based on NLMPC 64
4.1.5. Energy Consumption Minimization Considering Road Grade Based on NLMPC 66
4.2. Derivation of Predictive Optimization Problem 69
4.2.1. Predictive Model Transformation of Inter-Vehicle Longitudinal Dynamics Model 69
4.2.2. Predictive Model Transformation of Constraints and Cost Function 70
4.2.3. Predictive Optimization Problem Construction 71
4.3. System Robustness Enhancement Based on Feedback Correction 71
4.4. Summary of Chapter 4 73
Chapter 5. Simulation Experiments of Predictive Cruise Control for Eco-Driving 74
5.1. Establishment of Simulation Platform Based on CarSim and MATLAB/Simulink 74
5.2. Typical Case Study for Car-following Driving Scenario 77
5.3. Typical Case Study for Signal Anticipation Driving Scenario 81
5.4. Typical Case Study for Free Driving Scenario 83
5.5. A Comprehensive Simulation Test of PCC system in Synthetic Driving Scenario 86
5.6. Summary of Chapter 5 88
Chapter 6. Conclusion and Prospects 89
6.1. Conclusion 89
6.2. Research Prospects 90

Chapter 1. Introduction

1.1. Research Background and Significance

Worldwide concerns about climate breakdown, global heating and fossil fuel excessive consumption have prompted all walks of life to take the initiative in energy conservation and CO_2 emission reduction actions. The reach of the Paris Agreement, as a milestone breakthrough, has been intensifying the development of a sustainable low-carbon society. The public road transport sector consumes about 20% of global energy and is spearheaded nearly 25% of energy-related CO_2 emissions, 75% of which are discharged by public road transportation [1]. Moreover, according to the preliminary estimates, the energy consumption and CO_2 emissions of worldwide public transport in 2030 will be raised by more than 50% due to the requirement of population and economic growth [2]. Accordingly, the related policies and low emission strategies and technologies on the road transport system are imperatively needed to moderate the energy and environmental burden, ameliorate the tense energy demand prospect, and achieve the UN's Sustainable Development Goals (SDGs) in the transport sector [3].

Energy consumption during vehicle operation is not only pertinent to the status of the vehicle itself, but also subject to the road condition and traffic situation. Moreover, it largely depends on the motion or driving behavior of the vehicle in a complex road traffic environment. According to current research status, there are several directions to enhance the fuel economy and diminish the fuel or energy consumption during traveling, including advanced motor and engine technologies, the latest vehicle bodywork design and techniques, new energy, as well as advanced control and driving assistance systems, as indicated in Figure 1.1, and their respective potentiality of energy conservation shown in Table 1.1. Among these strategies and technologies, eco-driving, as one of the conceptual control technologies, has been considerably noted due to its capability of reducing energy consumption in whatever the local microscopic or global macroscopic level [4]~[13].

TABLE 1.1 Main Vehicle Energy Saving Technologies and their Potentiality

Technologies			Potentiality of Energy Saving (%)
Engine & Vehicle Design	Engine Technologies	Turbocharging Technology	1.8 ~ 4.8
		Direct Injection Technology	10 ~ 20
		Idling Start-Stop	5 ~ 8
		Cylinder Deactivation	3.9 ~ 5.5
	Transmission Technologies	Multiple Gears	1.4 ~ 3.4
		Double Clutch	2.7 ~ 7.5
		Continuously Variable Transmission	2 ~ 8
	Lightweight	-	2 ~ 8
	Small-Displacement		20
	Diesel Vehicle		20
	Others	Aerodynamic Resistance	2 ~ 3

	Reduction Rolling Resistance Reduction	1 ~ 2
Eco-Driving		15 ~ 35
Intelligent Traffic Management (ETC, Actuated Signalization, etc.)		15
Vehicle Electrification		10 ~ 40

The core concept of eco-driving is to improve vehicle energy economy on the premise of meeting the basic requirements of travel, such as time or speed limits. The main objective of eco-driving is to attain the best match between the host vehicle speed and the vehicle surroundings, including road environment and traffic flow, through the appropriate operation controlled by a driver or an autonomous driving system. Thus far, eco-driving has led a new way for energy saving and emission reduction in road transport and has always been the focus of research in academia and industry. Government departments, research institutes and automobile manufacturers in many developed countries have committed a great deal of human and financial resources in the research and development of eco-driving technology, such as the *Intelligent Transportation Systems Joint Program* in the US [14], *Energy-Saving Intelligent Transportation Systems* Project in Japan [15], and *Eco-Will* Project in Europe [16].

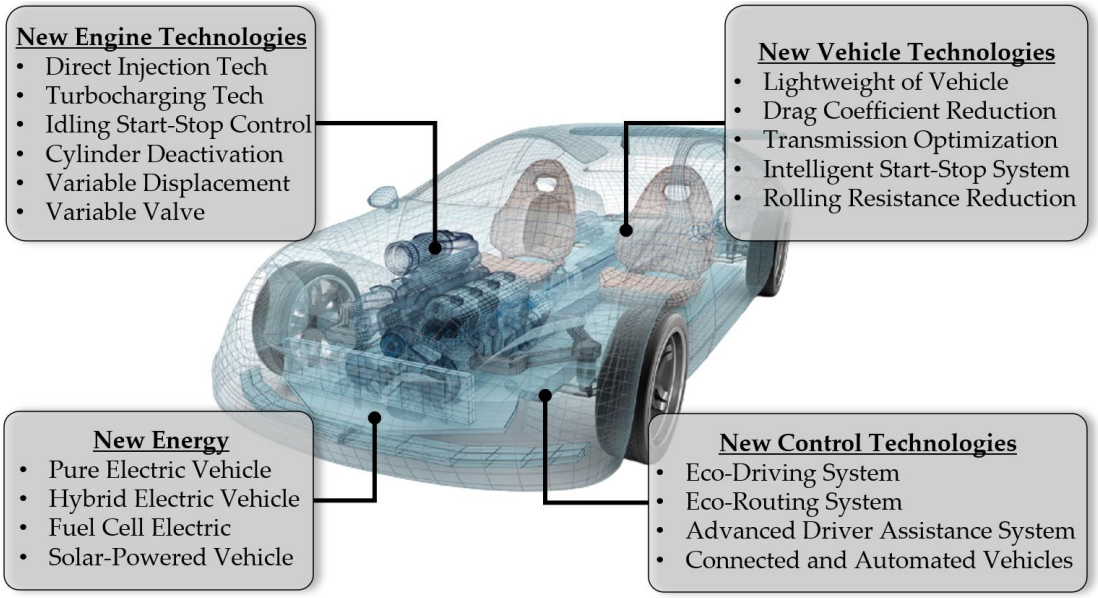

Fig. 1.1 Advanced Technologies for Ameliorating Energy Economy

A systematic classification of the current eco-driving system can be summarized as preplanning systems, real-time dynamic systems, and experience-based systems [17]. In comparison with others, the real-time dynamic optimization system, also called Eco-Driving Assistance System (EDAS), as the extension of advanced driver assistance systems (ADASs), presents transcendent energy economy improvement potential due to higher levels of engagement with the driving surroundings. The real-time dynamic system can be further categorized as online driving behavior evaluation systems (offering feedback guidance based on historical energy consumption versus driving pattern), online phonetic and haptic systems (providing a predictive, feedforward suggestion according to upcoming driving information), and predictive cruise control (involving autonomous driving features). Among these systems, predictive cruise control (PCC) is the ideal system to take full advantage of energy saving

of eco-driving because of two reasons: (1) Equipped with the intelligent hardware system including controllers, sensors and actuators, cruise control system can partially or entirely replace the human driver to realize the energy saving objective automatically, which promotes the development of Eco-Driving Assistance System (EDAS) for the future mobility; (2) Cruise control technology, as an embedded system into the vehicle, does not influence the energy-saving technologies of the vehicle itself, which means that the predictive cruise control system manipulates the vehicle to execute the eco-driving strategy, which can be combined with the energy-saving technologies of the vehicle itself to maximize the energy-saving potential simultaneously.

1.2. Literature Review

1.2.1. Research Status of Safety Distance Car-following Strategies

Car following, as the most primary microscopic traffic behavior, demonstrates the interaction of two vehicles next to each other restricted to a single lane. Car-following models utilize the inter-vehicle dynamics to reflect the corresponding driving behavior of a host vehicle with the change of state of motion of a preceding vehicle. Under the driving scenario of car following, the priority of the cruise system of a vehicle is to guarantee driving safety. Therefore, the establishment of a safety distance model between the preceding and host vehicle is the fundamental of developing the cruise system [18]. On the one hand, overlength inter-vehicle spacing may cause the cut-in of other vehicles from adjacent lanes, which will not only compromise the driving safety of car following but also get the host vehicle into a frequent acceleration or deceleration, or even stop-and-go situation lowering the fuel economy. On the other hand, too short an inter-vehicle spacing may increase the risk of traffic collision during car following, and force drivers to take over or interfere in the driving task [19]. Hence, selecting an appropriate inter-vehicle strategy can not only improve the efficiency of road resource utilization but also the performance of car following and driving safety.

Basically, the safety distance model can be classified into three classic categories: (1) Car-following safety distance model based on the braking maneuver of the preceding vehicle, (2) Safety distance model based on driver characteristics, and (3) safety distance model based on time headway. Most of the subsequent safety distance models are improved and developed based on the above three classic models.

i. Car-following safety distance model based on braking maneuver of the preceding vehicle [20]~[21]

Through the analysis of the vehicle kinematics, when the preceding vehicle suddenly brakes into stop, the safety distance model of the host vehicle to maintain a safe stop from cruise should be as follow:

$$D_s = v_h t_d + \frac{v_h^2}{2a_h} + d_{stop} - \frac{v_p^2}{2a_p} \tag{1.1}$$

where, D_s refers to the safe distance, v_h is the velocity of the host cruise vehicle, v_p is the velocity of the preceding vehicle, t_d represents total time delay from driver reaction time and braking system response time, a_h is the maximum deceleration of the host vehicle, a_p is the maximum deceleration of the preceding vehicle, and d_{stop} is the relative distance between preceding and host vehicle when after the stop.

It is intuitive to understand that $v_h t_d$ calculates the coverage during the total time delay of the host vehicle, $\frac{v_h^2}{2a_h}$ calculates the required distance of host vehicle under maximum deceleration, d_{stop} is the expected inter-vehicle distance when both vehicles are motionless, and $\frac{v_p^2}{2a_p}$ stands for the driving distance during deceleration of the preceding vehicle. It is noted that this model fully takes into account the driving safety of the following vehicle under the circumstance of the emergency stop of preceding vehicle. It is however relatively conservative in applying this model to the typical driving scenario because it tends to cause the waste of road resource,

decrement of traffic efficiency, and cut-in of vehicles from adjacent lanes.

In the follow-up study, several upgraded minimum safety distance models consider the braking process of the preceding vehicle and motion of the host vehicle separately to further subdivide the original safety distance model into different portions [22]. Although the exact precision is improved when calculating the required safe distance, it does greatly increase the complexity of the safety distance model.

ii. Car-following safety distance model based on driver characteristics

The influence of the subjective intention of drivers on the modeling of the safety distance is rarely considered among most of the safety distance models of the cruise system. Drivers with different driving habits have different subjective feelings about the safe distance. Driver preview safety distance model [23] is established based on the intention prediction of driving process in the actual traffic situation and the model parameters can be identified by the statistical process of many skilled drivers' operation. Once the driver predicts that after t_g seconds, the inter-distance between host and preceding vehicle is less than the critical value X_{lim}, the brake should be applied immediately for driving safety. The minimum safety distance required to be kept between host and preceding vehicle is defined by the relative distance at this moment. The mathematical expression of this model is shown as follow:

$$D_s = -v_{rel}t_g - \frac{a_p t_g^2}{2} + X_{lim} \tag{1.2}$$

where, D_s is the safety distance between host and preceding vehicle, X_{lim} represents the subjective critical value of drivers, v_{rel} represents the relative velocity between the host and preceding vehicle, and a_p is the acceleration (deceleration) of the preceding vehicle.

It is clear that subjective prediction of drivers is fully considered in this preview safety distance model, which is in line with the subjective judgment of drivers. However, the subjective prediction with a lot of uncertainty is hard to be quantified during modeling. Take the preceding vehicle's emergency braking as a typical example. As the driver preview model always takes a constant such as $1.5\mathrm{m}/s^2$ as the braking deceleration of the preceding vehicle, the calculated safety distance value by the model will be relatively small in the case of emergency braking of the preceding vehicle, which does not accord with the actual.

iii. Car-following safety distance model based on time headway [24]~[25]

Time headway between preceding and host vehicle, defined as the time intervals between the passage of successive vehicles past the same point, is categorized as constant time headway (CTH) and variable time headway (VTH). The constant time headway strategy was firstly proposed by Loannou [26] in 1993 in developing an autonomous intelligent cruise control system.

$$D_s = \mathrm{CTH} \cdot v_h + d_{min} \tag{1.3}$$

where, D_s is the safe distance between preceding and host vehicle, CTH represents the constant time headway (generally 1.2 ~ 2.0s), v_h is the velocity of the host vehicle, and d_{min} is the spacing when two vehicles are motionless (generally 2 ~ 5m).

It is obvious that the expected spacing is correlated directly with the velocity of the host cruise vehicle. The faster the host cruise vehicle, the larger the required braking distance. However, the constant value of time headway makes it difficult to work efficiently under complex traffic condition. Lin et al analyzed the influence on the traffic flow using different CTH under five different typical driving scenarios [27]. Simulation experiments show that it fails to meet the demand for different traffic flow using a fixed constant time headway, proving the limitation of the CTH strategy.

Broqua et al put forward that time headway should be proportional to the velocity of the host vehicle during the driving process [28], from which the significance of the velocity of host cruise vehicle was firstly emphasized

for time headway design.

$$\begin{cases} D_s = TH \cdot v_h + d_0 \\ TH = \lambda_1 \cdot v_h + \lambda_2 \end{cases} \tag{1.4}$$

where, D_s is the safe distance between preceding and host vehicle, TH refers to the time headway, v_h is the velocity of the host cruise vehicle, d_0 is the spacing between two vehicles after pulling up, and λ_1, λ_2 are the constant coefficient. On top of this, Yanakiev and Kanellakopoulos added that time headway should be correlated with not only the velocity of the host vehicle but also the relative velocity between preceding and host vehicle [29]. When the velocity of preceding vehicle is slower than the host vehicle, it is necessary to increase the time headway between two vehicles to ensure the driving safety, while if the velocity of the preceding vehicle is greater than host vehicle, the time headway can be appropriately decreased to improve the traffic flow capacity. A saturation function with an upper limit of 1 and a lower limit of 0 is used to describe the improved time headway.

$$TH = \text{sat}(\lambda_1 - \lambda_2 \cdot v_r) = \begin{cases} 1 & \lambda_1 - \lambda_2 \cdot v_r \geq 1 \\ \lambda_1 - \lambda_2 \cdot v_r & 0 < \lambda_1 - \lambda_2 \cdot v_r < 1 \\ 2 & otherwise \end{cases} \tag{1.5}$$

where, sat[ ] is the saturation function, $\lambda_1$and λ_2 are constants greater than 0, and v_{rel} refers to the relative velocity difference between preceding and host vehicles.

All the parameters of above time headway models reflect the characteristics of microscopic traffic, such as the velocity of host cruise vehicle and the relative velocity between two vehicles, while Swaroop et al. [30] and Rajamani et al. [31] holds the belief that the characteristic of macroscopic traffic flow should be considered as well in time headway. The correlation between time headway and macroscopic traffic flow speed and traffic jam density is proposed based on the theory of Greenshields [32]:

$$TH = \frac{1}{\rho_{jam}(v_{free} - v)} \tag{1.6}$$

where, ρ_{jam} is the density of traffic jam, and v_{free} is the velocity of free traffic flow.

Besides, based on a correlation between the velocity of host vehicle and drivers expected spacing, Seungwuk Moon and Kyongsu Yi proposed a Quadratic Desired Clearance (QDC) model [33]. The nonlinearity can more precisely describe the car-following behavior of the host vehicle compared with the linearized desired spacing model in [34].

$$D_{des} = c_0 + \tau v_h + r v_h^2 \tag{1.7}$$

where, D_{des} refers to the desired inter-distance between preceding and host vehicle, v_h is the velocity of host vehicle, and c_0, τ, and r are all coefficients to be calibrated.

Shengbo Li et al. hold that the coefficients in the above model are not labeled with a physical explanation although it can accurately describe the car-following characteristics, which makes it difficult for drivers to adjust these parameters according to their own driving behavior if the cruise control system is designed based on it [35]. Taking the Taylor Expansion of the quadratic term of the above model at the average speed and transforming it into a QDC model with clear physical significance for each parameter, the improved model is shown as follow:

$$D_{des} = r v_h (v_h - v_{h_{mean}}) + \tau_h v_h + d_0 \tag{1.8}$$

where, D_{des} refers to the desired inter-distance between preceding and host vehicle, r is the coefficient of quadratic term, v_h is the velocity of host vehicle, $v_{h_{mean}}$ is the average vehicle velocity under the car-following scenario, τ_h is the time headway, and d_0 denotes the spacing at motionlessness.

1.2.2. Research Status of Vehicular Energy Consumption Model

Numerous variables influence vehicular energy consumption and emission rates. These variables can be classified into six broad categories: travel-related, weather-related, vehicle-related, roadway-related, traffic-related, and driver-related factors, as suggested by Ahn et al in [36]. The primary elements of each subcategory are shown in Figure 1.2. The effects of the six influencing factors on fuel consumption are summarized in Table 1.2. As shown in Table 1.2, only some factors, such as road conditions, traffic-related factors and driver-related factors, significantly impact fuel consumption. It is important to note that the effects of these factors on fuel consumption are not cumulative but mutually reinforcing. When developing the fuel consumption model, the factors related to the state of the vehicle and driver are especially ought to be considered. However, the factors related to road conditions and traffic information, although having a great impact, are challenging to be reflected in the fuel consumption model and can be considered by optimizing the control algorithm. Environment-related factors contribute an insignificant share of fuel consumption and can be ignored during modeling [37].

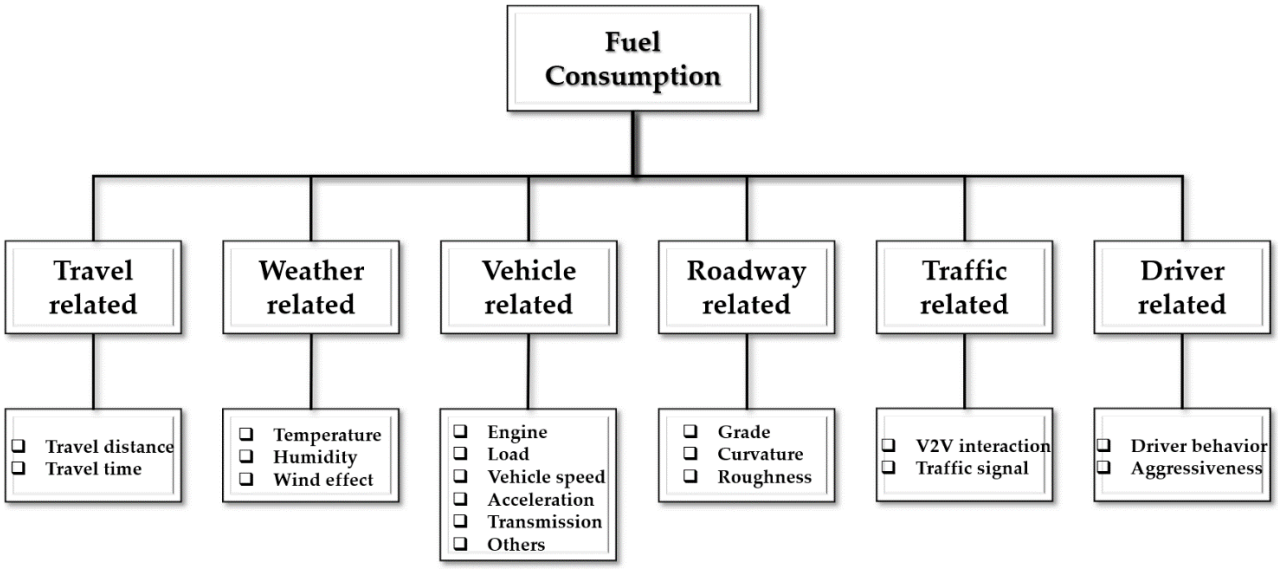

Fig. 1.2 Factors affecting vehicle energy consumption

Multifactorial influence on the vehicular energy consumption cannot be described by simple mathematical models. However, due to the real-time performance of eco-driving assistance system, the energy consumption model is required to be as simple as possible. Therefore, the main research objective is to simplify the model structure under the premise of adequate model accuracy. The current existing fuel consumption models can be roughly classified into three categories: microscopic fuel consumption models, mesoscopic fuel consumption models, and macroscopic fuel consumption models.

TABLE 1.2 Quantitatively Influence on Fuel Consumption from Primary Factors

Factors	Travel	Weather	Vehicle	Roadway	Traffic	Driver
Energy Saving (%)	8.74 ~ 42.15 [38]~[41]	1 [42]	Core Factors	3 ~ 20 [43]~[45]	22 ~ 50 [46]~[48]	4.35 ~ 40 [49]~[55]

i. Microscopic fuel consumption models:

Microscopic fuel consumption models, also called instantaneous fuel consumption models, basically estimate

the vehicle instantaneous fuel consumption by utilizing vehicle instantaneous state parameters. The inputs to this kind of models include engine rotation speed (rpm), torque, power, and vehicle instantaneous speed and acceleration. The models with engine power as input are the earliest ones, in which the most representative one was proposed by Post in 1984 [56], shown as follow:

$$\dot{m_{fm}} = f(x) = \begin{cases} \gamma + \beta P & P \geq 0 \\ \gamma & P < 0 \end{cases} \tag{1.9}$$

where, $\dot{m_{fm}}$ (ml/min) is the vehicular fuel consumption rate, $\gamma(ml/min)$ and $\beta\big(ml/(min \cdot kW)\big)$ are the vehicle-related parameters, and P (kW) is the vehicular instantaneous power. In 1989, Akcelik ameliorated this model and further enhanced its estimation precision [57]. This model takes the instantaneous power of the vehicle as the input, and models the positive and negative parts of the power respectively so that to guarantee the accuracy. When applied to the individual vehicle, the error between the total fuel consumption estimation given by the model and the actual values is 2%. Due to its simple model structure and adequate estimation accuracy, this model is still used by some scholars up to now [58]~[59]. After Post's model, fuel consumption models based on engine power and torque spring up, shown in Table 1.3.

TABLE 1.3 Microscopic Fuel Consumption Model Based on Power and Torque

Model sources	Model structure
Chang and Morlok [60]	$\dot{m}_f = \gamma_0 \cdot P$
Ahn [61]	$\dot{m}_f = \gamma_0 n_e + \gamma_1 P$
Rakha, H.A et al [62]	$\dot{m}_f = \begin{cases} \gamma_0 + \gamma_1 P + \gamma_2 P^2 & P \geq 0 \\ \gamma_0 & P < 0 \end{cases}$ $\dot{m}_f = \begin{cases} \gamma_0 + \gamma_1 P + \gamma_2 P^2 & P \geq 0 \\ \gamma_0 n_{idle} & P < 0 \end{cases}$ $P = \left(\frac{R(t) + 1.04ma(t)}{3600\eta} \cdot v(t) \right)$
Bart Saerens et al [63]	$\dot{m}_f = \gamma_0 + \gamma_1 n_e + \gamma_2 n_e^2 + \gamma_3 P + \gamma_4 P^2$ $\dot{m}_f = \gamma_0 n_e + \gamma_1 P + \gamma_2 P^2$ $\dot{m}_f = \gamma_0 n_e + \gamma_1 n_e^2 + \gamma_2 n_e^3 + \gamma_3 n_3 T_e + \gamma_4 n_e^2 T_e + \gamma_5 n_e T_e^2$ $\dot{m}_f = (\gamma_0 + \gamma_1 n_e^2)(\gamma_0 + \gamma_1 T_e + \gamma_2 T^2)$
Passenberg et al [64]	$m_f = \gamma_0 + \gamma_1 n_e + \gamma_2 n_e^2 + \gamma_3 n_e T_e + \gamma_4 T_e + \gamma_5 T_e^2$

where, $\dot{m}_f(mg/s)$is the vehicular fuel consumption rate, P (kW) is the instantaneous power demand of the vehicle, $n_e(rpm)$ is the engine rotation speed, $n_{idle}(rpm)$ is the engine idling rotation speed, T_e (Nm) is the engine torque, r_i is the model coefficient, $R(t)$ is the total resistance during driving, η_d is the transmission efficiency.

Ahn and Rakha proposed the VT-Micro model in 2002 with vehicular instantaneous velocity and acceleration as inputs to estimate the instantaneous fuel consumption [65]. The VT-Micro model uses different product combination of different powers of vehicle velocity and acceleration to fit the instantaneous fuel consumption, and its basic model description is shown as follow:

$$\ln MOE_e = \begin{cases} \sum_{i=0}^{3}\sum_{j=0}^{3}\left(L_{i,j}^{e} v^i a^j\right) & a \geq 0 \\ \sum_{i=0}^{3}\sum_{j=0}^{3}\left(M_{i,j}^{e} v^i a^j\right) & a < 0 \end{cases} \tag{1.10}$$

where, MOE_e is the vehicle transient fuel consumption rate, $L_{i,j}^{e}$ is the model regression coefficient of velocity to the power i and acceleration to the power j when the vehicle moves at a constant velocity or acceleration state; $M_{i,j}^{e}$ is the model regression coefficient of velocity to the power i and acceleration to the power j when vehicle moves at a deceleration state; $v(km/h)$is the vehicle instantaneous velocity and a $(m/s\text{^}2$)is the vehicle instantaneous acceleration.

There are two major characteristics of the VT-Micro model. Firstly, the positive and negative acceleration ranges are modeled respectively, which makes it take into account the different fuel consumption characteristics during acceleration and deceleration. Secondly, the logarithmic transformation is used to fit the logarithm of fuel consumption into the function of velocity and acceleration, which ensures that the output of the model is always non-negative. These two characteristics enable the VT-Micro model to possess high estimation accuracy ($R^2 \geq 90\%$). Wei Lei et al replaced the acceleration in the VT-Micro model with the composite acceleration within 9 seconds and thereby obtained the MEF model [66]. The composite acceleration is expressed as follow:

$$\bar{a}(t) = \varphi a(t) + (1-\varphi)\sum_{i=1}^{9}\frac{t-i}{9} \tag{1.11}$$

where, $\bar{a}(t)$ $(m/s\text{^}2$)is the composite acceleration at t, $a(t)$ $(m/s\text{^}2$) is the instantaneous acceleration at t, φ $(0 < \varphi < 1)$ is the weight coefficient.

ii. Mesoscopic fuel consumption models:

The input of the mesoscopic fuel consumption models is the different driving modes experienced by a vehicle during the driving process, such as acceleration mode, deceleration mode, constant speed mode and idling mode. Such models assume that the fuel consumption of each driving mode is independent and that the total fuel consumption of the vehicle is equal to the sum of the fuel consumption of all driving modes.

Akcelik proposed the Elemental model in 1982 based on driving modes [67]. The structure of this model is shown as follow:

$$\dot{m_{fm}} = \frac{f_1 L_c + f_2 t_s + f_3 n_s}{T_m} \tag{1.12}$$

where, $\dot{m_{fm}}$ is the instantaneous fuel consumption rate, $f_1(ml/min)$the fuel consumption rate during constant speed driving mode, $f_2(ml/min)$ the fuel consumption rate during idling driving mode, $f_3(ml/min)$the fuel consumption rate at a full stop, $L_c(m)$ is the distance covered during constant speed driving, $t_s(min)$ the idling time, n_s is the number of stops, and $T_m(min)$ is the total driving time.

The elemental model only considers two of the four driving modes, not including acceleration and deceleration modes. Hung et al developed a mesoscopic fuel consumption model including four driving modes taking vehicular instantaneous velocity and driving modes as inputs [68]. The idle mode and non-idle mode are modeled by piecewise interpolation function and negative exponential function respectively, and a high model accuracy (average absolute error $\leq 15\%$) is guaranteed. The model structure is shown as follow:

$$idling\ mode: F_I(t_I) = \begin{cases} ae^{-bt_I} & t_I < T_s \\ c & t_I \geq T_s \end{cases}$$
$$non-idling\ mode: f(x) = (\sum_{j=1}^{N} w(x_j)e_j)/(\sum_{j=1}^{N} w(x_j)) \quad (1.13)$$

where, $F_I(t_I)$ (g/s) is the fuel consumption rate during idling time t_I, $a, b, and\ c$ are model regression coefficient, $T_s(s)$ is the threshold of the idling time, x is the distance from data point to the central data point, $w(x_j) = 1 - x_j$ is the weight function, and $e_j(g/s)$is the fuel consumption rate at x_j.

M.A.S. Kamal utilized a modal-based fuel consumption model in the development of an eco-driving assistance system [69], in which M.A.S. Kamal held that the fuel consumption rates of idling mode and deceleration mode are constant, and the fuel consumption rate of acceleration and cruise mode are shown as follow:

$$\dot{m}_{f_{idling}} = constant$$
$$\dot{m}_{f_{decel}} = constant$$
$$\dot{m}_{f_{accel}} = (c_1 + c_2 av) \quad (1.14)$$
$$\dot{m}_f = \left(k_1\left(1 + \frac{1}{2}\left(\frac{v}{v_m}\right)^3\right) + k_2 v\right)$$

iii. Macroscopic fuel consumption models:

The inputs to the macroscopic fuel consumption models are ordinarily the driving time, distance and average driving velocity. The average-velocity fuel consumption model, as one representative one of macroscopic fuel consumption models, is to estimate the fuel consumption of the whole region by establishing the relationship between the average velocity of vehicles in a particular region and the total fuel consumption. The Environmental Protection Agency (EPA) utilizes MOBILE series fuel consumption models to estimate the vehicles fuel consumption while conducting transportation planning [70]. As a typical average-velocity macroscopic model, it takes average velocity of all the vehicle in certain region, different vehicle technologies, year of use, ambient temperature, fuel parameters and driving modes as model inputs. The average-velocity fuel consumption model is seldom used in practice, and is not applicable to this research, so it will not be expounded too much here.

1.2.3. Research Status of Vehicular Eco-Driving

The integration of eco-driving and intelligent driving originated from fuel-efficient cruise control, called predictive cruise control (PCC) in 2004 [71]. A representative research work done by Hellström E et al. is the transportation task of a given route, in which the optimal control algorithm is applied to obtain the economic velocity [72]. Generally, eco-driving research combined with intelligent driving can be categorized as highway-based and urban-roadway-based strategies.

i. Freeway-based eco-driving considering the road terrain to minimize the fuel consumption

For freeway-based eco-driving, it mainly considers the influence of road terrain (road grade) on the vehicular fuel economy, planning the economic (or ecological) velocity of a single vehicle in freeway driving situation, without considering the influence from surrounding vehicles on the cruise vehicle. In 1977, Schwarzkopf and Leipnik carried out the eco-speed optimization considering the road slope [73]. Based on a nonlinear vehicle dynamics model, the eco-speed passing through a constant slope road was obtained by solving an optimal fuel economy problem. In 2005, Chang and Morlok also the influence of road slope on fuel economy [74]. The author assumed that there was a linear relationship between vehicle fuel consumption and work done. Under

this premise, when the road slope was constant within a certain range, driving with a constant velocity entailed an optimal fuel economy. Erik Hellström. et al [75]~[78] conducted a series of studies on the fuel economy problem of heavy trucks driving on the sloped road from 2005 to 2010, and developed a fuel-optimal look-ahead controller utilizing road topography information. This look-ahead controller took the weighted functions of fuel consumption, velocity variation, gear shifting, braking times into the optimization objective function, transforming it as a dynamic programming (DP) problem. This research achieved higher fuel economy by generating smooth speed profiles with the result of fuel consumption reduction by 2.5%. However, this look-ahead controller needs to constantly search for the optimal control signal, which is computationally burdensome. Obtaining the optimal velocity trajectory once for the whole driving route using the dynamic programming algorithm instead of multiple optimizations, Fredrik Söderstedt alleviated the computation inefficiency [79]. The eco-velocity trajectory obtained by the proposed algorithm was used as the reference velocity of the conventional cruise controller. The proposed method was fast, and fuel-saving effect was similar to the performance of the look-ahead controller designed by Erik Hellström et al.

In 2009, Nicholas [80] proposed a method to improve the fuel economy utilizing traffic data and model predictive control (MPC). The author held that vehicles could respond in advance according to the traffic conditions ahead, which significantly improved the travel efficiency and provided driving information to the driver. In addition, simulation results showed that the proposed method requires less hardware modification, so it is highly feasible for passenger vehicles.

In 2010, Tu Luu et al. [81] designed a driver assistance system for light vehicles to improve the vehicular fuel economy. Based on the vehicle longitudinal dynamics model, the objective function, consisting of the weighted functions of fuel consumption rate, driving time, and driving comfortability, was solved by dynamic programming to obtain the fuel-efficient optimized speed profile. In 2011, Kamal et al. [82] utilized the model predictive control algorithm, combined with the information of road gradient, vehicle dynamics model and fuel consumption model, to plan the vehicular speed passing up and down the hilly road. The results demonstrated that the fuel consumption could be effectively reduced by accelerating avant climbing the uphill in a preplanned manner so as to avoid hard acceleration. In downslope, it took advantage of downhill gradient, and without any braking, the velocity is allowed to increase to some extent and finally settled at a specified speed.

In 2014, Yu [83] designed a hierarchical eco-driving system with two layers. For the first layer, it applied the Dijkstra algorithm to optimize the average eco-speed at multiple signalized intersections considering the traffic lights information, traffic flow and speed constraints at certain road sections. For the second layer, it considered the road slope information and calculated the real-time eco-speed.

In 2015, Themann et al. [84] proposed an energy efficiency optimization strategy for autonomous driving based on average driving behavior and driver preferences. This model firstly obtained the predicted speed vector through map data, such as road slope, curvature, speed limitation, distance to traffic signal light and other information. Then the driver's expectation on travel time and fuel consumption was directly considered to ensure that the optimization results meet the driver's demand. The ACC InnoDrive system of Porsche adopted a similar method and achieved fuel consumption reduction by about 10% [85]. The InnoDrive integrated adaptive cruise control (ACC) system, GPS, and GIS to analyze driving intention based on real-time road traffic information. Then, the optimal velocity profile can be obtained based on the above information. Finally, it cooperatively controlled the engine, transmission, and braking system to follow the obtained optimal velocity profile to minimize the fuel consumption.

ii. Urban roadway eco-driving considering the traffic signal lights information

In urban driving conditions, optimization of speed trajectory is performed to minimize the fuel consumption by

using the upcoming traffic signal phase and timing (SPaT) information with the advancement of V2X technology, including Vehicle-to-Vehicle (V2V) communication and Vehicle-to-Infrastructure (V2I) interaction. Furthermore, the intelligent transport system (ITS) makes it possible to engage higher levels of real-time dynamic monitoring of the vehicle performance, enabling the eco-driving system to perform more efficiently.

In 2011, Asadi and Vahidi [86] proposed a vehicle-centered predictive cruise control system that controlled the vehicle based on traffic signal lights information through the ITS to reduce the waiting time at the red interval of traffic signal lights and avoid unnecessarily frequent acceleration or deceleration. The simulation results showed that 47% fuel consumption and 56% CO_2 emissions can be reduced by the predictive use of signal timing. And this research offered the possibility of applying model predictive control (MPC) framework to formulate the travel optimization considering traffic signal lights information.

In 2013, Kamal et al. [87] developed a comprehensive and innovative eco-driving model based on MPC, predicting the velocity of preceding vehicle, taking into account the changing traffic signals at intersections to compute the optimal vehicle control input. The breakthrough of this research is that the MPC vehicle uses the upcoming signal status to choose its acceleration/deceleration behind a preceding vehicle so that it can stop at a red signal by smooth deceleration instead of use of hard braking. The simulation results showed that up to 13.21% fuel savings could be achieved.

In 2014, Mahler and Vahidi [88] proposed a predictive optimal velocity-planning algorithm that uses probabilistic traffic SPaT information to increase a vehicle's energy efficiency. The best velocity trajectory that maximizes the chance of passing through green lights can be calculated based on a signal-phase prediction model. Through multi-signal simulation, the fuel economy improvement can be realized by 16% and 6%, respectively, by fixed-time and actuated signals.

In 2015, De Nunzio et al. [89] further improved the energy efficiency for vehicles going through many successive signalized intersections. The presented pruning algorithm is capable of finding the energy-efficient path and returning the speed advisory to the drivers in a sub-optimal way. Although the simulated vehicles are independently equipped with the proposed algorithm and do not share information among vehicles, the noticeable traffic energy consumption reduction can be achieved without affecting travel time.

In 2019, an optimal parametric approach [90] was proposed to analytically solve an eco-driving problem for autonomous vehicles crossing multi-intersections without stopping. The traffic light information was described as spatial equality and temporal inequality constraints. The simulation results showed the advantages of considering multiple intersections jointly rather than dealing with them individually. An ecological Adaptive Cruise Control (Eco-ACC) was proposed [91] to minimize energy consumption while avoiding collisions and complying with traffic signals, which was the extension of the conventional ACC system. In the higher-level controller, Eco-ACC computes the energy-optimal velocity reference incorporating red light duration. In the lower level, the ACC controller ensures safety against a collision with the preceding vehicle.

iii. Urban roadway eco-driving under car-following driving scenario

The development of optimal fuel economy under the circumstance of car following requires considering the car-following safety. Due to the high unpredictability of driver behavior, the eco-driving cruise control under the mode of car following is a more challenging task. In 2006, Zhang and Ioannou [92] designed a PID controller for the truck following system. This paper proposed that fuel consumption could be reduced by avoiding unnecessary acceleration and braking, and the goal of the controller was set to track the speed of the preceding vehicle while maintaining the specified inter-distance. In 2008, Li et al. [93] took vehicle tracking and fuel efficiency into consideration in the study of adaptive cruise control. The research group used the inverse model

to compensate for the nonlinearity of vehicle longitudinal dynamics. Given the tradeoff between fuel economy and vehicle tracking capability, the MPC framework was used to manage the optimization problem. The experimental results showed that the fuel-saving rate of the model is 8.8% and 2% on city roads and expressways, respectively. In 2011, Wu et al. [94] developed a new fuel economy optimization system (FEOS). This system received the information from the vehicle and its surroundings to calculate the optimal acceleration/deceleration with the Lagrange multiplier method. The optimal control command can be sent to the driver through an interactive interface or automatic control system of the autonomous vehicle. This FEOS can be used in both the free driving situation and car-following driving scenario. The experimental results showed that, without sacrificing traffic safety, the vehicles equipped with the FEOS system could save 22% ~ 31% fuel during acceleration and 12% ~ 26% fuel during deceleration compared with those without FEOS. Therefore, as opposed to the relatively costly design and improvement of vehicle technology, FEOS provides a straightforward and feasible way to minimize fuel consumption. Moreover, the system can be applied in both driver assistance systems (ADS) and human-machine interactive interfaces of autonomous driving vehicles. In 2013, Kamal et al. [95] developed a new control system aiming at controlling the vehicle to improve its fuel economy in the changing urban transport system. By measuring the current road and traffic-related information, the system predicted the future traffic state of the preceding vehicle and calculated the optimal input signal into the vehicle. The experimental simulation results showed that the controller saved 13% fuel consumption in the urban traffic environment.

In 2015, Luo et al. [96] proposed a controller based on nonlinear predictive control in order to improve the energy efficiency and integration of the control system for hybrid electric vehicles. With stable tracking constraints, the coordinated optimal control problem of safe tracking and fuel consumption minimization was established, which was solved by multi-step offline dynamic programming and an online look-up table for practical implementation of the algorithm. The experimental results indicated that the proposed i-HEV ACC enhanced the driving safety, fuel efficiency as well as driving comfortability. There are similar methods in subsequent research. For instance, Zhao et al. [97], in 2017, proposed a new spacing control technique based on model predictive control for the ACC system, which considered both the fuel economy and driving comfortability simultaneously.

Another approach for fuel efficiency is based on the utilization of new technologies. In 2007, Manzie et al. [98] proposed to remotely acquire the vehicle surrounding traffic information through an intelligent transportation system, and thereby adjust driving strategy according to such required information. Experiments showed that the acquisition of remote traffic information enabled the vehicle with 7 seconds ahead preview capability, resulting in the improvement of fuel economy. In 2012, Li et al. [99] proposed a servo-loop control design of a Pulse-and-Gliding (PnG) strategy to minimize the fuel consumption in the automated car following scenario. Simulation experimental results show that compared with the linear-quadratic (LQ) -based benchmark controller, the PnG controller improved the fuel economy up to 20%.

The recent representative research works are reviewed and listed in Table 1.4.

TABLE 1.4 A Review of Recent Studies on Eco-Driving

Research Purpose	Modeling Approach	Achievements	Ref.
To improve fuel economy while maintaining a safe following distance	Car-following-oriented MPC	Maintaining a safe distance between leading vehicle while obtaining fuel economy	[100]
To reduce fuel	Model predictive multi-	Fuel consumption can	[101]

consumption and emissions, considering the car-following scenario	objective control framework	be reduced by 10.49% with the proposed controller compared with conventional controllers in Advanced Vehicle Simulator (ADVISOR)	
To improve fuel economy under the vehicle-to-vehicle communication structure	Ecological cooperative adaptive cruise control (eCACC) strategy	Better car-following performance results in significant energy savings in different driving cycles	[102]
To improve fuel economy of the vehicle driving by incorporating traffic information into the energy management strategies	Deep deterministic policy gradients approach	Fuel economy improvement, by taking traffic information into account	[103]
To realize better power allocation of hybrid EV and optimize the fuel economy	Fuzzy adaptive PMP optimization	Fuel economy improvement and maintaining the state of charge of battery	[104]
To enhance eco-driving in the urban traffic system, considering multiple signalized intersections	Open-loop optimal control problem (OCP) combined with three-stage operation rules and Dijkstra algorithm	About 10.14% and 5.04% fuel consumption reduction can be achieved for the urban and suburban area, respectively	[105]
Eco-speed trajectory planning in real-time considering upcoming traffic and road constraints	Energy Adaptive Cruise Control (EACC) based on MPC in the space domain	The proposed MPC achieves 2.5% more energy savings than linear MPC in the time domain	[106]
To improve fuel economy and air quality in a traffic system with signalized intersections in the city of Riverside, CA, USA	Cooperative eco-driving (CED) system with a role transition protocol	About 7% reduction in energy consumption and 59% reduction in pollution emission can be achieved, using full utilization of the connected and autonomous vehicles (CAVs)	[107]
To improve fuel economy for CAV platoon driving through successive signalized intersections	Ecological cooperative adaptive cruise control (Eco-ACC) based on the combination of DP and OCP approaches	About 8.02% improvement in fuel economy and 2.92% reduction in trip time can be achieved	[108]
To enhance CAVs eco-driving control on signalized roadways	MPC algorithm with traffic management strategies and road geometry constraints, using DRCC	About 23.6% energy savings through Smooth trajectories generation with shorter idling time at the intersection	[109]

1.2.4. Research Status of Eco-Driving Control Strategies

According to above review about research status of eco-driving, the working mechanism of the eco-driving cruise control system consists of three categories, including eco-cruise considering the road slope information, the minimization of the fuel consumption considering the constraints of upcoming traffic signal lights information in the urban transport system, and fuel economy optimization during the car-following mode. The proportional-integrative-derivative (PID) algorithm can be widely employed when only the speed control is considered [110]. However, in real process control, taking the minimization of fuel consumption as the optimization objective, various soft and hard constraints in the actual driving process are required to be considered. Classic PID controller is hard to handle such complex systems. Consequently, many advanced control algorithms have been developed and applied to the development of eco-driving cruise control systems, such as sliding mode control for fixed Vehicle-to-Vehicle spacing [111], linear quadratic control for adaptive time headway [112], nonlinear decoupled control [113], and model predictive control, etc.. Several commonly used control algorithms are systematically listed as follow:

(1) PID Control:

PID control algorithm, as one of the most classic control algorithms in industrial control field, is widely utilized in various industries. PID control has been widely used in the development of vehicle cruise control systems but taking into account the spacing control under the car following model is the difficulty of PID control algorithm. In 2001, Yi et al. [114] designed a vehicle stop-and-go cruise control algorithm combining PI control and feedforward strategy, which includes upper-level speed and spacing control algorithm and lower-level throttle and braking actuator control. In 2006, Zhang and Ioannou [115] designed a truck following controller using the PID control algorithm. The author selected PID control parameters through the zero-pole placement theory, adjusted inter-vehicle spacing error and relative speed to obtain the smooth speed trajectory, and improved fuel economy of the truck driving. PID control algorithm is characterized by fast response but poor robustness, so it is not suitable for multi-objective control.

(2) Optimal Control:

Optimal control, as an important branch of modern control theory, searches for the optimal control signal to obtain the maximum or minimum value of the objective function under certain constraints. In 2003, Möbus et al [116] calculated optimal acceleration according to traffic rules, safe distance, and driver intention in the multi-objective traffic scenario. The objective function was formulated as the quadratic cost function of discretized piecewise affine system and solved by dynamic programming. Yi et al. [117] proposed a vehicle spacing control algorithm for the stop-and-go driving situation. The acceleration of the control algorithm was regulated by spacing and throttle/brake control, and the expected acceleration was obtained by using linear quadratic control theory.

(3) Sliding Mode Control:

The difference of sliding mode control from other controllers involves in so-called variable structures systems, which consists of a set of continuous subsystems with a proper switching logic and, as a result, control actions are discontinuous functions of the system state, disturbances and reference inputs. The sliding mode surface is designed according to the desired dynamic characteristics of the system, and the control law makes the system arrive at the origin along the sliding mode surface from any initial position. In 2002, Lu et al. [118] designed a cooperative adaptive cruise control (CACC) system combining the variable time headway (VTH) and sliding mode control, analyzed the robustness of the closed-loop system, and established the clear relationship between spacing, control variables and preceding vehicle’s speed and acceleration. In 2005, Bin et al. [119] designed a sliding mode controller based on the study of nonlinear characteristics of acceleration dynamic response for

vehicle stop-and-go cruise control system. Simulation experimental results indicated the enhanced system robustness using proposed sliding mode controller. In 2014, Ganji et al. [120] developed an adaptive cruise control system based on sliding mode control for hybrid electric vehicles and compared its performance with the PID controller. In 2015, Li et al. [121] presented a sliding mode controller for an automatic car following system and validated its effectiveness through simulation and experimental bench. Therefore, through the above analysis, sliding mode control features fast dynamic response, better system robustness, and easier real implementation. The disadvantages of this controller involve chattering problem for utilization in real control systems.

(4) Fuzzy Logic and Neural Network Control:

Fuzzy logic imitates uncertainty, the reasoning process, and working mechanism of the human brain to make the fuzzy judgment on problems with unclear boundaries. The neural network simulates structural and functional characteristics of biological neural network to realize self-learning, enabling the system to realize self-improvement by adjusting weights according to the variation of environment. With the advantages of self-learning and self-adaptation, both fuzzy logic and neural network are capable of solving nonlinear problem so that they are widely used in vehicular adaptive cruise control system.

In 2002, Ohno [122] proposed a neural-network-based adaptive cruise control system to predict the optimal driving behavior, which was a kind of application of digital twin using the neural network to simulate an experienced driver. In 2006, Naranjo et al. [123] conducted experimental analysis on a stop-and-go adaptive cruise control system. Based on fuzzy logic control, the input variables were velocity error, acceleration, time headway and its derivative, and the output variables were throttle and brake pedal manipulation. The real test bench results showed that the control algorithm had a wide range of adaptive control and improved the driving safety. In 2010, Alonso et al. [124] used the genetic algorithm to optimize the adaptive cruise control system based on ultrasonic sensors, which overcame the shortcoming that ACC can only be applied at expressway with large spacing. In 2012, Khayyam et al. [125] held that although the conventional analytical adaptive cruise control system could perform well, it was difficult to design and handle the burdensome computation problem. To reduce the computational costs, an ACC-based adaptive neuro-fuzzy inference system (ANFIS) was proposed to calculate fuel consumption under integrated dynamic loads such as wind resistance, road slope, rolling friction. The Look-ahead strategy with ANFIS could predict upcoming road slope. The experimental results indicated that 3% averaged fuel consumption reduction can be achieved.

(5) Model Predictive Control:

Model predictive control (MPC) is a closed-loop optimal control strategy based on system model. In 1978, Richalet et al [126] proposed “three principles” for MPC: predictive model, receding horizon optimization, and feedback control. MPC can effectively handle multi-objective optimization problems within multiple hard or soft system constraints. Meanwhile, the MPC algorithm is characterized by solid robustness by timely compensating for the uncertainties caused by model mismatch and disturbance.

In 2008, Corona and De Schutter [127] proposed an adaptive cruise control system based on MPC for nonlinear system dynamics. In 2012, Shakouri et al. [128] integrated the conventional upper controller and lower controller into a single control loop, and extended the linearized vehicle dynamics LTI model based on relative distance and speed between the host and preceding vehicles. The objective of maintaining constant spacing was introduced into the single nonlinear MPC, and pedal position control of throttle/brake was realized by using the state-dependent method.

Especially, the research group at Tsinghua University has conducted a lot of research on the application of the MPC algorithm to vehicle cruise control. In 2010, Shengbo Eben Li [129] solved and optimized the problems

in MPC practical application. In 2011, Shengbo Eben Li et al. [130] conducted a comprehensive design of the upper-level controller of the ACC system under the framework of MPC. Considering the minimization of fuel consumption and car following performance, the quadratic cost function was established. The optimal control problem was numerically solved by quadratic programming. Subsequently, in 2013 and 2015, Shengbo Eben Li et al. [131]~[132] extended their study on the application of MPC in the ACC system. A fuel-economy-oriented inter-distance control algorithm was developed based on the MPC framework. Multiple objectives, such as fuel economy, car following, and driver expected response, were transformed into cost function and constraints. Compared with the linear quadratic algorithm, the proposed strategy improved the car-following performance as well as fuel economy. Then, Shengbo Eben Li focused on the computational efficiency of the MPC algorithm for real-time application. By combining the "move blocking" strategy with a "constraint-set compression" strategy, a lower-dimensional MPC algorithm was formulated using partially relaxing inequality constraints in the prediction horizon.

1.2.5. Summary of Research Status

Through the above analysis and review of current research status on safety distance model, energy consumption model, ecological cruise control system and related control algorithm, it can be concluded respectively as follow:

(1) For the aspect of safety distance model: the safety distance model directly influences the driving safety, traffic flow and platoon stability, road utilization efficiency and the driver's acceptance to of car-following system. Specifically, if the safety distance is too small, such as the model based on time headway, although it can increase the traffic flow and road utilization rate, the actuation time of braking system or response time for drivers is insufficient, which makes drivers feel uneasy and prone to traffic accidents. If the safety distance is too large, such as the model based on braking process, although the driving safety can be guaranteed, the road utilization rate is hard to be fully exploited. There may be vehicles from adjacent lanes cutting into the lane of the host vehicle so that the stability of the vehicle platoon cannot be ensured. Therefore, research emphasis should be placed on developing a safety distance model which can not only ensure driving safety but also improve the road utilization rate.

(2) For the aspect of the fuel/energy consumption model: it is found that most of the modeling data for existing microscopic fuel consumption is fed and collected during engine's stable conditions. In most real driving scenarios, vehicles operate in a transient condition, which causes the noticeable estimation error and is hard to satisfy the fuel consumption prediction accuracy in developing eco-driving system. On the other hand, the existing instantaneous fuel consumption model is blamed for too many model parameters. Consequently, it is necessary to develop an instantaneous fuel/energy consumption model with a simple and clear model structure as well as adequate estimation accuracy for eco-driving system.

(3) For the aspect of the eco-driving system: considering different traffic scenarios, eco-driving system is generally classified into two categories. The first research direction does not consider extra complexity from the interaction between vehicles, and only takes into account the information of road terrain to optimize the fuel economy. The second direction focuses on fuel economy optimization during car-following situation or considers the information upcoming traffic signal lights to get the optimal velocity trajectory, during which the interactions between vehicle to vehicle and vehicle to infrastructure, as the determinant of driving behavior, are integrated into the control objective. Moreover, the nonlinearity of energy consumption and motion of the preceding vehicle will aggravate the computational complexity. Therefore, in order to realize efficient online system optimization, problem formulation needs to be ingeniously designed.

(4) For the aspect of control algorithm: There exists a lot of uncertainties and constraints for a comprehensive multi-objective eco-driving system that considers the influences from either preceding vehicle, or upcoming traffic signal lights timing and phase information, or the road terrain ahead. Hence, an advanced control algorithm is required to optimize dynamic control objectives according to real-time driving condition. Model predictive control is capable of handle multi-objective optimization problem with various system constraints. What's more, MPC's superior robustness can timely make up for the uncertainty caused by model mismatch and disturbance, which is suitable for the control strategy design of complex systems.

1.3. What will be elucidated in this research

As reviewed, current research are mostly focused on the specific driving scenario eco-driving strategy development, either car-following scenario, or speed regulation based on traffic signal lights, or simply speed optimization considering road grade information. However, a vehicle may experience an integrated traffic system with synthetic driving scenarios in an actual day-to-day trip. For example, a host vehicle may start up from a complete stop and accelerate until its velocity reaches the road speed limitations during which road gradient variation will influence the fuel/energy consumption. When the host vehicle approaches the signalized intersection, the SPaT information can be anticipated and influences the energy consumption. At any time instant, a host vehicle may encounter following a preceding vehicle which may disappear after the host vehicle implements lane-changing maneuver.

To fill the research gap in previous studies, a comprehensive predictive cruise control for electric vehicles (EVs) eco-driving is developed in this research to handle the mixed and integrated driving scenarios in both urban and suburban areas. According to the relevance and difference of the overall research contents, this thesis is divided into six chapters and the main research works of each chapter are expounded as follow:

- Chapter 1, introduction. The research background and the significance of this research are introduced in detail. Then, according to the main technologies covered in this research, the relevant literature is sorted out and analyzed from four aspects: car-following strategies, vehicular energy consumption model, eco-driving system, and eco-driving control algorithms. It follows that the research idea is determined.
- Chapter 2, eco-driving system architecture design and dynamics modeling. According to the detection of the surrounding driving environment, the proposed predictive cruise control system is designed with three driving scenarios (free driving scenario, car following scenario, and signal anticipation scenario) and an instantaneous driving scenario switch logic. The overall scheme for each driving scenario is designed with the explanation of critical technologies. The vehicle longitudinal model and inter-vehicle longitudinal dynamics model are established, respectively, laying the model basis for the development of the predictive cruise control system in the following chapters. The reference velocity planning model is presented based on traffic signal phase and timing (SPaT) information.
- Chapter 3, artificial-neural-network-based instantaneous energy consumption model (ANN-IECM). The analysis of similarities and differences between energy consumption model for EVs and the fuel consumption model for ICEVs is conducted, which presents the necessity and feasibility of the development of energy consumption model. The dataset for neural network training is prepared and neural network structure and training algorithm are determined. Finally, the model effectiveness is validated.
- Chapter 4, predictive cruise control system for eco-driving based on MPC algorithm is presented.

Optimization problems for three driving states are formulated respectively under the framework of MPC. Then, detailed mathematical derivations of the predictive optimization problem are presented. For the real application of the proposed predictive cruise control system, the system robustness, feasible region expansion, and computation efficiency are further discussed in detail.

- Chapter 5, simulation experiments of predictive cruise control for eco-driving. The simulation platform is firstly established based on CarSim and MATLAB/Simulink. Typical case studies for different driving modes are conducted to verify the effectiveness of proposed predictive cruise control system. The comparative simulation results are analyzed and discussed.
- Chapter 6, conclusion, and prospects. Summarize the research contents and results of the overall thesis and elaborate on the originality of the research. Finally, future work is proposed in view of the defects in this study.

1.4. Technical Route

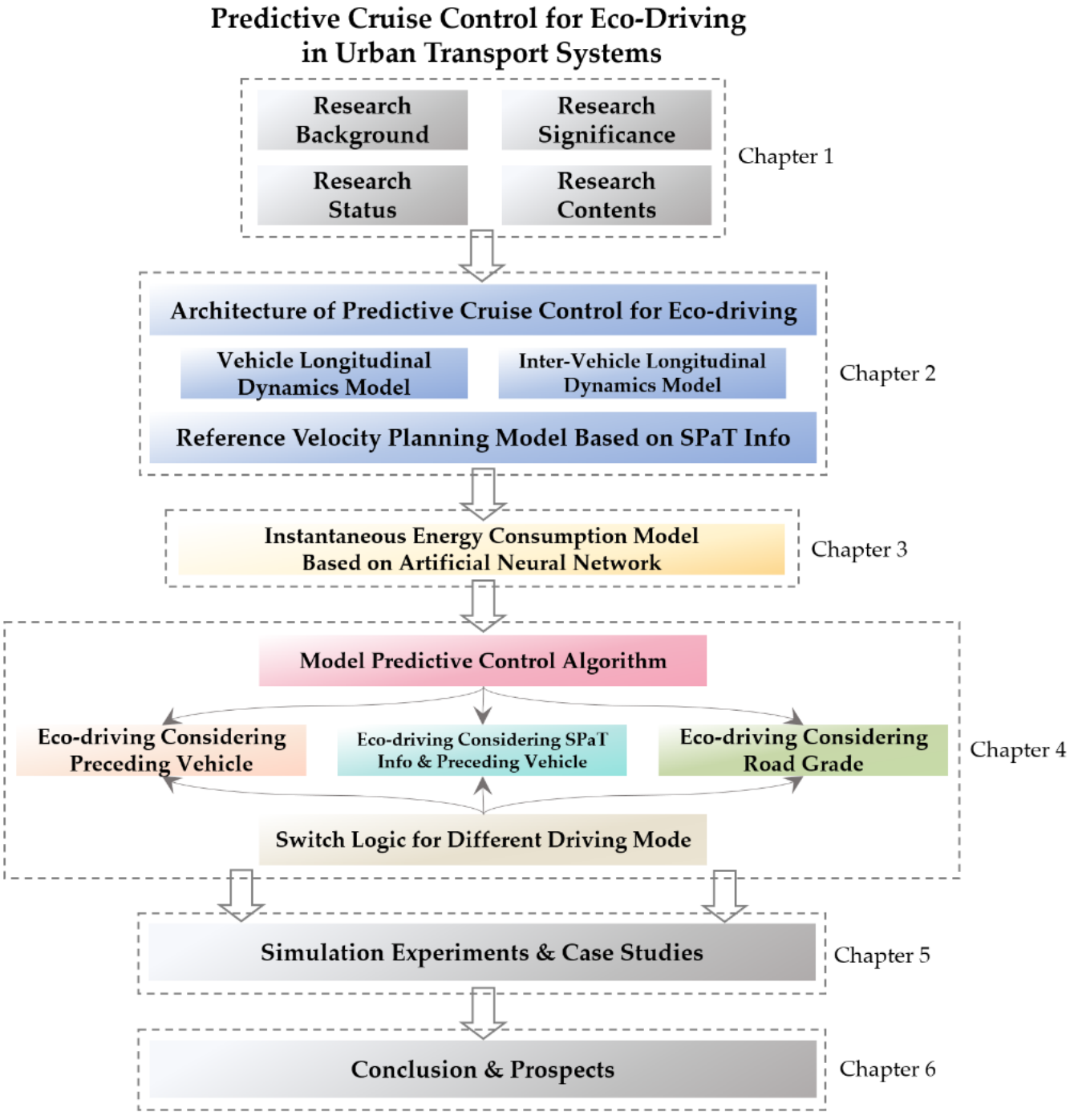

Fig. 1.3 Technical Route of overall research

1.5. Summary of Chapter 1

This chapter elaborates on the relevant research background and significance of vehicle eco-driving cruise control system. It systematically summarizes the research status of the key technologies of the eco-driving cruise control system involved in this research. Based on this, the research content of this thesis is determined, followed by the overall technical route.

Chapter 2. Eco-Driving Predictive Cruise Control System Architecture and Dynamics Modeling

2.1. Eco-Driving Predictive Cruise Control System Architecture

During the automatic cruise, for a given driving task with enough driving range, it may cover multiple complex driving scenarios, including driving on the straight road, curved road, hilly road, free driving, car-following driving, acceleration, deceleration, or emergent braking, etc. Simultaneously, vehicles driving is highly constrained by traffic signal lights and speed limitations in the certain road section. Different road conditions, driving conditions and traffic constraints are coupled with each other, making the driving task too complex and difficult to obtain an optimal solution. Even if the solution is obtained, the obtained economic speed profile only reflects a specific driving task under specific working conditions. The influence of various factors is difficult to be decoupled and quantitatively analyzed, making it difficult to get the practical eco-driving control law. Consequently, it is insignificant to optimize a specific driving task with the fact that there exist infinite types of driving tasks in reality.

Based on the fact stated above that a comprehensive eco-driving system is required to develop so that it can both handle the mixed and integrated driving scenarios with multiple constraints and realize the decoupled optimization for the different driving scenario for the significance of practical implementation. For this purpose, instead of deriving the global optimal control for the whole driving task, the mixed and coupled driving scenarios are divided into three categories, including the free driving scenario and car following scenario and signal anticipation scenario. The decoupling of each single driving scenario makes it possible to explore its internal mechanism and obtain the universal control strategy. Therefore, the proposed predictive cruise control system for eco-driving in this research will be designed scenario by scenario and combined through an instantaneous driving scenario switch logic.

2.1.1. Predefined Assumption on ITS and CAVs

In this research, the overall predictive cruise control system for electric economic driving is developed based on the ITS and technology background of connected and automated vehicles (CAVs). The ITS enables Vehicle-to-Vehicle (V2V) and Vehicle-to-Infrastructure (V2I) communication for the host vehicle to access real-time information in making optimal driving decisions.

Vehicle-to-Vehicle (V2V)

The V2V data interaction provides the real-time driving state information of the surrounding vehicles so that, e.g., in the car following driving situation, the velocity of the preceding vehicle is crucial to the maintenance of safety distance. The data exchange used in this research includes real-time inter-vehicle distance or relative spacing between host and preceding, d_{rel}, and the real-time velocity of the preceding vehicle v_{pre}, as explained in the following Table 2.1.

TABLE 2.1 Vehicle-to-Vehicle Communication data in the research

Parameter	Explanation	Unit
d_{rel}	The relative distance between host and preceding vehicle in	m

	the same lane	
v_{pre}	The real-time driving speed of the preceding vehicle	m/s

Vehicle-to-Infrastructure Communication

The real-time traffic and road condition are important in working out an operative and eco-cruise strategy. The V2I communication realizes the data real-time transmission from the roadside to vehicle side, such as driving speed limitation on certain road sections, the traffic signal phase and timing (SPaT) information, the distance to the upcoming signalized intersection, road altitude information according to the driving position, etc. In this research, the V2I interaction contains the dynamic distance to the upcoming signalized intersection d_{TSL}, the speed limitation $[v_{min}, v_{max}]$, the road altitude for certain driving position h, the traffic signal lights state S_{TSL}, and the remaining time for the current traffic signal light t_{remain}, as explained in the following Table 2.2.

TABLE 2.2 V2I data interaction in this research

Data	Variable Definition	Unit
d_{TSL}	The distance to the upcoming signalized intersection	m
$[v_{min}, v_{max}]$	Allowable speed limitation on a certain road section	m/s
h	Road altitude at a certain position	m
S_{TSL}	The traffic signal lights state, including Green, Red, Yellow	-
t_{remain}	The time left for the traffic light of the upcoming intersection	s

Connected and automated vehicles

With the coordination of automated vehicle connection, the advancement of connected and automated vehicles (CAVs) enables the information interaction through ITS. Besides, the AV is capable of realizing more accurate and consistent vehicular control compared to the human driver, which makes it an ideal platform for developing the predictive cruise control system for eco-driving.

The V2I and V2V data are visualized in the following Figure 2.1.

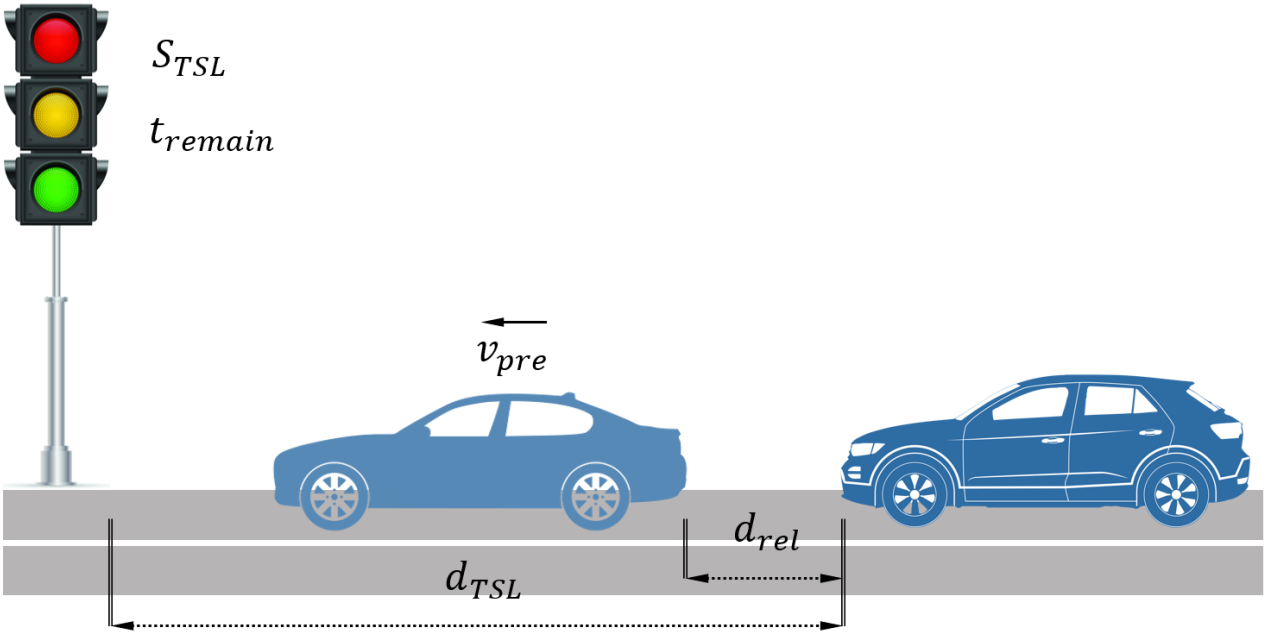

Fig. 2.1 Visualization of parameters in ITS

2.1.2. Predictive Cruise Control System Overall Scheme

Before developing the predictive cruise control system for eco-driving, it is indispensable to declare the research object and its position in the whole vehicular control. As illustrated in Figure 2.2, the overall cruise control system is distributed hierarchically. The perception of the driving environment for the host vehicle is supported by assumed ITS and CAVs and these data streams are fed into the upper-level controller. The upper-level controller calculates the desired acceleration utilizing the optimization algorithm according to multiple control objectives based on the vehicle longitudinal dynamics model. The lower-level controller takes the desired acceleration obtained from the upper-level controller as input to adjust the throttle and brake pedal pressure and control the vehicle to track the desired acceleration. The main research content in this thesis is the upper-level controller design of the economic predictive cruise control system.

The control objectives of the proposed predictive cruise control system for eco-driving are different according to different traffic road condition. Without considering the constraints from surrounding traffic conditions, the vehicle is operating freely, during which the energy consumption is optimized only considering the road gradient information; while driving under daily urban transport situation, the motion of the preceding vehicle has to be considered as constraints of energy consumption optimization; besides, the traffic signal lights information, as an influential factor to traffic flow, is considered additionally as a constraint to optimize the vehicular energy consumption. Therefore, because of the difference of control objectives and system complexity and to make the proposed predictive cruise control (PCC) system adapting to the comprehensive traffic system with synthetic driving scenarios, three typical driving scenarios, including road gradient information access-based free driving, the motion of preceding vehicle based-car following, and upcoming SPaT information-based signal anticipation scenario, are discussed separately. In actual daily travel, however, the proposed PCC system for eco-driving is required to be able to automatically switch catering to different driving scenarios with different optimization objectives. Hence, a driving scenario switching logic (DSSL) is required to be designed precisely.

To formulate the DSSL of the host vehicle, a general vehicular braking distance model is firstly introduced [133], as follow:

$$d_{brk} = d_{min} + v_{host}(k) \cdot t_{brk} + \frac{v_{host}^2(k)}{2 \cdot a_{brk}} \tag{2.1}$$

where d_{brk} (m) refers to the braking distance, d_{min} (m) denotes the minimum critical distance, $v_{host}(k)$ (m/s) represents the host vehicle velocity at instant k, t_{brk} (s) is the reaction time before braking, a_{brk} (m/s^2) is the deceleration during braking.

The thresholds value for the distance to an upcoming signalized intersection d_{TSL} and the relative distance between the host and preceding vehicles in the same lane d_{rel} are defined as $d_{TSL,limit}$ and $d_{rel,limit}$, respectively. They are numerically equal to the maximum braking distance based on equation 2.1 using the parameters from [133], shown as follow:

$$d_{TSL,limit} = d_{rel,limit} = 10 + v_{host}(k) + 0.0825 \cdot v_{host}^2(k) \tag{2.2}$$

Once the actual distance to the upcoming signalized intersection, d_{TSL}, is smaller than the threshold value, $d_{TSL,limit}$, the DSSL switches into the signal anticipation scenario. Once the actual relative distance between host and preceding vehicle, d_{rel}, is smaller than the threshold value, $d_{rel,limit}$, the DSSL switches into the car following scenario. Otherwise, the free driving scenario considering the road gradient information will be triggered by the DSSL.

The real-time estimated time length to pass the upcoming signalized intersection is defined as follow:

$$t_{limit} = \begin{cases} \dfrac{d_{TSL}}{v_{host}(k)} & v_{host}(k) > 0 \\ \dfrac{d_{TSL}}{a_{max}} & v_{host}(k) = 0 \end{cases} \tag{2.3}$$

where a_{max} denotes the maximum physical allowable acceleration of the vehicle.

Thus, the detailed driving scenario switching logic (DSSL), shown in Figure 2.3, can be designed, and used to switch into one of three studied typical driving scenarios. In order to mathematically describe the real-time driving scenario of the vehicle, a vector $\begin{bmatrix} d_1 \\ d_2 \\ d_3 \end{bmatrix}$ is defined. The $\begin{bmatrix} 1 \\ 0 \\ 0 \end{bmatrix}$ stands for the free driving scenario, $\begin{bmatrix} 0 \\ 1 \\ 0 \end{bmatrix}$ means that the vehicle is under signal anticipation driving scenario, and $\begin{bmatrix} 0 \\ 0 \\ 1 \end{bmatrix}$ denotes the vehicle is under the car following driving scenario.

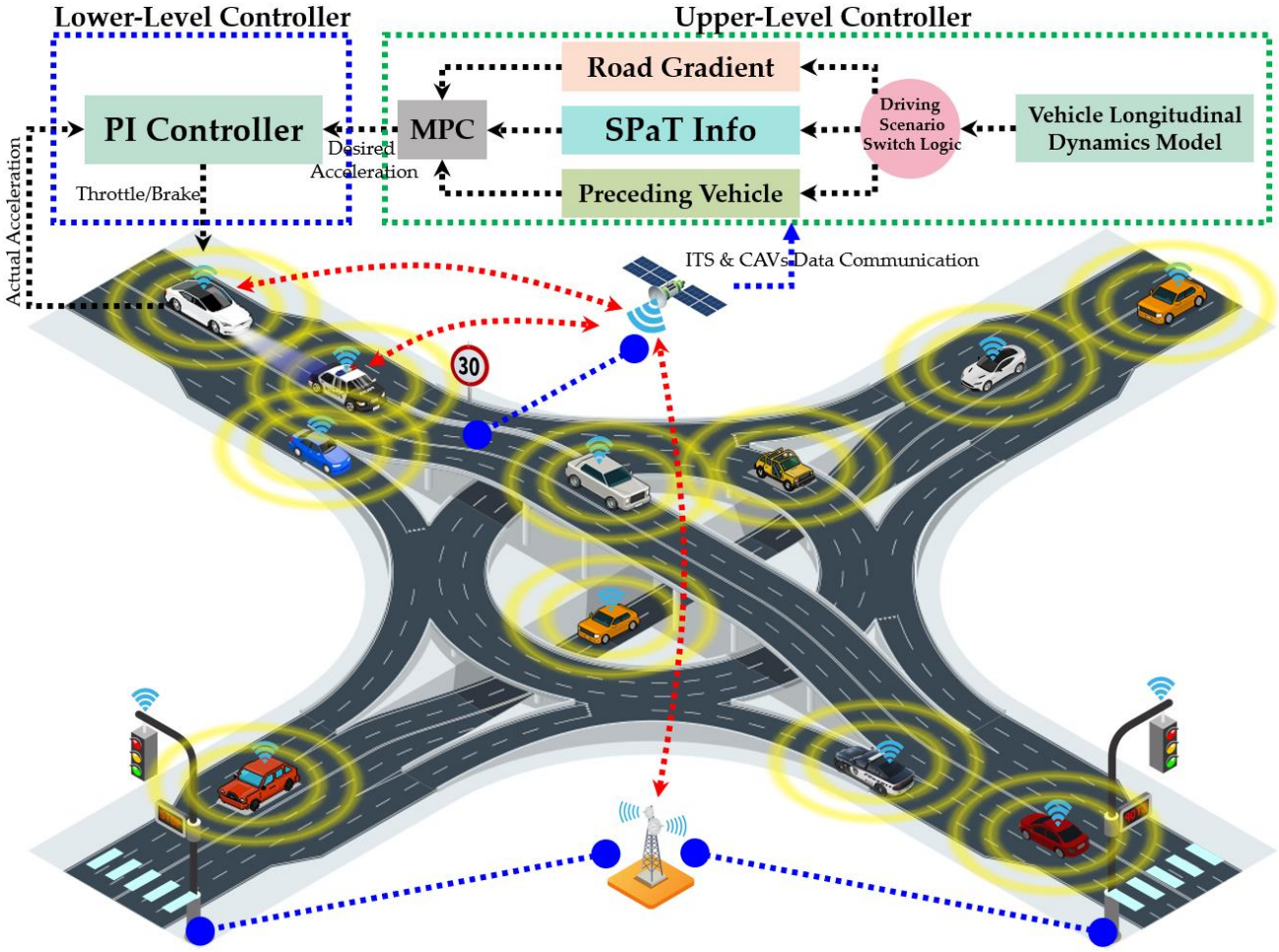

Fig. 2.2 Schematic of Predictive Cruise Control System for Eco-Driving

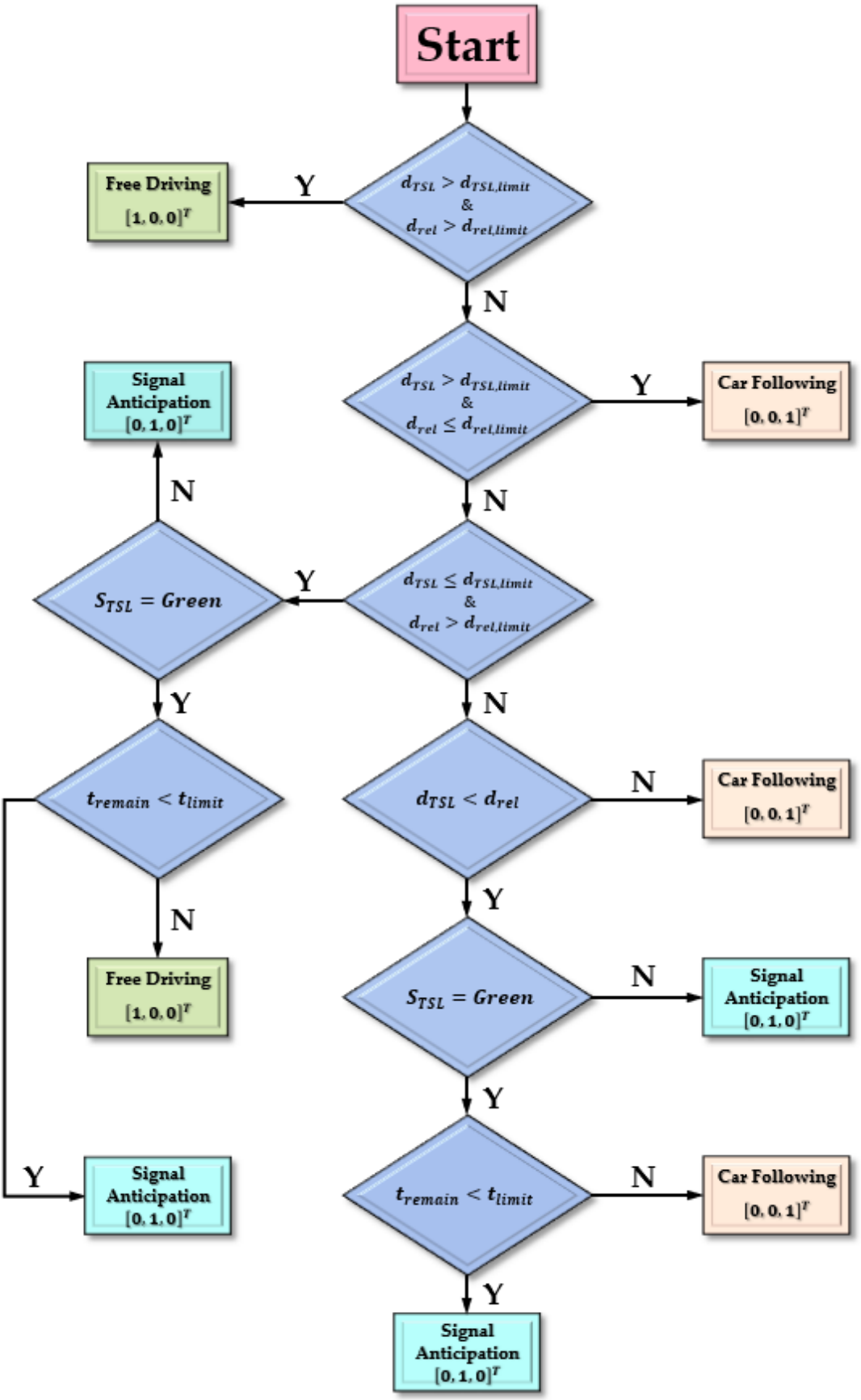

Fig. 2.3 Flow Chart for Driving Scenario Switching Logic (DSSL)

For free driving scenario $[1,0,0]^T$, the PCC system executes the eco-driving algorithm under the framework of MPC based on vehicle longitudinal dynamics model and instantaneous energy consumption model with access to real-time road gradient information to minimize the energy consumption. For signal anticipation scenario $[0,1,0]^T$, the PCC system executes the eco-driving algorithm under the framework of MPC based on vehicle longitudinal dynamics model and instantaneous energy consumption model with access to upcoming real-time traffic SPaT information to optimize the energy consumption. For car following scenario $[0,0,1]^T$, the PCC system executes the eco-driving algorithm under the framework of MPC based on vehicle longitudinal dynamics model, inter-vehicle dynamics model and instantaneous energy consumption model with access to the motion states of preceding vehicle to realize both driving safety and energy economy. The eco-driving system architecture based on the MPC algorithm for three typical driving scenarios is shown as follow in Figure 2.4:

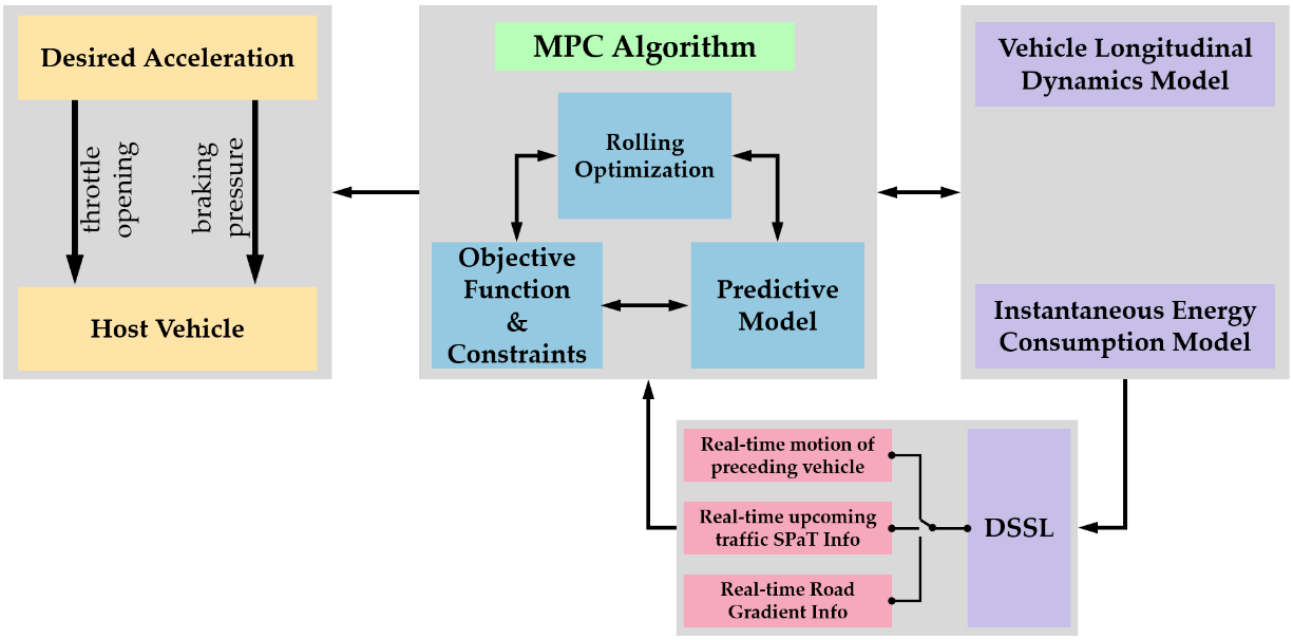

Fig. 2.4 Three Typical Driving Scenarios of PCC System Architecture based on MPC algorithm

The proposed predictive cruise control (PCC) system for eco-driving is based on the model predictive control algorithm. For each sampling time step, the MPC takes the state of the system at the current moment, solves a finite time-domain open-loop online optimization problem to obtain a sequence of desired acceleration within certain system constraints, and inputs the first element of the derived control sequence into the system to realize the closed-loop control, which inherently ensures the robustness of the control system. In the next time step, the rolling optimization problem is solved in real-time with the prediction horizon moving forward. Thus, repeatedly, the overall driving task with certain control and optimization objectives can be completed.

The general vehicular longitudinal dynamics system includes inter-vehicle longitudinal dynamics model and vehicle dynamics model. The inter-vehicle longitudinal dynamics model describes the car-following behavior using a safety distance strategy and transfers the desired acceleration output by the MPC to the host vehicle.

2.2. System Dynamics Modeling

According to the specific requirements for different driving scenarios proposed above, the corresponding system dynamics modeling is the prerequisite of developing the PCC system for eco-driving. For free driving scenario and signal anticipation scenario, the vehicle longitudinal dynamics model is required to reflect the real-time vehicle driving condition. For car following driving scenario, the inter-vehicle longitudinal dynamics model is

necessary to represent the coupling between inter-vehicle and vehicle dynamics. Once the DSSL switches into the signal anticipation scenario, the driving objective at this specific moment is to find the optimal reference velocity that reduces the idling at red lights given the upcoming state of traffic signal lights. Therefore, a rule-based reference velocity planning model that calculates an instantaneous optimal vehicle velocity trying to avoid stopping at the red light is proposed.

2.2.1. Vehicle Longitudinal Dynamics Modeling

The vehicle longitudinal dynamics is modeled based on the sum of all forces acting in the longitudinal direction illustrated in Figure 2.5. During the motion of the vehicle, the longitudinal acceleration a_{host} is calculated as follow:

$$a_{host}(t) = \frac{\mathrm{d}v_{host}(t)}{\mathrm{d}t} = \frac{1}{m_{eq}}[F_{trac}(t) - F_{res}(t)] \tag{2.4}$$

where m_{eq} denotes the equivalent vehicle mass which is the sum of vehicle weight, driver, and rotational equivalent masses, F_{trac} is the traction force, and F_{res} is the collectively resistance forces from different aspects as follows:

$$F_{res}(t) = F_{roll}(t) + F_{aero}(t) + F_g(t) \tag{2.5}$$

$$F_{roll}(t) = c_r \cdot m_{eq} g \cos\big(\theta(t)\big) \tag{2.6}$$

$$F_g(t) = m_{eq} g \sin\big(\theta(t)\big) \tag{2.7}$$

$$F_{aero}(t) = \frac{1}{2}\rho_a A_f C_D v_{host}^2(t) \approx \frac{1}{2}\rho_a A_f C_D(\kappa_1 v_{host}(t) + \kappa_2) \tag{2.8}$$

where F_{roll} is the rolling resistance correlated with rolling resistance coefficient c_r, F_g is the gradient resistance due to the gravity when driving on an uphill road, F_{aero} is the aerodynamics drag force correlated with air density ρ_a, the frontal area of the vehicle A_f, and aerodynamic drag coefficient C_D. The aerodynamics drag force F_{aero} can be approximated through linear fitting, i.e., $v_{host}^2(t) = \kappa v_{host}(t) + \kappa_2$.

The powertrain of the electric vehicle consists of the battery pack, a DC-AC converter, an electric motor, and a single ratio transmission. The electrical energy is converted into mechanical energy delivered to the wheels through a single gear ratio gearbox. Hence, the traction force F_{trac} can be calculated according to the motor output torque as follow:

$$F_{trac} = \frac{T_m(t) i_g \eta_e}{r_w} \tag{2.9}$$

where T_m is the electric motor output torque, i_g is the single gear ratio of the gearbox, η_e is the transmission efficiency, and r_w is the radius of the vehicle wheel.

The electric motor utilizes energy from the onboard battery to generate torque. Reversely, during vehicles' braking, it works as a generator using regenerative braking power to recharge the battery. As the mapping of motor torque and rotation speed, electric motor efficiency can be expressed using following formula [134]:

$$\eta_m(t) = f\big(T_m(t), \omega_m(t)\big) \tag{2.10}$$

Then the motor power P_m can be calculated using defined motor efficiency η_m, as follow:

$$P_m(t) = T_m(t) \cdot \omega_m(t) \cdot \eta_m^{\alpha} \tag{2.11}$$

where $\alpha = \begin{cases} 1 & working\ as\ a\ generator \\ -1 & working\ as\ a\ electric\ motor \end{cases}$.

The battery model can be simplified as an internal resistance model [135] shown as Figure 2.6, wherein R_{batt} is the internal resistance, I_{batt} is the equivalent current in the circuit, and U_{batt} is the open-circuit voltage. Thus, the battery power providing energy to electric motor can be obtained as following [136]:

$$P_{batt} = U_{batt}I_{batt} - I_{batt}^2 R_{batt} \tag{2.12}$$

The variation rate of the state of charge (SOC), as an indicator of the remaining battery energy, is expressed as follow:

$$\dot{SOC} = -\frac{I_{batt}}{Q_{batt}} \tag{2.13}$$

where Q_{batt} denotes maximum battery capacity.

Substituting equation 2.12 into equation 2.13, the following equation can be obtained:

$$\dot{SOC} = -\frac{U_{batt} - \sqrt{U_{batt}^2 - 4P_{batt}R_{batt}}}{2Q_{batt}R_{batt}} \tag{2.14}$$

Consequently, the electric motor output torque can be calculated using power transition from the onboard battery and the electric motor showing below:

$$T_m(t) = \frac{P_{batt}}{\omega_m} \tag{2.15}$$

When the motor output power T_m is a positive value, the battery works as discharging process. While T_m is negative, the battery works in the charging procedure.

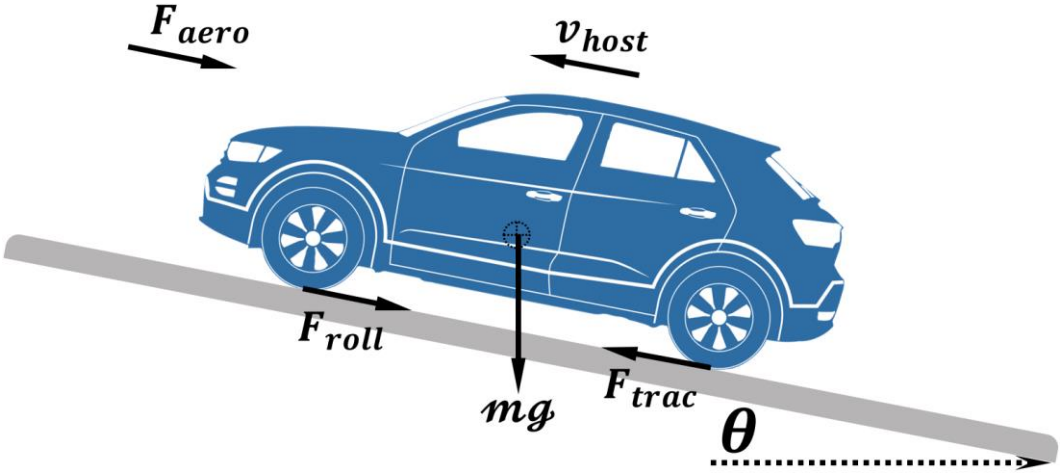

Fig. 2.5 Longitudinal Forces Acting on the Vehicle Driving on Slope Road

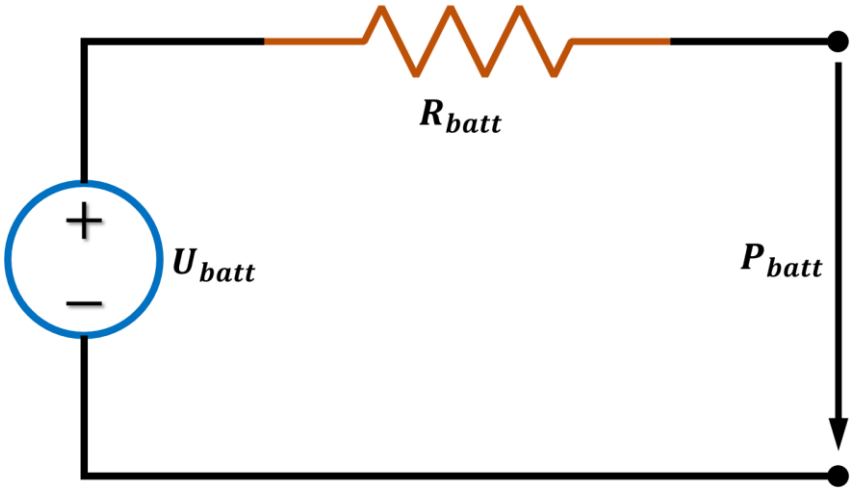

Fig. 2.6 Equivalent Internal Resistance Model for Battery

Accordingly, based on the above derivation, the vehicle longitudinal dynamics model can be obtained explicitly as follow:

$$\begin{aligned} \frac{\mathrm{d}x_{host}}{\mathrm{d}t} &= v_{host} \\ \frac{\mathrm{d}v_{host}}{\mathrm{d}t} &= \frac{1}{m_{eq}}\left[\frac{T_m(t) i_g \eta_e}{r_w} - c_r \cdot m_{eq} g\, cos\big(\theta(t)\big) - m_{eq} g\, sin\big(\theta(t)\big) - \frac{1}{2}\rho_a A_f C_D(\kappa_1 v_{host}(t) + \kappa_2)\right] \end{aligned} \tag{2.16}$$

The related parameters used to model the electric vehicle are listed in Table 2.3.

TABLE 2.3 Specification of Vehicle Longitudinal Dynamics Model

Specification	Values
Equivalent total mass of the electric vehicle, m_{eq}	$1260kg$
Gear ratio, i_g	3.905
Total mechanical efficiency of the driveline, η_e	0.95
Effective radius of the vehicle wheel, r_w	$287mm$
Frontal area of the vehicle, A_f	$2.22m^2$
Rolling resistance coefficient, c_r	0.028
Aerodynamic drag coefficient, C_D	0.316
Air density, ρ_a	$1.206kg/m^3$
Motor	Maximum available power: P_{m_max} = $55kW$; Maximum output torque: $305Nm$;
Battery	Battery voltage: 6~$9V$; Packs: 40; Initial charge level: 0.8; Q_{batt}: $93Ah$

2.2.2. Validation of Dynamic and Stability Performance

The part of an actual vehicle trip is measured as the test velocity profile to validate the accuracy of the vehicle longitudinal dynamics model. The model dynamics responses of longitudinal velocity, acceleration, motor

torque, battery output power, and battery state-of-charge is shown in Figure 2.7.

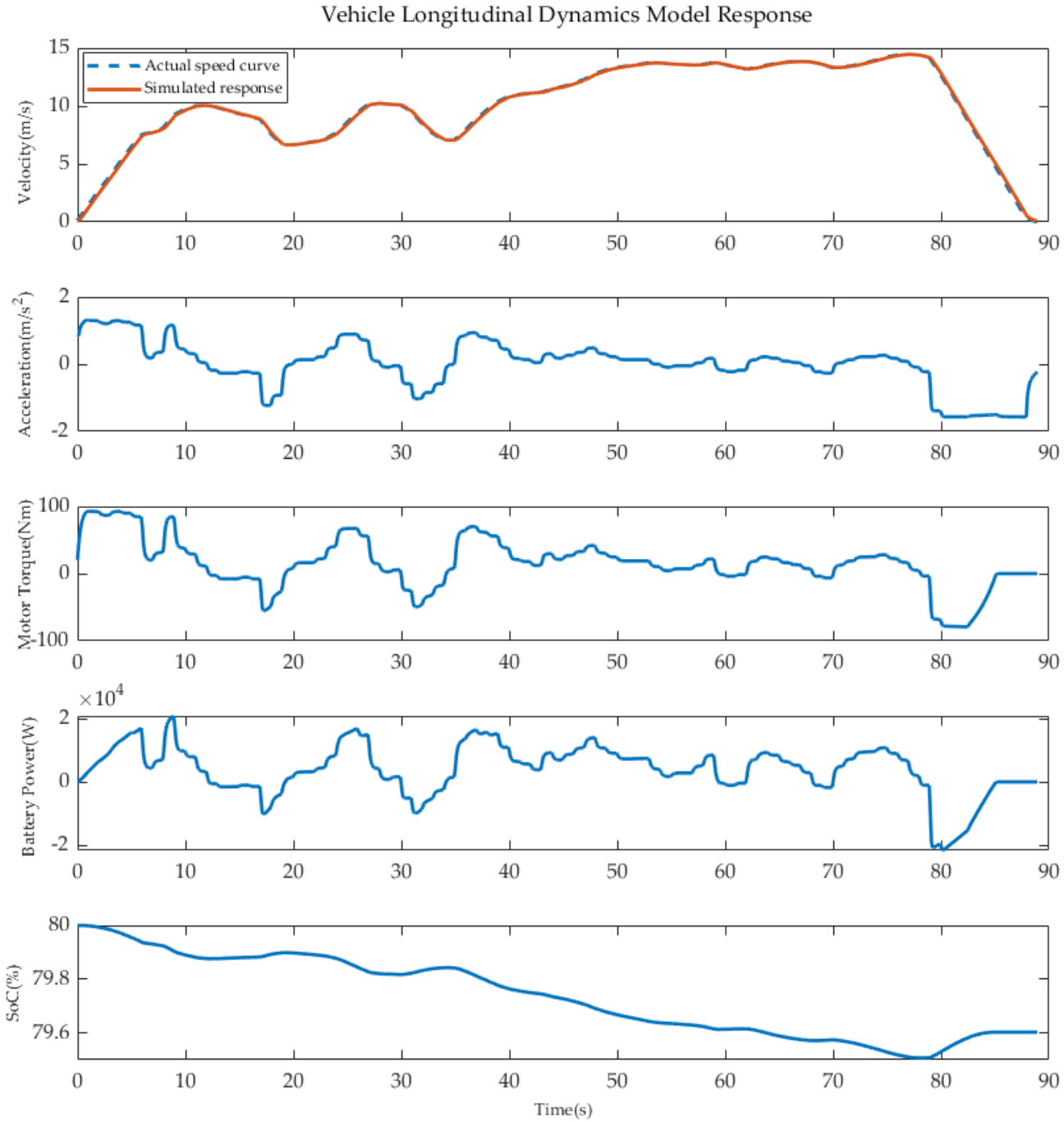

Figure 2.7 Model dynamics response of the real drive cycle

From the model output speed response, the model can track the actual speed curve well. Therefore, the established vehicle longitudinal dynamics model can accurately reflect the stability and dynamic characteristics of the vehicle longitudinal dynamics system.

2.2.3. Safety Distance Modeling Based on Variable Time Headway Strategy

During the car following driving scenario, the inter-vehicle longitudinal dynamics model describes the car-following characteristics. Among all the parameters of modeling the inter-vehicle longitudinal dynamics, the

most critical one is the desired safety distance, which calculates the spacing between host and preceding vehicles. According to the review of existing safety distance models, this research will combine both the strategy of constant time headway (CTH) and variable time headway (VTH) to design a novel safety distance model, which will consider not only the velocity of the host vehicle but also the relative velocity between host and preceding vehicles.

For conventional CTH strategy, it adopts the constant headway, which can be manually set by the driver. The mathematical expression is shown as follow:

$$D_{safe} = CTH \cdot v_{host} + d_{min} \tag{2.17}$$

where D_{safe} denotes the safety distance, CTH is the constant time headway, v_{host} is the velocity of the host vehicle, and d_{min} is the minimal critical spacing when two vehicles pull on.

Now instead of using a constant time headway CTH, a customized variable time headway VTH is designed, taking into account both the velocity of host vehicle v_{host} and relative velocity v_{rel} ($v_{rel} = v_{pre} - v_{host}$), and also the maximum allowable velocity v_{max}. The explicit mathematical equation is shown as follow:

$$VTH = \begin{cases} \tau_1 + \tau_2 v_{host} - \tau_3 v_{rel} & v_{host} < v_{max} \\ \tau_1 + \tau_2 v_{max} - \tau_3 v_{rel} & otherwise \end{cases} \tag{2.18}$$

where τ_1,τ_2, and τ_3 are constant coefficients greater than 0.

Replacing the CTH in equation 2.17 with the customized VTH, an adaptive safety distance model can be obtained as follow:

$$D_{safe} = VTH \cdot v_{host} + d_{min} = \begin{cases} \tau_1 v_{host} + \tau_2 v_{host}^2 - \tau_3 v_{rel} v_{host} + d_{min} & v_{host} < v_{max} \\ \tau_1 v_{max} + \tau_2 v_{max}^2 - \tau_3 v_{rel} v_{max} + d_{min} & otherwise \end{cases} \tag{2.19}$$

2.2.4. Stability Analysis of Safety Distance Model

As the basis of the inter-vehicle longitudinal dynamics model, it is indispensable to check whether the proposed safety distance model is reasonable and can adapt to the complex traffic situation. The prerequisite of system stability is that the inter-distance of the safety distance model converges when the preceding is operating under stable condition without any acceleration.

Assume the error between actual inter-distance D_{actual} and safety distance D_{safe} is Δd, then:

$$\Delta d = D_{actual} - D_{safe} \tag{2.20}$$

Taking "$v_{rel} \to 0 \Rightarrow \Delta d \to 0$" as the condition of system stability, substitute D_{safe} in equation 2.20 with equation 2.19 to obtain the following equation:

$$\Delta d = D_{actual} - VTH \cdot v_{host} - d_{min} \tag{2.21}$$

Take the derivative with respect to time simultaneously for both sides of the equation 2.21:

$$\dot{\Delta d} = v_{rel} - \dot{VTH} \cdot v_{host} - VTH \cdot \dot{v_{host}} \tag{2.22}$$

Rewrite stability condition "$v_{rel} \to 0 \Rightarrow \Delta d \to 0$" as:

$$v_{rel} + \kappa \Delta d = 0 \tag{2.23}$$

Plug equation 2.23 into equation 2.22:

$$\dot{\Delta d} = -\kappa \Delta d - \dot{VTH} \cdot v_{host} - VTH \cdot \dot{v_{host}} \tag{2.24}$$

Take the derivative for both sides of equation 2.19 when $v_{host} < v_{max}$, and plug it into equation 2.24:

$$\dot{\Delta d} = -\kappa \Delta d - (\tau_2 \cdot \dot{v_{host}} - \tau_3 \cdot \dot{v_{rel}}) v_{host} - VTH \cdot \dot{v_{host}} \tag{2.25}$$

Take the derivative for equation $v_{rel} = v_{pre} - v_{host}$ and equation 2.23, and with the condition of stability of preceding vehicle:

$$\dot{v_{rel}} = -\dot{v_{host}} = -\kappa \cdot \dot{\Delta d} \tag{2.26}$$

Plug equation 2.26 into equation 2.25:

$$\kappa \cdot \Delta d + [1 + VTH \cdot \kappa + (\tau_2 + \tau_3) \cdot \kappa \cdot v_{host}] \cdot \dot{\Delta d} = 0 \tag{2.27}$$

Since VTH, τ_2, τ_3, v_{host} and κ are all greater than 0, then $[1 + VTH \cdot \kappa + (\tau_2 + \tau_3) \cdot \kappa \cdot v_{host}] > 1$ and let it to be $\kappa_{\Delta d}$, the equation 2.27 is rewritten as:

$$\dot{\Delta d} = -\frac{\kappa}{\kappa_{\Delta d}} \Delta d \tag{2.28}$$

According to equation 2.28, when $\Delta d > 0$, $\dot{\Delta d} < 0$, equivalent to the decrease of the inter-distance error; conversely, when $\Delta d < 0$, $\dot{\Delta d} > 0$, equivalent to the increase of the inter-distance error. But for both conditions, the error tends to be 0. From equation 2.23, the v_{rel} converges to 0 as well. Thus, it can be concluded that the proposed safety distance model satisfies the condition of system stability: "$v_{rel} \to 0 \Rightarrow \Delta d \to 0$".

2.2.5. Inter-Vehicle Longitudinal Dynamics Modeling and Discretization

For the car following driving scenario, since the controlled plant is the inter-vehicle longitudinal dynamics, the prerequisite of developing the controller is to model the controlled plant. In this research, the inter-vehicle longitudinal dynamics model is designed taking the inter-vehicle distance error, relative velocity, and acceleration of host vehicle as state variables, desired acceleration of host vehicle as a control input, acceleration of preceding vehicle as system disturbance. To calculate the desired acceleration, the state-space model between host and preceding vehicle is firstly established.

Take the derivative of equation $\Delta d = D_{actual} - D_{safe}$ and equation $v_{rel} = v_{pre} - v_{host}$:

$$\begin{gathered} \dot{\Delta d} = v_{rel} - \left[2\tau_1 v_{host} + 3\tau_2 v_{host}^2 - 2\tau_3 v_{rel} v_{host} + \tau_3 v_{host}^2 - d_{min}\right] a_{host} + \tau_3 v_{host}^2 a_{pre} \\ \dot{v_{rel}} = a_{pre} - a_{host} \end{gathered} \tag{2.29}$$

where a_{pre} denotes the acceleration of the preceding vehicle, and a_{host} is the acceleration of host vehicle.

When applying the optimal desired acceleration obtained by the upper-level controller to the lower-level PI controller, there exists the time delay corresponding to the finite bandwidth of the vehicle's dynamic response. To eliminate the time delay and process the obtained desired acceleration signal in time, the first-order lag model is used to model the inter-vehicle longitudinal dynamics.

$$a_{host,actual} = \frac{K_g}{T_g + 1} \cdot a_{host,desired} \tag{2.30}$$

where K_g is the system gain, T_g is the time constant, $a_{host,actual}$ is the actual acceleration of host vehicle, and $a_{host,desired}$ is the optimal desired acceleration of the host vehicle.

Accordingly, the differential equation about desired and actual acceleration can be modeled as:

$$\dot{a_{host,actual}} = \frac{K_g}{T_g} a_{host,desired} - \frac{1}{T_g} a_{host,actual} \tag{2.31}$$

Take the inter-vehicle distance error Δd, relative velocity v_{rel}, and actual host vehicle acceleration $a_{host,actual} \asymp a_{host}$, as system state variables:

$$\boldsymbol{x} = \begin{bmatrix} \Delta d \\ v_{rel} \\ a_{host} \end{bmatrix} \tag{2.32}$$

Take the calculated desired acceleration as the control input, acceleration of the preceding vehicle as system disturbance, the system state-space equation can be obtained as follow:

$$\dot{\boldsymbol{x}} = \boldsymbol{A}\boldsymbol{x} + \boldsymbol{B}u + \boldsymbol{G}w \tag{2.33}$$

where system matrices $\boldsymbol{A}, \boldsymbol{B}, \boldsymbol{G}$ are derived as:

$$(\text{let } \mathcal{H} = 2\tau_1 v_{host} + 3\tau_2 v_{host}^2 - 2\tau_3 v_{rel} v_{host} + \tau_3 v_{host}^2 - d_{min})$$

$$\boldsymbol{A} = \begin{bmatrix} 0 & 1 & -\mathcal{H} \\ 0 & 0 & -1 \\ 0 & 0 & -\frac{1}{T_g} \end{bmatrix}, \boldsymbol{B} = \begin{bmatrix} 0 \\ 0 \\ \frac{K_g}{T_g} \end{bmatrix}, \boldsymbol{G} = \begin{bmatrix} \tau_3 v_{host}^2 \\ 1 \\ 0 \end{bmatrix},$$

$$u = a_{host,desired} \asymp a_{desired}, w = a_{pre}.$$

i.e.

$$\begin{bmatrix} \dot{\Delta d} \\ \dot{v_{rel}} \\ \dot{a_{host}} \end{bmatrix} = \begin{bmatrix} 0 & 1 & -\mathcal{H} \\ 0 & 0 & -1 \\ 0 & 0 & -\frac{1}{T_g} \end{bmatrix} \begin{bmatrix} \Delta d \\ v_{rel} \\ a_{host} \end{bmatrix} + \begin{bmatrix} 0 \\ 0 \\ \frac{K_g}{T_g} \end{bmatrix} a_{desired} + \begin{bmatrix} \tau_3 v_{host}^2 \\ 1 \\ 0 \end{bmatrix} a_{pre} \tag{2.34}$$

In the real control system, the inter-vehicle longitudinal dynamics model is usually applied in the discrete domain, so the system state-space equation is discretized. However, due to the quadratic terms in the safety distance model proposed in this research, the continuous inter-vehicle longitudinal dynamics model is nonlinear. According to the modern control theory, the integration of a matrix polynomial needs to be found for the discretization of a continuous state-space equation. For the nonlinear model, however, taking the integration of a matrix polynomial is complex. According to the real experimental test in research [137], the coefficient of quadratic terms in the safety distance model is small enough to be negligible within a unit control step. Consequently, under the premise of not affecting the accuracy of the system, the quadratic terms in the safety distance model can be temporarily ignored to simplify the overly calculation. The discretized inter-vehicle longitudinal dynamics model can be expressed as follow:

$$\begin{aligned} \boldsymbol{x}(k+1) &= \overline{\boldsymbol{A}}\boldsymbol{x}(k) + \overline{\boldsymbol{B}}u(k) + \overline{\boldsymbol{G}}w(k) \\ \boldsymbol{y}(k) &= \boldsymbol{C}\boldsymbol{x}(k) \end{aligned} \tag{2.35}$$

where k refers to the kth sampling time step, $\overline{\boldsymbol{A}}$, $\overline{\boldsymbol{B}}$, and $\overline{\boldsymbol{G}}$ are discretized system coefficient matrices, $\boldsymbol{y}$ represents the system output, $\boldsymbol{C}$ is an identity matrix.

Assume T_s as the sampling period, $\overline{\boldsymbol{A}}$, $\overline{\boldsymbol{B}}$, and $\overline{\boldsymbol{G}}$ can be obtained as follow:

$$\overline{\boldsymbol{A}} = \sum_{k=0}^{\infty} \frac{\boldsymbol{A}^k T_s^k}{k!}, \overline{\boldsymbol{B}} = \sum_{k=0}^{\infty} \frac{\boldsymbol{A}^{k-1} T_s^k}{k!} \boldsymbol{B}, \overline{\boldsymbol{G}} = \sum_{k=0}^{\infty} \frac{\boldsymbol{A}^{k-1} T_s^k}{k!} \boldsymbol{G} \tag{2.36}$$

2.2.6. Reference Velocity Planning Modeling Based on SPaT Information

When DSSL switches into signal anticipation scenario, a reference velocity v_{ref} is required to be calculated based on the real-time driving state and upcoming traffic signal phase and timing information. The basic idea of calculating the v_{ref} is to accelerate when the time of green signal light is enough and decelerate until the start of next green signal light so that the host vehicle can pass through the signalized intersection without any stop. According to research work [86], a non-empty intersection checking algorithm based on a set of logical rules is proposed.

Once entering signal anticipation scenario, a vehicle plans cross the first green interval of the upcoming traffic signal at the current time step with the velocity range:

$$\left[\frac{d_{TSL}}{r_1}, \frac{d_{TSL}}{g_1}\right] \tag{2.37}$$

where r_1 and g_1 denote the start time of the first red and green interval of the upcoming traffic signal light, respectively.

Then, the feasibility of crossing the signalized intersection using current velocity depends on if the above velocity range has the intersection with the allowable speed limits on a certain road section $[v_{min}, v_{max}]$. If the set intersection is empty, the following green interval will be checked until a non-empty set intersection can be found. The mathematical expression of the "non-empty set intersection checking algorithm" is represented by:

$$\left[\frac{d_{TSL}}{r_i}, \frac{d_{TSL}}{g_1}\right] \cap [v_{min}, v_{max}] \tag{2.38}$$

Finally, the reference velocity v_{ref} at each time step can be obtained by the following rule:

$$v_{ref} = max\left[\left[\left[\frac{d_{TSL}}{r_i}, \frac{d_{TSL}}{g_1}\right] \cap [v_{min}, v_{max}]\right]\right] \tag{2.39}$$

2.3. Summary of Chapter 2

This chapter starts with the three typical driving scenarios classified by a DSSL, including free driving scenario considering road gradient information, signal anticipation scenario considering upcoming traffic SPaT information, and car following driving scenario considering the constraints from preceding vehicle. And then propose the overall system design architecture. The predictive cruise control system dynamics models including vehicle longitudinal dynamics model, safety distance model, inter-vehicle longitudinal dynamics model and reference velocity planning model are developed and analyzed, respectively.

Chapter 3. Instantaneous Energy Consumption Model (IECM)

As the foundation of the design of the predictive cruise controller for eco-driving, it is crucial to develop a vehicular energy consumption model which is not only capable of accurately estimating the energy consumption during driving, but also characterized by a simple model structure and suitable for transient state energy consumption estimation. Moreover, there are currently few researches on the estimation of electric vehicles (EVs) energy consumption, which limits the further exploration of EVs' driving range potential. Considering that electric vehicles share the same longitudinal dynamics characteristics as internal combustion engine vehicles (ICEVs), and the conversion efficiency from battery electrical energy to motor output power is higher and more direct. Given the strong mapping relations between the energy consumption of battery and motor output power, vehicle driving condition, etc., a new instantaneous energy consumption for electric vehicle is proposed based on the idea of machine learning and data mining, which lays the foundation for the following development of predictive cruise control system for eco-driving.

3.1. Analysis of IECM

The current existing energy consumption model can be classified into two categories. The first type is steady-state models taking engine torque, engine rotational speed and power as inputs to fit the fuel consumption rate. These type of models is characterized by high estimation accuracy when the vehicle operates under steady state and by large estimation error when the vehicle operates under unsteady state. The second type is transient state models based on the "steady-state preliminary estimation + transient correction" method or "direct dynamics variable". The transient state models give dual attention to both steady-state and transient-state driving conditions so that the fuel consumption estimation can be ensured.

Table 3.1 shows several typical transient state models with their corresponding dynamic variables, where $\dot{m_{air}}$ (g/s) refers to the transient air mass flow rate, ΔT (Nm/s) and $\Delta\omega$ (rad/s^2) are the transient engine torque and speed, respectively, v (km/h) and a (m/s^2) are the vehicle instantaneous velocity and acceleration, $\bar{a}(t)$ (m/s^2) is the composite acceleration at time t, P_{MOE_e} is the instantaneous fuel consumption rate (mg/s), $L_{i,j}$ and $M_{i,j}$ are the model regression coefficients, α is the acceleration impact factor.

TABLE 3.1 Typical Transient Fuel Consumption Models

Modeling Methodology	Mathematical expression of models	Dynamic variables
Steady-state estimation + transient correction	Engine fuel map + fuel-to-air ratio limitation correction [138]	$\dot{m_{air}}$
	Engine fuel map + engine speed and torque variation correction [139]	$\Delta T, \Delta\omega$
	Engine fuel map + torque variation correction [140]	ΔT
Direct dynamics	$ln\, P_{MOE_e} = \sum_{i=0}^{3}\sum_{j=0}^{3}\left(L_{i,j}v^i a^j\right), a \geq 0$ $ln\, P_{MOE_e} = \sum_{i=0}^{3}\sum_{j=0}^{3}\left(M_{i,j}v^i a^j\right), a > 0$	a

variable [141]

$$ln\, P_{MOE_e} = \sum_{i=0}^{3}\sum_{j=0}^{3}\left(L_{i,j} v^i \bar{a}^j\right), \bar{a} \geq 0$$

$$ln\, P_{MOE_e} = \sum_{i=0}^{3}\sum_{j=0}^{3}\left(M_{i,j} v^i \bar{a}^j\right), \bar{a} \geq 0$$

$$\bar{a}(t) = \alpha a(t) + (1-\alpha)\sum_{i=1}^{9}\frac{a(t-i)}{9} \qquad \bar{a}$$

[142]

Min. Z and Hui. J [143] pointed out that vehicular transient-state fuel consumption is higher than steady-state fuel consumption by about 6%~30%. Therefore, the transient correction considering the features of vehicle velocity and acceleration is indispensable for precisely estimating the actual fuel consumption. However, if only transient vehicle velocity and acceleration are used to estimate the fuel consumption, the models using the direct-dynamics-variable-based method do not contain the engine torque and speed which can reflect the influence from the variation of road gradient on fuel consumption [144]. The transient fuel consumption models based on the "steady-state estimation + transient correction" method include the engine map, which enables it to reflect the influence on the fuel consumption from road terrain variation. But compared with the direct-dynamic-variable-based method, modeling using the steady-state estimation + transient correction" method tends to be complicated. More importantly, the variables used for correction, such as $\dot{m_{air}}$, is not accessible during real driving process.

Accordingly, based on the analysis above, to fill the research gaps and adapt to the objective of developing a predictive cruise control system for electric vehicle eco-driving, the following key points in terms of the energy consumption estimation model is summarized:

i. Instead of using $\dot{m_{air}}$, ΔT, or $\Delta\omega$, instantaneous driving velocity $v(t)$ and acceleration $a(t)$ is required as input features due to their readily accessibility.
ii. As shown in Figure 3.1, the rotational speed and output torque of the electric vehicle motor is concerned with motor efficiency, which directly relates to the energy consumption. And in analogy with the engine torque and engine speed, motor output torque and speed can reflect the impact of the road slope variation on energy consumption.
iii. Catering to the nonlinearity and time-varying property of vehicular longitudinal energy consumption and for simplifying the modeling process, machine learning based on the artificial neural network (ANN) is applied to conduct the nonlinear fitting for the development of the instantaneous energy consumption model (IECM).

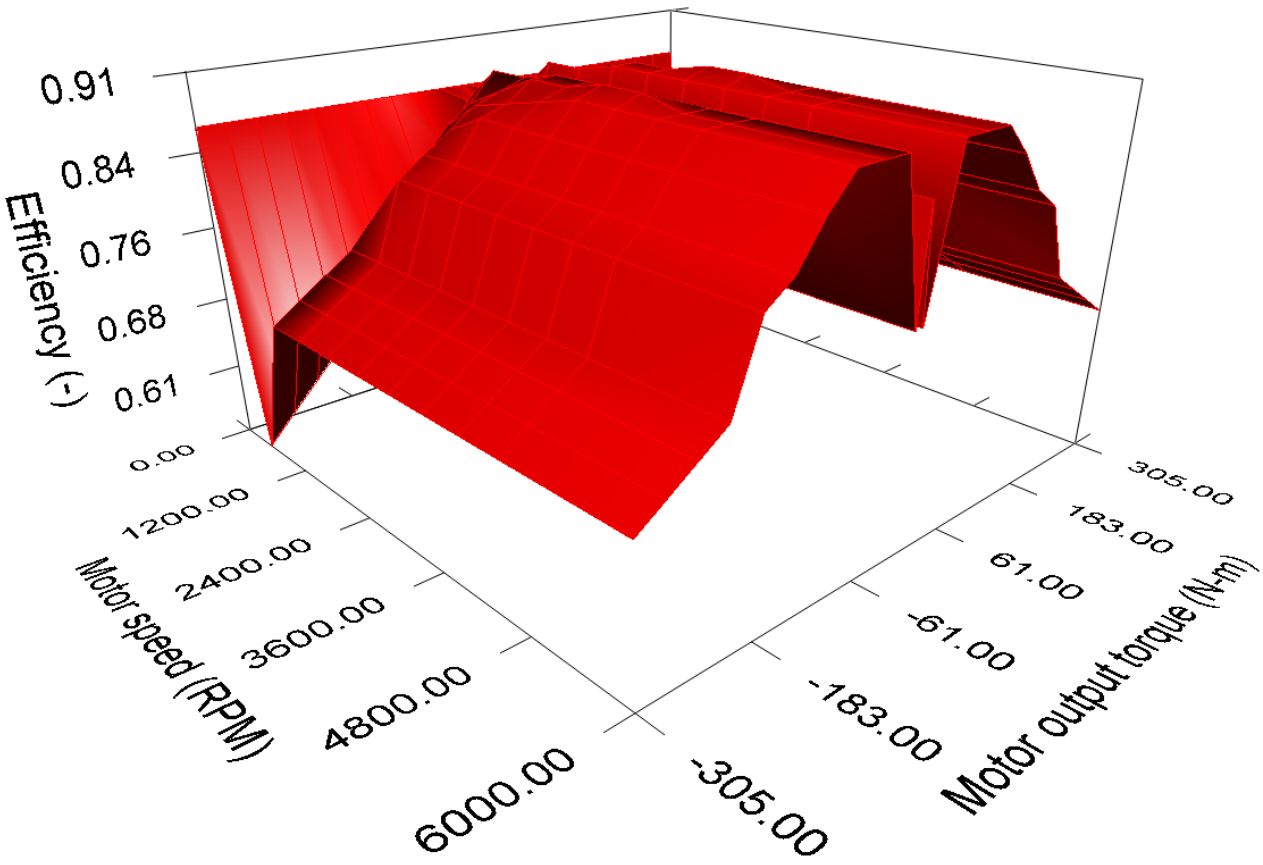

Fig. 3.1 EV Electric Motor Efficiency as a Function of Rotational Speed and Output Torque

As shown in Figure 3.2, using the artificial neural network as the fitting tool, the IECM takes motor torque $T_m(N \cdot m)$, motor speed $\omega_m(rpm)$, transient vehicle velocity $v(m/s)$, and transient vehicle acceleration $a(m/s^2)$ as input features to calculate the mapping $0.1s$ output instantaneous energy consumption $E_{ins}(W \cdot 0.1s)$.

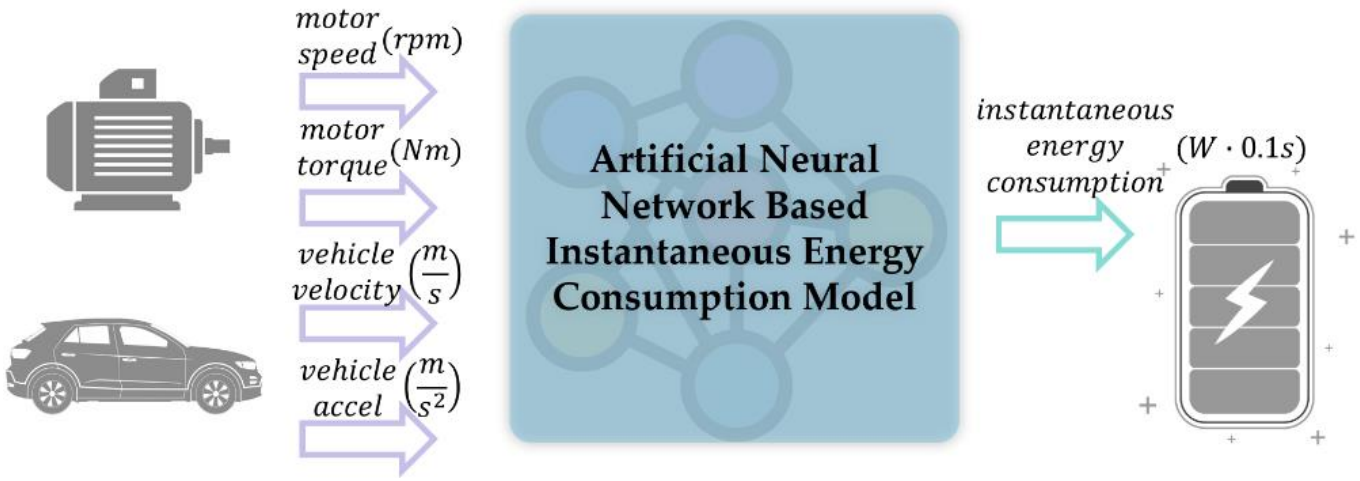

Fig. 3.2 Diagram of Inputs and Output for ANN-Based IECM

3.2. Modeling Data Collection and Process

The energy consumption data that were used to develop the ANN-based IECM were derived from the Downloadable Dynamometer Databased and were generated at the Advanced Mobility Technology Laboratory

(AMTL) at Argonne National Laboratory under the funding and guidance of U.S. Department of Energy (DOE) [145]. Argonne's Downloadable Dynamometer Database (D^3) offers publicly available testing data regarding advanced vehicle technologies. The electric vehicle database under AMTL includes 10 different types of EVs. The experimental driving cycles comprise Steady-state Drive Cycle, US06 Drive Cycle, UDDS Drive Cycle and Highway Drive Cycle. The sampling time of experimental data collection is $0.1s$, with total sampling period varying from $900s \sim 1500s$ according to different drive cycles. The database obtained by dynamometer test bench includes dynamometer speed (mph), dynamometer tractive effort (N), battery current (A), battery voltage (V), battery SOC (%), motor speed (rpm), integrated power reported by power analyzer (kW), etc.

The driving pattern is determined by different drive cycle. Steady-state Drive Cycle refers to the driving pattern of the vehicle at various steady velocities, under which the electric motor works steadily. US06 Drive Cycle is the driving pattern with high velocity and acceleration. UDDS Drive Cycle refers to the driving condition on the city road with frequent braking action under low speed and acceleration. Highway Drive Cycle situates between US06 and UDDS. Since the objective of this research is to develop an instantaneous energy consumption used for general driving task, the driving pattern is required to be within a wide velocity range and suitable for both steady-state and transient-state driving. Accordingly, a B-class electric vehicle with an asynchronous motor ($132kW/340Nm$) is selected from D^3, its Steady-state Drive Cycle dataset and US06 Drive Cycle dataset are used to train the neural network, and its Highway Drive Cycle dataset is used to verify the proposed ANN-Based IECM.

The accuracy of the IECM is determined by the validity of the data used for modeling. The raw data collected through CAN bus from chassis dynamometer experiments are mixed with noise, which is undesirable for the identification of model parameters. Besides, there exists some abnormal values during the measurement by sensor due to the experimental facilities. To keep the accuracy of the model from the impact of the noise and abnormal values, the raw data are filtered to improve the quality before being applied to train the neural network. In this research, the raw data are processed using moving average filtering. A moving average filter smooths data by replacing each data point with the average of the neighboring data points defined within the span, which is equivalent to lowpass filtering with the response of the smoothing given by the difference equation:

$$y_{smooth}(i) = \frac{1}{2N+1}[y_{raw}(i+N) + y_{raw}(i+N-1) + \cdots + y_{raw}(i-N)] \tag{3.1}$$

where $y_{smooth}(i)$ is the smoothed value for the ith data point, N is the number of neighboring data points on either side of $y_{smooth}(i)$, and $2N+1$ is the span.

For example, suppose smooth data using a moving average filter with a span of 5. Using the rules above, the first four elements of y_{smooth} are given by:

$y_{smooth}(1) = y_{raw}(1)$,

$y_{smooth}(2) = \frac{[y_{raw}(1)+y_{raw}(2)+y_{raw}(3)]}{3}$,

$y_{smooth}(3) = \frac{[y_{raw}(1)+y_{raw}(2)+y_{raw}(3)+y_{raw}(4)+y_{raw}(5)]}{5}$,

$y_{smooth}(4) = \frac{[y_{raw}(2)+y_{raw}(3)+y_{raw}(4)+y_{raw}(5)+y_{raw}(6)]}{5}$.

Note that $y_{smooth}(i)$ refers to the order of the data after sorting, and not necessarily the original order.

The required modeling data, such as vehicle velocity, acceleration, motor speed and instantaneous energy consumption, can be directly accessed from D^3, but the indirect information like motor torque is required to be calculated based on vehicle dynamics theory in equation 2.15. The data processing including original data sheet importing and reading, unit conversion, dynamics derivation, smoothing, logging and visualization, are

completed automatically through the $CarSim/Simulink$ co-simulation platform, shown as Figure 3.3.

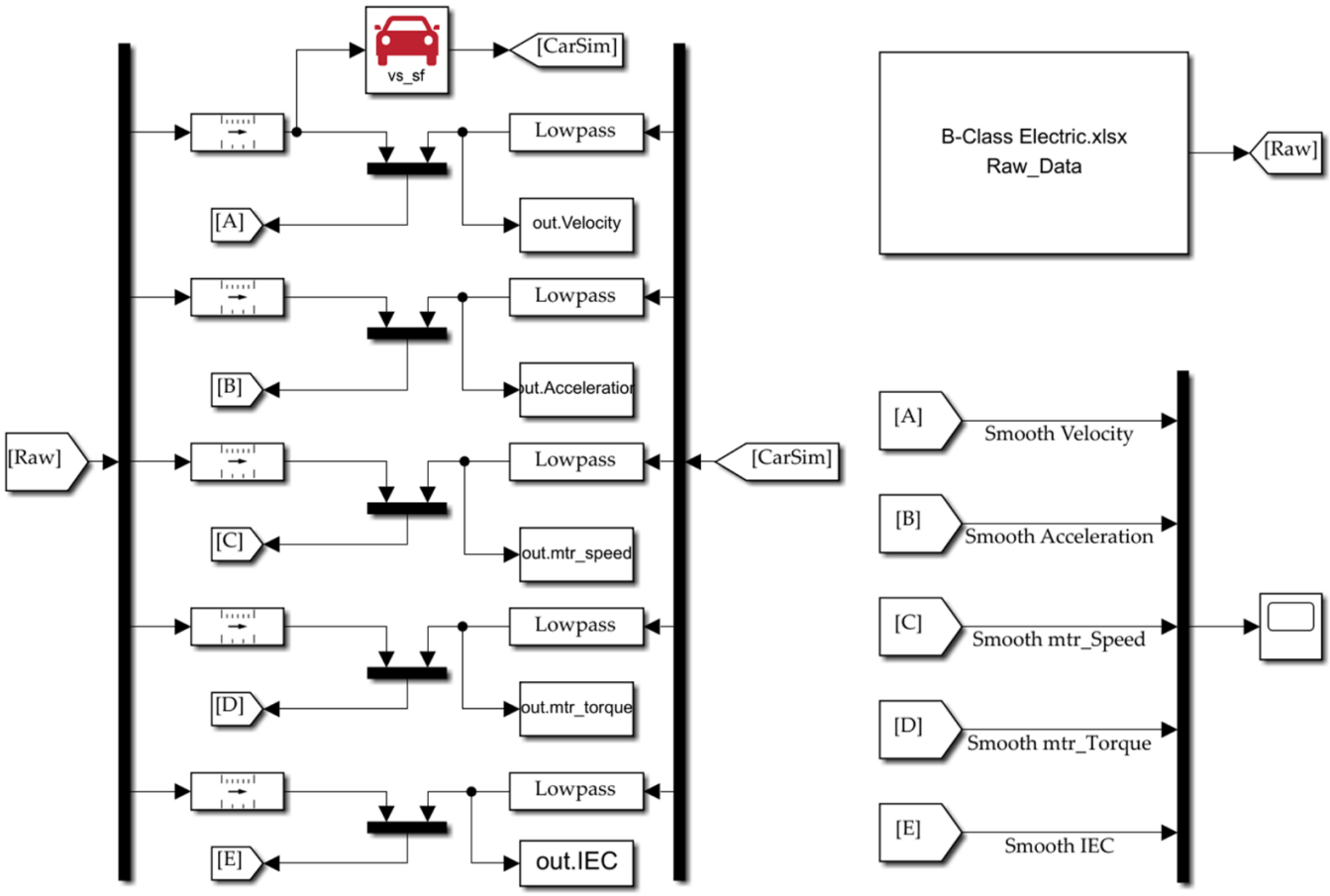

Fig. 3.3 Modeling Data Processing Using CarSim/Simulink

The original raw data with noise and filtered datasets used for actually training the neural network, including the input features vehicle velocity $v(t)$ (m/s), acceleration $a(t)$ (m/s^2), motor speed $\omega_m(t)$ (rpm), motor torque $T_m(t)$ $(N \cdot m)$ and output feature instantaneous energy consumption E_{ins} $(W \cdot 0.1s)$ are shown in Figure 3.4.

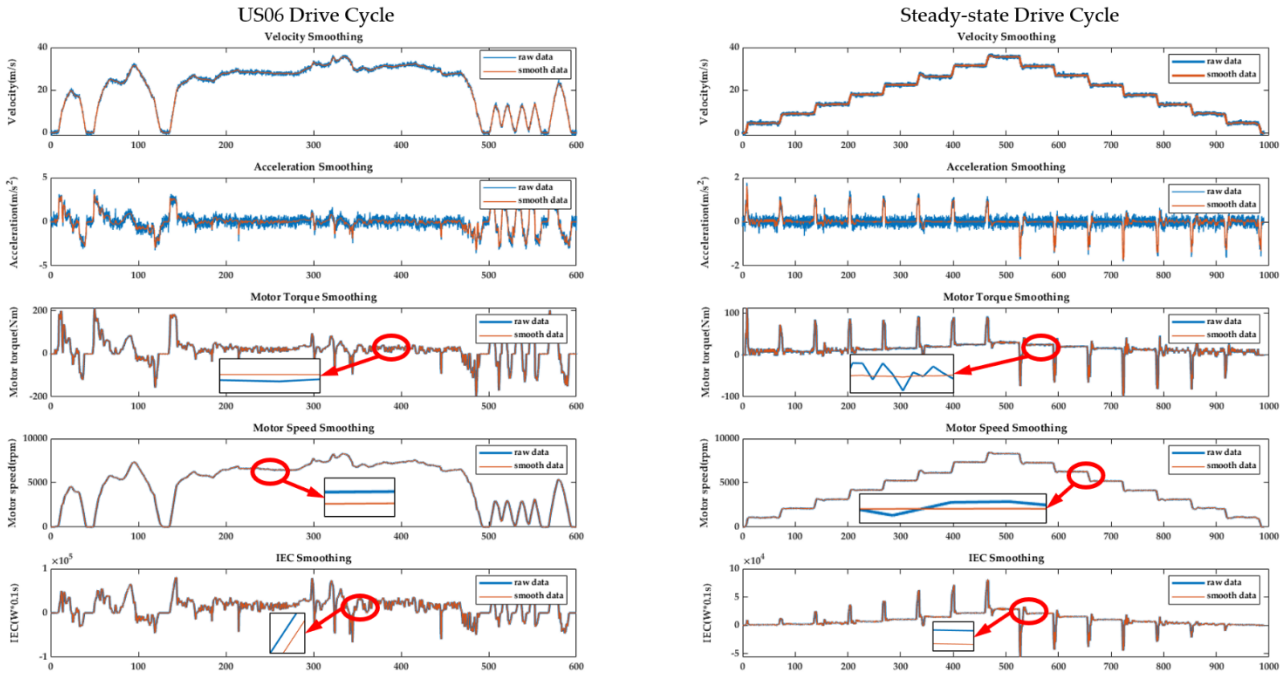

Fig. 3.4 Smoothing Data for neural network training

3.3. Artificial-Neural-Network-Based IECM

By analyzing the physical mechanism of EV's energy consumption, it is manifest that there exists strong mapping between energy consumption and vehicle motion characteristics (velocity and acceleration) and electric motor operation characteristics (torque and speed). Such a nonlinearity can be precisely approximated by the advantages of neural network fitting. In 1990, Hornik. K et al proposed the universal approximation of an unknown mapping and its derivatives using multilayer feedforward networks [146], in which it pointed out that, for any continuous system, a neural network with two layers and a sigmoid activation function can be a universal approximator. Therefore, in this research, instead of using common statistical polynomial regression, a computational-based artificial neural network is used to develop the IECM.

3.3.1. Establishment of Neural Network Structure

The fitting accuracy of a backpropagation neural network is highly related to the network structure, determined by the number of hidden layers and the number of neurons in each layer. Goodfellow. I et al. [147] generalized how to determine the number of hidden layers, shown in Table 3.2.

TABLE 3.2 Determination the number of Hidden Layers

Num. of Hidden Layers	Result
0	Only capable of representing linear separable functions or decisions
1	Can approximate any function that contains a continuous mapping from one finite space to another
2	Can represent an arbitrary decision boundary to arbitrary

	accuracy with rational activation functions and can approximate any smooth mapping to any accuracy
> 2	Additional layers can learn complex representations

Theoretically, the deeper the layers are, the better the function fitting ability will be. In fact, however, deeper layers may bring about the problem of overfitting, and at the same time increase the network training difficulty, making it difficult for the model to converge.

The second step to construct the neural network is to determine the number of neurons for each layer. Too few neurons in the hidden layer will result in underfitting. Conversely, using too many neurons may also cause problems, such as overfitting. More neuron nodes mean greater information processing capability. Since the limited information contained in the training dataset is not enough to train all the neurons in the hidden layer, it will lead to overfitting. Even if the training data contains enough features, too many neurons will increase the training time, difficult to achieve the desired modeling effect. Therefore, in this research, the structure construction starts with 1 hidden layer and 1 neurons for each layer (5 neurons for the first hidden layer), increasing or decreasing the number of hidden layers and neurons according to the approximation of underfitting or overfitting.

Part of the network structure with its corresponding mean squared error are shown in Table 3.3. According to the results, the structure of ANN-Based IECM in this research is determined as "$4 \backsim 10 \backsim 1 \backsim 1$", seen in Figure 3.5.

TABLE 3.3 Approximation of Different Network Structure

Network Structure	MSE	Network Structure	MSE
⋮	⋮	$4 \backsim 10 \backsim 1 \backsim 1$	$1.062e$-5
$4 \backsim 5 \backsim 1$	$2.168e$-5	$4 \backsim 10 \backsim 5 \backsim 1$	$1.335e$-5
$4 \backsim 10 \backsim 1$	$1.453e$-5	$4 \backsim 15 \backsim 1 \backsim 1$	$1.426e$-5
$4 \backsim 15 \backsim 1$	$1.218e$-5	⋮	⋮

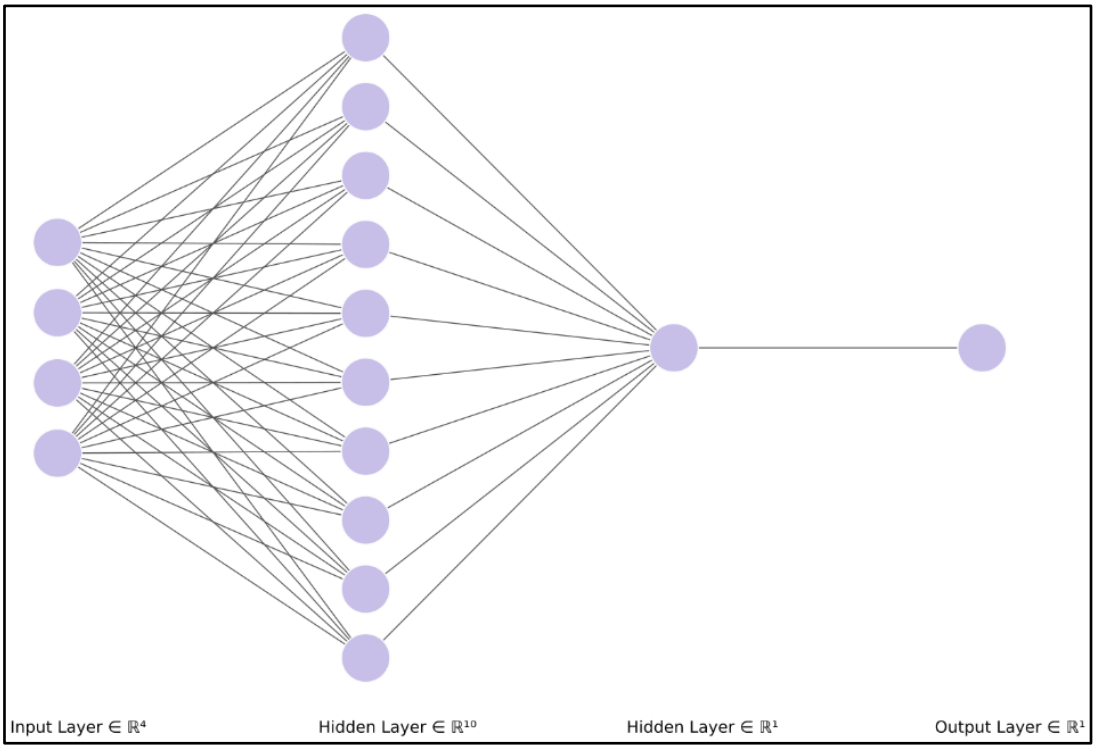

Fig. 3.5 Detailed Structure of Proposed Neural Network

The overall training proceeds as follows: first, the training dataset is fed into the neural network allocated with different weights and biases; second, the estimation of the instantaneous energy consumption is carried out; third, given a performance function correlated with real instantaneous energy consumption and estimation value from ANN model, the Levenberg-Marquardt Backpropagation algorithm is implemented so that the weight and bias variables are updated along with the calculation of a Jacobian matrix of the performance function. Iteratively, then the ANN estimates the instantaneous energy consumption based on updated weights and biases at the next time step until the sum of squares reduces to some target error or the norm of the gradient becomes less than some predefined value, during which the ANN-Based IECM is well-trained. The system architecture with the proposed methodology is shown in Figure 3.6.

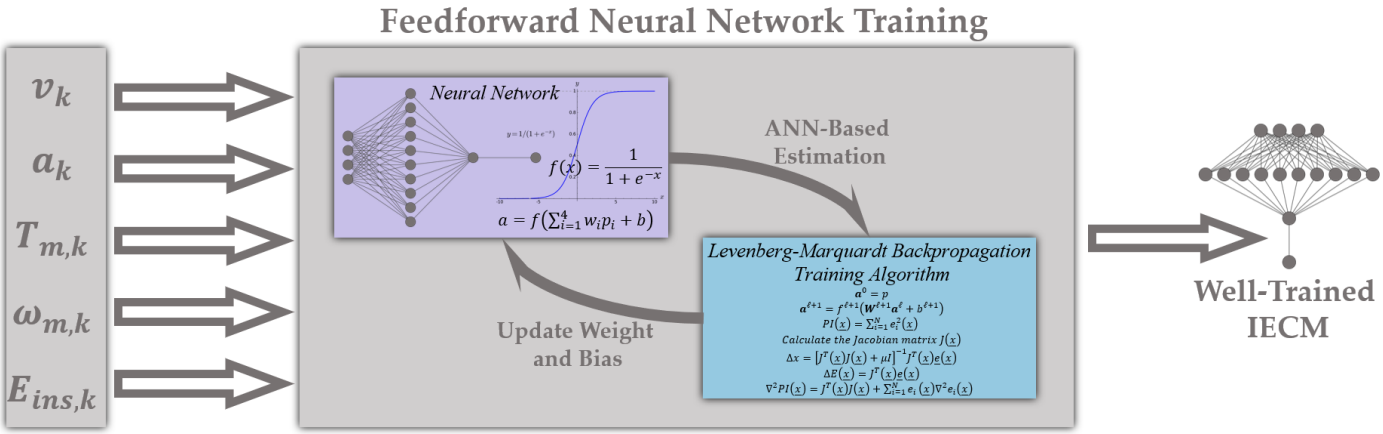

Fig. 3.6 Architecture of Proposed Feedforward Neural Network Training Algorithm

As the basic element of the network, the neuron is the functional unit that conducts the mathematical calculation. A neuron accepts more than one input, which constitutes the input vector $\boldsymbol{p} = \left[v_k, a_k, T_{m,k}, \omega_{m,k}\right]^T$. Multiplied

by a weight matrix $\boldsymbol{W}$ and summed with a bias b, the net input n to the neuron is expressed as:

$$n = \sum_{i=1}^{k} w_i p_i + b = \boldsymbol{W} \cdot \boldsymbol{p} + b \tag{3.2}$$

Next, through the activation function f, the neuron output a is obtained by:

$$a = f(n) \tag{3.3}$$

In this research, the logistic sigmoid activation function is applied, which is expressed as:

$$f(x) = \frac{1}{1 + e^{-x}} \tag{3.4}$$

The neuron with vector input, as the fundamental building block, is illustrated in Figure 3.7.

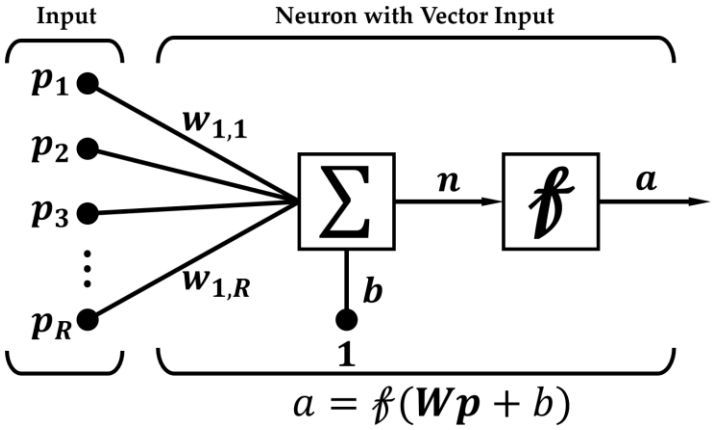

Fig. 3.7 Diagram of Neuron with Vector Input

3.3.2. Feedback Training Algorithm

As an approximation to Newton's method, the Levenberg-Marquardt Backpropagation [148] training algorithm is demonstrated in Figure 3.8. Total layer $\mathcal{L}$ is 3, $\boldsymbol{a}_q^{\mathcal{L}}$, namely E_q, is the estimated energy consumption output of the network given the qth input $\boldsymbol{p}_q = \left[v_k, a_k, T_{m,k}, \omega_{m,k}\right]^T$, $\boldsymbol{r}_q$ is the actual energy consumption, e_q denotes the error for the qth input, $\Delta\omega^{\ell}$ and Δb^{ℓ} are the steepest descent algorithm parameters, κ refers to the learning rate, δ^{ℓ} refers to the sensitivity of the performance index $\mathcal{P}$ to changes in the ith element of the net input in layer ℓ, $\mathcal{P}(x)$ denotes a function intended to be minimized with respect to the parameter vector x, $\mathcal{J}(x)$ is the Jacobian matrix.

After training the neural network using the above Levenberg-Marquardt algorithm, the relationships between the outputs of the neural network and the targets are shown in Figure 3.9. The regression values for training, testing, validation, and all dataset reach to 0.99, which indicates that the network outputs and the targets are precisely matched, and the neural network model is well-trained.

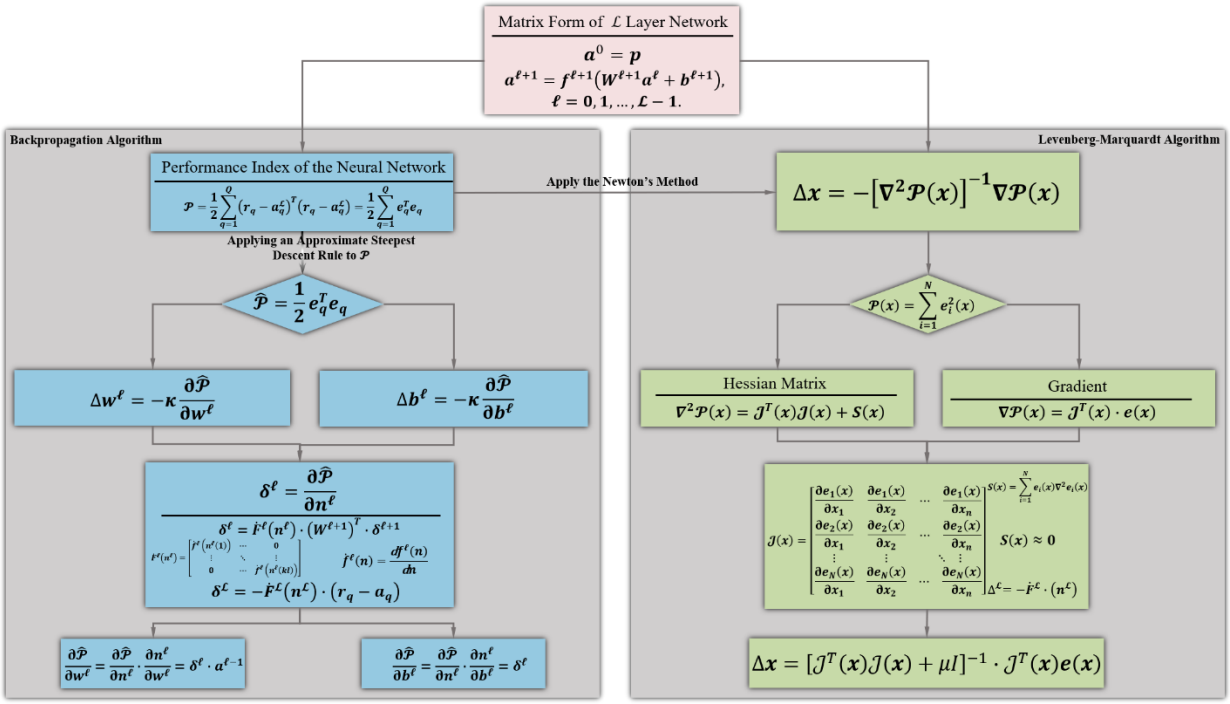

Fig. 3.8 Flow Diagram of Levenberg-Marquardt Feedforward Neural Network Training Algorithm

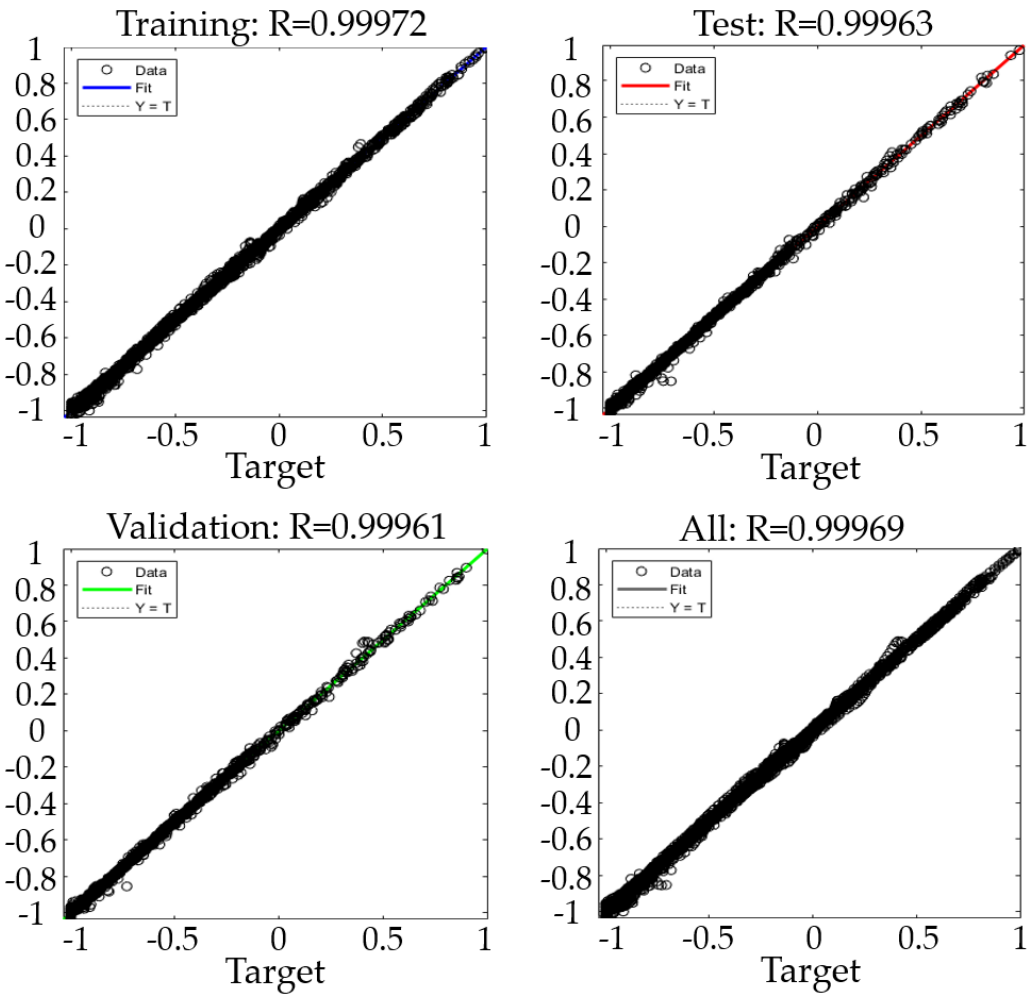

Fig. 3.9 Regression Plots of Training, Testing, Validation and ALL Dataset

3.3.3. ANN-Based IECM Application Deployment

Once the proposed network is well-trained, it is required to explicitly define it as a deployable IECM. Note that the IECM is proposed mainly for the development of the predictive cruise control system for eco-driving to evaluate the instantaneous energy economy for specific driving conditions. Therefore, to ensure the interactivity between each part of the PCC system, the well-trained ANN-Based IECM is deployed in the MATLAB environment as a callable function, shown in Figure 3.10.

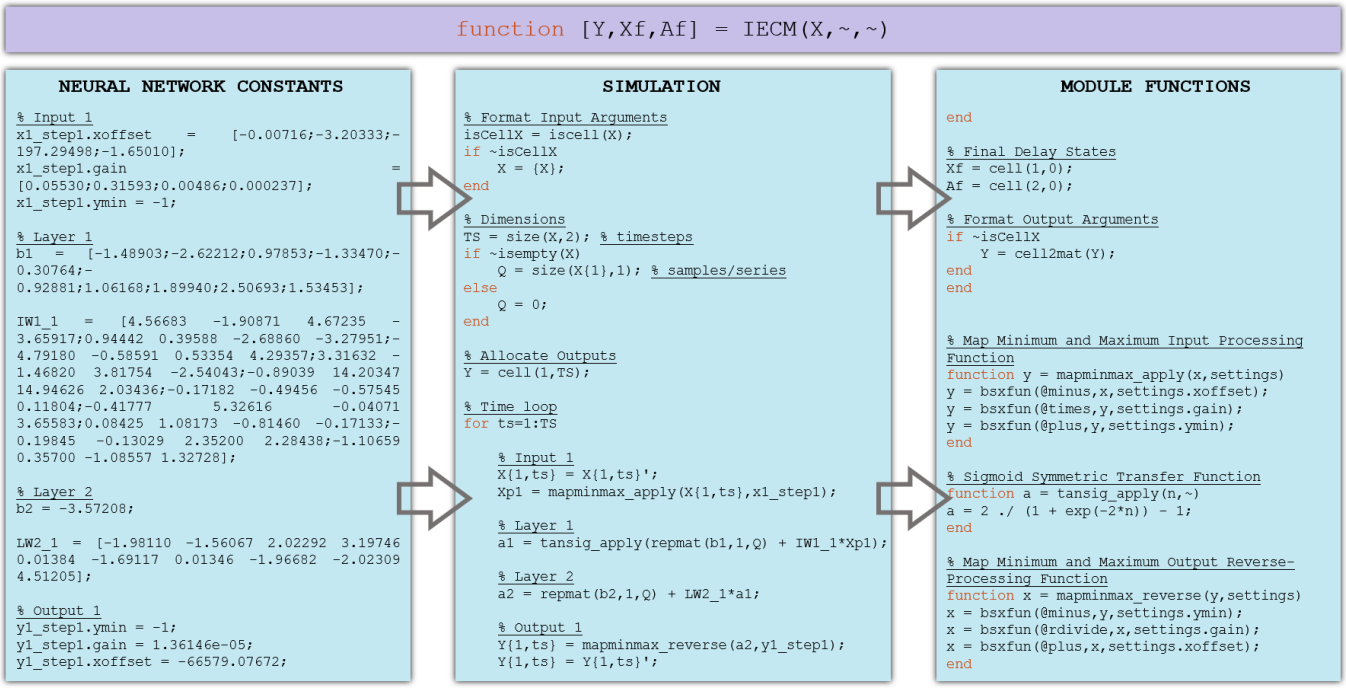

Fig. 3.10 Deployable Function of ANN-Based IECM

where $Y = E_{ins}(t), X = [v(t), a(t), T_m(t), \omega_m(t)]^T$, *i.e.*

$$E_{ins(t)} = IECM\big(v(t), a(t), T_m(t), \omega_m(t)\big) \tag{3.5}$$

3.4. Validation of ANN-Based IECM

Before applying the proposed instantaneous energy consumption estimation model into the development of the PCC system, a standard Highway Drive Cycle, seen in Figure 3.11, is adopted to validate the IECM. For an assessment to be effective, the Mean Absolute Percentage Error ($MAPE$) and the Mean Square Error (MSE) are used as model evaluation indexes.

$$MAPE = \frac{1}{n}\sum_{i=0}^{n}\left|\frac{E_{actual}(i) - E_{estimate}(i)}{E_{actual}(i)}\right| \times 100\% \tag{3.6}$$

$$MSE = \frac{1}{n}\sum_{i=0}^{n}[E_{actual}(i) - E_{estimate}(i)]^2 \tag{3.7}$$

where n is the number of sample data, E_{actual} is the actual measurement of instantaneous energy consumption, $E_{estimate}$ is the model estimation value.

To better validate the accuracy of the proposed ANN-Based IECM, a multivariate fitting energy consumption model for electric vehicle (EV-MFECM) from reference [149] is compared to show the estimation improvement of ANN-Based IECM. EV-MFECM, based on the method of "steady-state estimation + transient correction", consists of two modules. It took vehicle velocity and acceleration as steady-state module inputs, motor speed and torque as transient correction inputs to estimate the instantaneous energy consumption for the electric

vehicle. The mathematical expression is shown as follow:

$$\begin{cases} \mathcal{W}_{bc} = \alpha_0 + \alpha_1 T_m \omega_m + \alpha_2 T_m^2 + \alpha_3 \omega_m \\ \mathcal{W}_{bs} = \beta_0 + \beta_1 va + \beta_2 v^2 a + \beta_3 v a^3 + \beta_4 v^2 a^2 \\ \mathcal{W}_{bfit} = \mathcal{W}_{bc} + \mathcal{W}_{bs} \end{cases} \tag{3.8}$$

where $\mathcal{W}_{bc}$, $\mathcal{W}_{bs}$, and $\mathcal{W}_{bfit}$ are steady-state module energy consumption estimation, transient correction module energy consumption estimation, and total estimation, respectively. $\alpha_0 \sim \alpha_3$ are regression coefficients for the steady-state module, $\beta_0 \sim \beta_4$ are regressions coefficients for the transient correction module.

Using the previous dataset for training the neural network, Steady-state Drive Cycle and US06 Drive Cycle, the coefficients can be calibrated so as to conduct the comparative validation with the ANN-Based IECM.

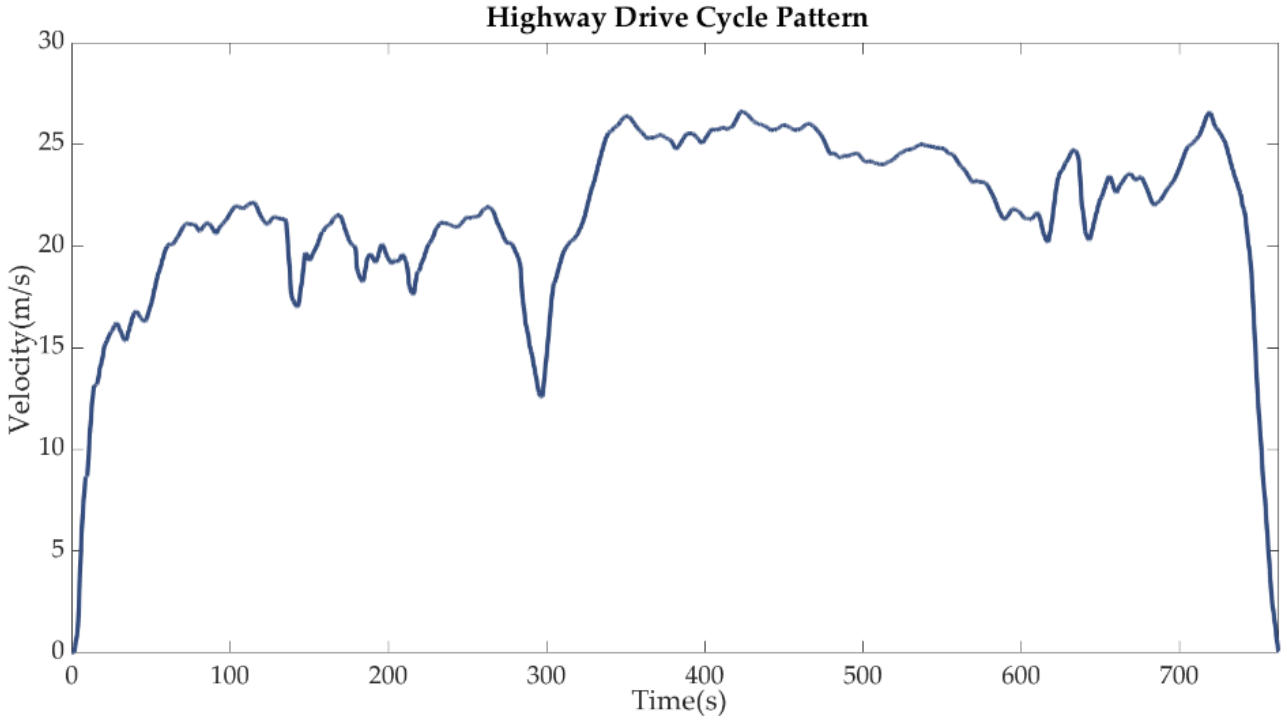

Fig. 3.11 Highway Drive Cycle Pattern

TABLE 3.4 The Comparative Validation Result of ANN-Based IECM

	$MAPE(\%)$	$MSE(W \cdot 0.1s)$
ANN-Based IECM	1.25	$1.4231e+6$
EV-MFECM	3.20	$1.6850e+6$

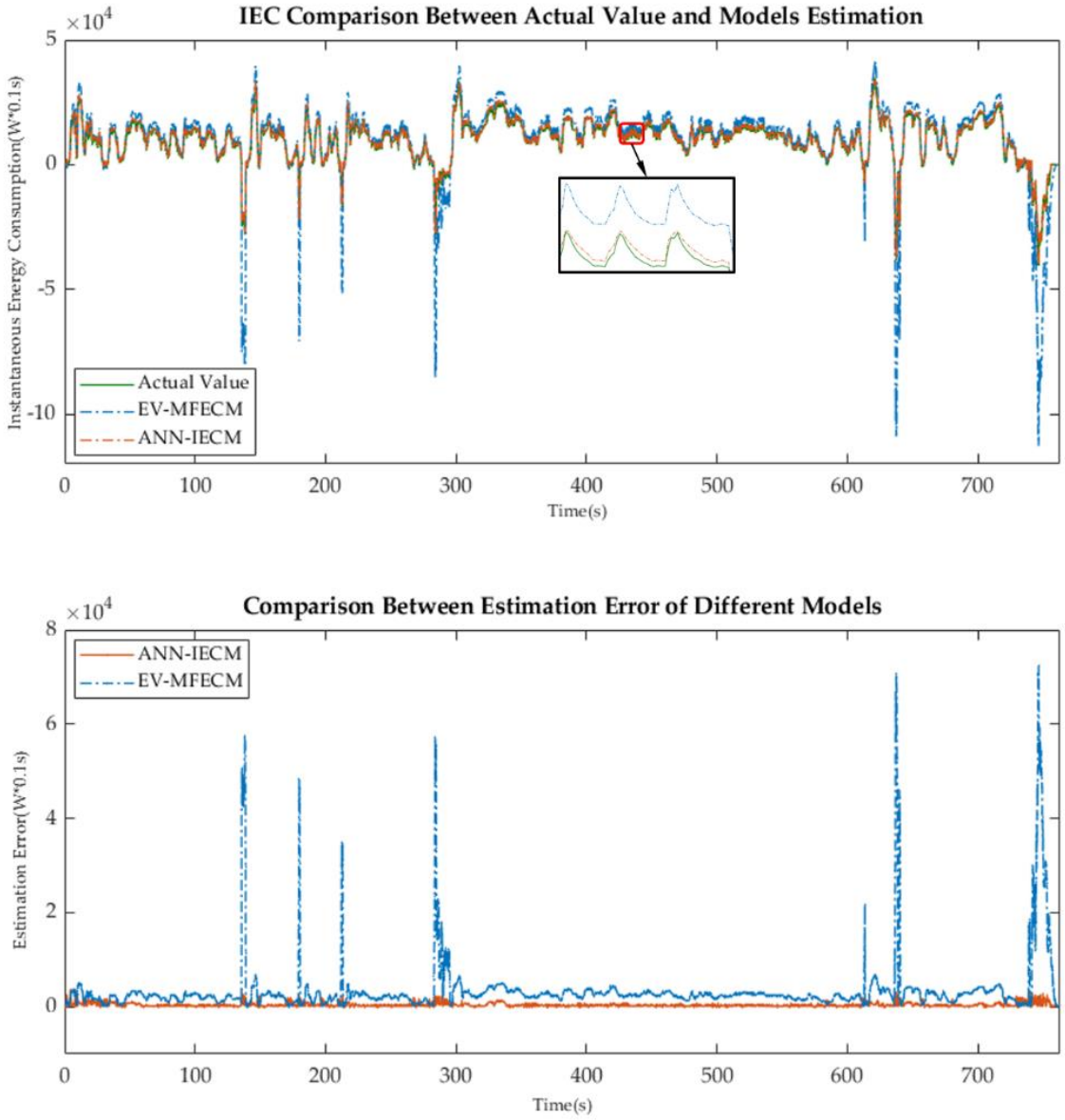

Fig. 3.12 Comparison of Estimation of Models with Actual Value and Estimation Error of Different Models

From Table 3.4, the comparative result shows that, under the Highway Drive Cycle, both the MSE and $MAPI$ values of proposed ANN-Based IECM are lower than the corresponding values of baseline EV-MFECM, which indicates that estimation performance of ANN-Based IECM is superior to the one based on statistical multivariate regression method. From Figure 3.12, it is easy to see that both ANN-Based IECM and EV-MFECM are capable of reflecting the trend of energy consumption under the Highway Drive Cycle. However, it is evident that the proposed ANN-Based IECM fits better and is more accurate than the baseline. The error of ANN-Based IECM is closer to zero without any spikes. Besides, the EV-MFECM contains the polynomial combination, which makes it too complicated to be deployed in real applications. On the contrary, ANN-Based IECM features an explicit model structure and is easy to be encoded into the hardware, which makes it more suitable for vehicle eco-driving optimization system.

3.5. Summary of Chapter 3

By analyzing the existing vehicle energy consumption models, an instantaneous energy consumption based on

machine learning – data mining is proposed catering to the driving characteristics of electric vehicle. After smoothing the real chassis dynamometer experimental Drive Cycle data and determining the network structure, the Levenberg-Marquardt training algorithm is applied to train the neural network and encapsulates it as a callable function. Model validation is then performed to illustrate its estimation performance.

Chapter 4. Predictive Cruise Control System for Eco-Driving Based on MPC

This chapter presents the core methodology used to develop the predictive cruise control system for eco-driving. To begin with, the basics of model predictive control (MPC) algorithm is introduced. Then, the optimization problems are formulated separately for each driving scenario: free driving scenario, car following scenario, and signal anticipation scenario. For each optimization problem, detailed controller structure, control objectives, cost function, and constraints are precisely designed. The mathematical derivations of prediction form transformation for system dynamics model, cost function and constraints are included. Finally, in response to the practical implementation of MPC, low robustness of model mismatch, the infeasibility of the optimal control law, and online computing complexity are discussed, and corresponding solutions are proposed, respectively.

4.1. Eco-Driving System Based on MPC

4.1.1. MPC Theory

The idea of predictive control can be traced back to the rolling optimization control strategy proposed by Propoi et al in 1963 [150]. After more than 50 years, many branches have been developed, such as model algorithm control (MAC), dynamic matrix control (DMC), generalized predictive control (GPC), predictive function control (PFC), etc. As the combination of control theory and optimization, model predictive control, also known as receding horizon control (RHC), is one of the branches and has been of high interest in academic and industrial research in recent years. As the extension of the linear quadratic regulator (LQR) and linear quadratic gaussian (LQG) control, MPC adopts modern control theory to analyze its internal mechanism, for example, taking state-space equation as its model. Proposed by Mayne. D. Q et al in 1988 [151], the essence of the MPC is using optimization to solve a control problem or obtaining the controller's command by solving an optimization problem. Therefore, the external of MPC is the control concept, and the internal layer contains the idea of optimization. MPC can handle multi-input multi-output (MIMO) system that have interactions between their inputs and outputs. Most importantly, MPC is capable of explicitly handling constraints of input and output, which enables it to satisfy the industrial development requirements of economic, safe, environmental-friendly. During each control interval, MPC utilizes the controlled plant model to predict the system states or output within a prediction horizon. By optimizing the performance index of the prediction horizon, it uses system real-time output to realize the feedback correction to the prediction model, making the overall control strategy to be a closed-loop online optimization. By solving this optimization problem, an optimal control sequence is obtained, and the first element of the control sequence is applied to the system. Repeatedly, the next optimization is solved with the prediction horizon moving forward. Three representative characteristics of MPC thereby can be summarized as: prediction model, rolling-horizon optimization, feedback correction:

i. Prediction model: as the basics of the MPC, the prediction model is capable of predicting the future output based on the past information and control input. Note that what really matters is the function to predict rather than the concrete form of the model. Convolution model, (such as step response model, pulse response model), state-space model (mechanism model), transfer function model, neural network model, etc. all can be used as a prediction model.

ii. Rolling-horizon optimization: MPC obtains the optimal control signal by optimizing a certain performance

assessment index. This optimization process is not carried out offline, but rolling online, which is the fundamental difference between MPC and conventional optimal control.

iii. Feedback correction: to diminish the control error caused by the model mismatch or environmental disturbance, the plant actual output is first checked at the next sampling time, and use the actual output to correct the prediction based on the model.

Based on these three features, the fundamental principle of MPC is shown in Figure 4.1. Shown as curve - 1, there always exists a reference trajectory. Taking time instant k as current time instant (the position of the vertical axis of the coordinate frame), the controller predicts the system output (seen as curve - 2) for a period of prediction horizon based on the system current state and control signal. By solving an optimization problem under the objective function and various constraints, a series of control sequences (shown as a rectangular wave - 4) can be obtained within the control horizon $[k, k+N_c]$. The first element of this control sequence is input into the controlled plant. When it comes to the next time step $k+1$, the above process is repeated to complete the optimization problem with constraints in a rolling horizon way so as to realize the continuous control of the controlled plant.

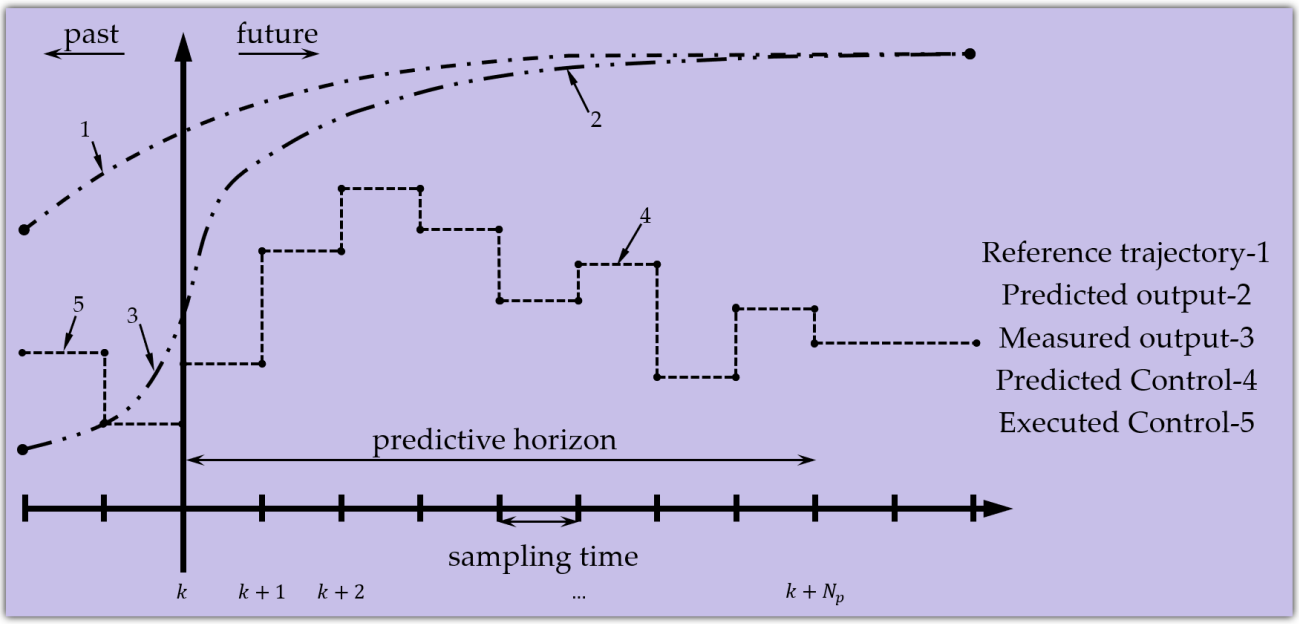

Fig. 4.1 Schematic Diagram of Model Predictive Control

The block diagram of MPC is shown in Figure 4.2, which consists of the controller, controlled plant and state estimator. The MPC controller calculates the optimal control sequence u^* based on the prediction model, objective function, and constraints. The plant is controlled based on current control signal and output the state signal $x(t)$ into the state estimator. The state estimator, e.g., Kalman filter, is used to estimate the state signal, which cannot be obtained by sensor observation or the observation cost is too high.

MPC is commonly categorized into linear MPC and nonlinear MPC, which is usually transformed into quadratic programming (QP) problem. As a classic mathematical optimization problem, the objective function of QP is a quadratic function with linear or nonlinear constraints, which is commonly solved using the active-set or interior-point method. However, due to the defects of the MPC algorithm itself, there are three aspects of practical problems, namely, low robustness for model mismatch, insolvability of the optimal control, the high computational complexity of online optimization.

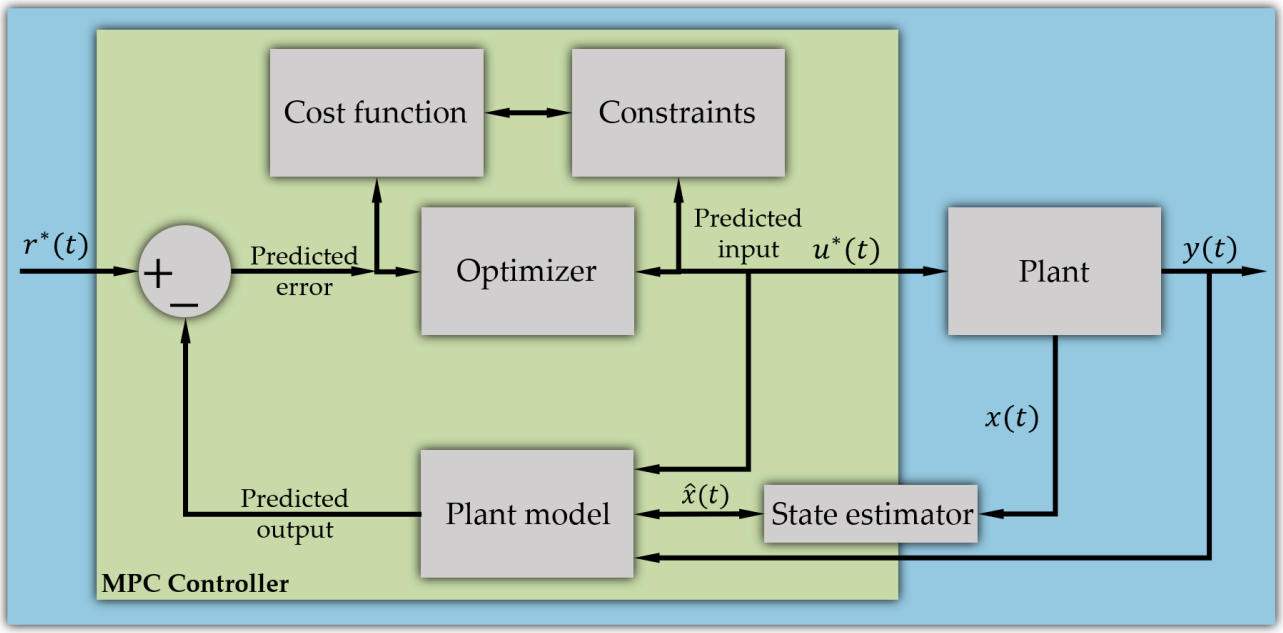

Fig. 4.2 Block Diagram of Model Predictive Control

The first kind of problem is mainly caused by the modeling error of the controlled plant. There are inevitable uncertainties such as parameter measurement error, unmodeled dynamic and external disturbance, etc. Therefore, there is always a mismatch between the established mathematical model and the controlled plant. When the model mismatch is serious, the conventional MPC is unable to compensate for the prediction error caused by the model mismatch, which tends to bring about the decline of optimal control performance, especially for the rapid-changing plants.

The second kind of problem is closely related to the feasible region of the predictive optimization problem. The reasons are as follows: (1) Restricted by the constraints of the controlled plants, the free space of the system state is limited; (2) When the external disturbance or model mismatch is too large, the mechanical inertia of the controlled plant causes the system state to run beyond the feasible region of the predictive optimization problem; (3) In order to ensure the stability of the closed-loop system, the stability constraint conditions are added, which inversely reduces the feasible region of the predictive optimization problem. Whatever the feasible region is reduced, or the state runs out of the feasible region, the direct result is the insolvability of the predictive optimization problem. When the predictive optimization problem is insolvable, the optimal control signal does not exist, and the control process is interrupted.

The third kind of problems is related to the scale of the predictive optimization problem, the efficiency of the numerical optimization algorithm and the real-time requirement of the controlled plant. During a single control period, MPC uses numerical optimization algorithm to solve the predictive optimization problem and obtain the optimal control signal. For rapid-changing plants such as vehicles, the control period is usually at the level of the seconds or milliseconds, which requires the high performance of real-time solving capability. When the prediction horizon is too long, or there are many system states and control inputs, the predictive optimization problem is computationally burdensome and difficult to solve within a single control period due to the limitation of the efficiency of the numerical optimization algorithm. This problem is especially serious when the predictive optimization problem is nonlinear. Therefore, even if each step of the predictive optimization problem has a feasible solution, the control process will be interrupted if the problem cannot be solved within a single control period.

4.1.2. A Complete Example – Using MPC to Realize Velocity Tracking

To articulate the basic concept of designing a practical MPC algorithm, this section is particularly introduced to explain a complete algorithm design process, laying an epitome and directive groundwork for the following sections.

Problem description:

Vehicle speed tracking system for eco-driving can be hierarchically divided into upper level and lower level controller. The upper-level controller calculates the desired acceleration to track the reference speed trajectory quickly and smoothly, while the lower-level controller realizes the desired acceleration by coordinating the acceleration and braking mechanism.

The block diagram of the speed tracking control system is shown in Figure 4.3. The upper-level controller using MPC to calculate the desired acceleration a_{des} according to current vehicle velocity v, current acceleration a, and reference velocity v_{ref}. The lower-level controller firstly determines the braking or acceleration based on a switch logic, and then transforms the desired acceleration into control input to the executor based on a PI controller. For a simulated vehicle, the control input is either throttle opening α_{thdes} or braking pressure p_{bdes}.

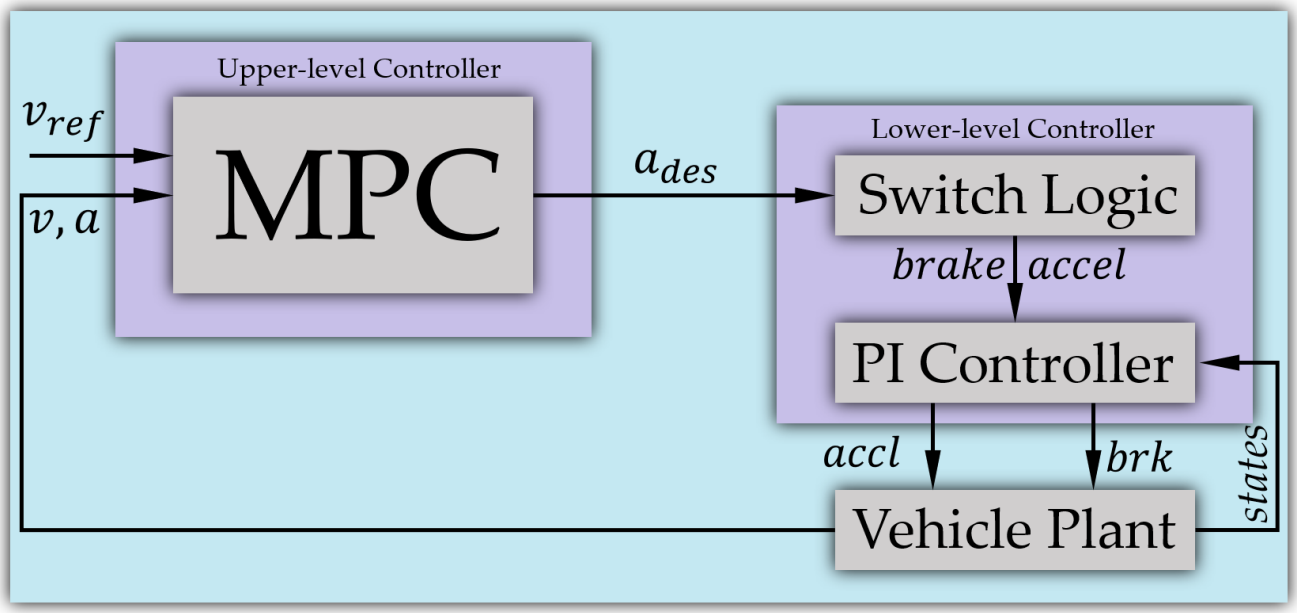

Fig. 4.3 Block Diagram of Speed Tracking Control System

MPC problem modeling for vehicle speed tracking:

Similar to the previous discussion, the vehicle longitudinal control can be expressed as a first-order inertial system:

$$\dot{a} = \frac{K}{\tau_d}(a_{des} - a) \tag{4.1}$$

where $K = 1.05$ is the system gain, τ_d is the time constant.

The continuous system state equation of the vehicle longitudinal dynamics can be expressed as:

$$\dot{\boldsymbol{x}} = \boldsymbol{A}\boldsymbol{x} + \boldsymbol{B}\boldsymbol{u}$$
$$\boldsymbol{A} = \begin{bmatrix} 0 & 1 \\ 0 & -\frac{1}{\tau_d} \end{bmatrix}, \quad \boldsymbol{B} = \begin{bmatrix} 0 \\ \frac{K}{\tau_d} \end{bmatrix} \tag{4.2}$$

where $\boldsymbol{x} = [v \quad a]^T$ is the system state vector, $\boldsymbol{u} = a_{des}$ is the system control input.

By applying the Forward Euler (FE) method, the system state equation can be discretized as:

$$\boldsymbol{x}(k+1) = \boldsymbol{A}_k\boldsymbol{x}(k) + \boldsymbol{B}_k\boldsymbol{u}(k)$$
$$\boldsymbol{A}_k = \begin{bmatrix} 1 & T_s \\ 0 & 1 - \frac{T_s}{\tau_d} \end{bmatrix} \quad \boldsymbol{B}_k = \begin{bmatrix} 0 \\ \frac{kT_s}{\tau_d} \end{bmatrix} \tag{4.3}$$

where k is the current sampling time instant, $k+1$ is the next sampling time instant, T_s is the sampling period.

Since the velocity v is the system output, the output equation can be expressed as:

$$\boldsymbol{y}(k) = \boldsymbol{C}\boldsymbol{x}(k)$$
$$\boldsymbol{C} = [1 \quad 0] \tag{4.4}$$

In order to ensure the system control objective – velocity tracking accuracy and to avoid excessive acceleration and jerk, the cost function is defined as [152]:

$$\boldsymbol{J}\big(\boldsymbol{x}(t), \boldsymbol{u}(t-1), \Delta\boldsymbol{u}(k)\big) = \sum_{i=1}^{N_p} \big\|\boldsymbol{y}_p(k+i|k) - \boldsymbol{y}_{ref}(k+i|k)\big\|_{\boldsymbol{Q}}^2 + \sum_{i=1}^{N_c} \|\Delta\boldsymbol{u}(k+i)\|_{\boldsymbol{R}}^2 \tag{4.5}$$

where $t-1$ is the sampling time instant at last step, N_p is the predictive horizon, N_c is the control horizon, $\boldsymbol{y}_p(k+i|k)$ is the control output prediction value, $\boldsymbol{y}_{ref}(k+i|k)$ is the reference control output, $(k+i|k)$ represents predicting the value at $k+i$ time instant at k sampling time instant, where $i = 0, 1, \cdots, N_c - 1$. $\boldsymbol{Q}$ and $\boldsymbol{R}$ are the system weight matrix of the system output and control increment. The first term on the right side of the equation reflects the capability of the system to follow the reference trajectory. The second term reflects the requirement for the steady variation of the control signal. The significance of the entire cost function enables the system to follow the desired trajectory as quickly and steadily as possible.

System constraints are applied to the acceleration and its changing rate – jerk, expressed as follow:

$$\boldsymbol{u}_{min} \le \boldsymbol{u}(k+i) \le \boldsymbol{u}_{max}, i = 0,1,\cdots,N_e - 1 \tag{4.6}$$

$$\Delta\boldsymbol{u}_{min} \le \Delta\boldsymbol{u}(k+i) \le \Delta\boldsymbol{u}_{max}, i = 0,1,\cdots,N_e - 1 \tag{4.7}$$

where $\boldsymbol{u}_{min}$ and $\boldsymbol{u}_{max}$ are the thresholds of acceleration, $\Delta\boldsymbol{u}_{min}$ and $\Delta\boldsymbol{u}_{max}$ are the thresholds of jerk.

The basic concept of MPC is to minimize the cost function 4.5 under the control constraints 4.6 and 4.7, solving the following optimization problem during each control period:

$$\min \boldsymbol{J}\big(\boldsymbol{x}(k), \boldsymbol{u}(k-1), \Delta\boldsymbol{u}(k)\big) \tag{4.8}$$

$s.t.$

$$\boldsymbol{x}(k+1) = \boldsymbol{A}_k\boldsymbol{x}(k) + \boldsymbol{B}_k\boldsymbol{u}(k)$$
$$\boldsymbol{A}_k = \begin{bmatrix} 1 & T_s \\ 0 & 1 - T_s/\tau_d \end{bmatrix} \quad \boldsymbol{B}_k = \begin{bmatrix} 0 \\ kT_s/\tau_d \end{bmatrix}$$
$$\boldsymbol{u}_{min} \le \boldsymbol{u}(k+i) \le \boldsymbol{u}_{max}, i = 0,1,\cdots,N_e - 1$$

$$\Delta \boldsymbol{u}_{min} \le \Delta \boldsymbol{u}(k+i) \le \Delta \boldsymbol{u}_{max}, i = 0,1,\cdots,N_e - 1$$

The above optimization problem is solved by transforming it into a standard quadratic programing (QP) problem.

The transformation from MPC problem to QP problem:

For the discrete vehicle longitudinal dynamics state equation 4.3, a new state vector $\boldsymbol{\xi}(k|t) = [\boldsymbol{x}(k) \quad \boldsymbol{u}(k-1)]^T$ can be formulated to obtain a new state-space equation [152]~[155]:

$$\begin{aligned} \boldsymbol{\xi}(k+1) &= \widetilde{\boldsymbol{A}}_k \boldsymbol{\xi}(k) + \widetilde{\boldsymbol{B}}_k \Delta \boldsymbol{u}(k) \\ \boldsymbol{\eta}(k) &= \widetilde{\boldsymbol{C}}_k \boldsymbol{\xi}(k) \end{aligned} \tag{4.9}$$

where $\widetilde{\boldsymbol{A}}_k = \begin{bmatrix} \boldsymbol{A}_k & \boldsymbol{B}_k \\ \boldsymbol{0}_{m\times n} & \boldsymbol{I}_m \end{bmatrix}$, $\widetilde{\boldsymbol{B}}_k = \begin{bmatrix} \boldsymbol{B}_k \\ \boldsymbol{I}_m \end{bmatrix}$, $\widetilde{\boldsymbol{C}}_k = [\boldsymbol{C}_k \quad \boldsymbol{0}]$, $\boldsymbol{I}_m$ are 1-D identity matrix and 2-D identity matrix, respectively, with $m = 1$, $n = 2$. According to equation 4.9, the state prediction can be obtained as [156]:

$$\begin{aligned} \boldsymbol{\xi}(k+1) &= \widetilde{\boldsymbol{A}}_k \boldsymbol{\xi}(k) + \widetilde{\boldsymbol{B}}_k \Delta \boldsymbol{u}(k) \\ \boldsymbol{\xi}(k+2) &= \widetilde{\boldsymbol{A}}_k \boldsymbol{\xi}(k+1) + \widetilde{\boldsymbol{B}}_k \Delta \boldsymbol{u}(k+1) = \widetilde{\boldsymbol{A}}_k^2 \boldsymbol{\xi}(k) + \widetilde{\boldsymbol{A}}_k \widetilde{\boldsymbol{B}}_k \Delta \boldsymbol{u}(k) + \widetilde{\boldsymbol{B}}_k \Delta \boldsymbol{u}(k+1) \\ \boldsymbol{\xi}(k+3) &= \widetilde{\boldsymbol{A}}_k \boldsymbol{\xi}(k+2) + \widetilde{\boldsymbol{B}}_K \Delta \boldsymbol{u}(k+2) = \widetilde{\boldsymbol{A}}_k^3 \boldsymbol{\xi}(k) + \widetilde{\boldsymbol{A}}_k^2 \widetilde{\boldsymbol{B}}_k \Delta \boldsymbol{u}(k) + \widetilde{\boldsymbol{A}}_k \widetilde{\boldsymbol{B}}_k \Delta \boldsymbol{u}(k+1) + \widetilde{\boldsymbol{B}}_k \Delta \boldsymbol{u}(k+2) \\ &\vdots \\ \boldsymbol{\xi}(k+N_p) &= \widetilde{\boldsymbol{A}}_k \boldsymbol{\xi}(k+N_p-1) + \widetilde{\boldsymbol{B}}_k \Delta \boldsymbol{u}(k+N_p-1) = \widetilde{\boldsymbol{A}}_k^{N_p} \boldsymbol{\xi}(k) + \widetilde{\boldsymbol{A}}_k^{N_p-1} \widetilde{\boldsymbol{B}}_k \Delta \boldsymbol{u}(k) + \widetilde{\boldsymbol{A}}_k^{N_p-2} \widetilde{\boldsymbol{B}}_k \Delta \boldsymbol{u}(k+1) + \cdots + \widetilde{\boldsymbol{B}}_k \Delta \boldsymbol{u}(k+N_p-1) \end{aligned} \tag{4.10}$$

According to equation 4.11, the system output of the new state-space equation is thereby can be calculated as follow [156]:

$$\begin{aligned} \boldsymbol{\eta}(k+1) &= \widetilde{\boldsymbol{C}}_k \boldsymbol{\xi}(k+1) = \widetilde{\boldsymbol{C}}_k \widetilde{\boldsymbol{A}}_k \boldsymbol{\xi}(k) + \widetilde{\boldsymbol{C}}_k \widetilde{\boldsymbol{B}}_k \Delta \boldsymbol{u}(k) \\ \boldsymbol{\eta}(k+2) &= \widetilde{\boldsymbol{C}}_k \widetilde{\boldsymbol{A}}_k \boldsymbol{\xi}(k+1) + \widetilde{\boldsymbol{C}}_k \widetilde{\boldsymbol{B}}_k \Delta \boldsymbol{u}(k+1) = \widetilde{\boldsymbol{C}}_k \widetilde{\boldsymbol{A}}_k^2 \boldsymbol{\xi}(k) + \widetilde{\boldsymbol{C}}_k \widetilde{\boldsymbol{A}}_k \widetilde{\boldsymbol{B}}_k \Delta \boldsymbol{u}(k) + \widetilde{\boldsymbol{C}}_k \widetilde{\boldsymbol{B}}_k \Delta \boldsymbol{u}(k+1) \\ \boldsymbol{\eta}(k+3) &= \widetilde{\boldsymbol{C}}_k \widetilde{\boldsymbol{A}}_k \boldsymbol{\xi}(k+2) + \widetilde{\boldsymbol{C}}_k \widetilde{\boldsymbol{B}}_k \Delta \boldsymbol{u}(k+2) = \widetilde{\boldsymbol{C}}_k \widetilde{\boldsymbol{A}}_k^3 \boldsymbol{\xi}(k) + \widetilde{\boldsymbol{C}}_k \widetilde{\boldsymbol{A}}_k^2 \widetilde{\boldsymbol{B}}_k \Delta \boldsymbol{u}(k) + \widetilde{\boldsymbol{C}}_k \widetilde{\boldsymbol{A}}_k \widetilde{\boldsymbol{B}}_k \Delta \boldsymbol{u}(k+1) + \widetilde{\boldsymbol{C}}_k \widetilde{\boldsymbol{B}}_k \Delta \boldsymbol{u}(k+2) \\ &\vdots \\ \boldsymbol{\eta}(k+N_p) &= \widetilde{\boldsymbol{C}}_k \widetilde{\boldsymbol{A}}_k \boldsymbol{\xi}(k+N_p-1) + \widetilde{\boldsymbol{C}}_k \widetilde{\boldsymbol{B}}_k \Delta \boldsymbol{u}(k+N_p-1) = \widetilde{\boldsymbol{C}}_k \widetilde{\boldsymbol{A}}_k^{N_p} \boldsymbol{\xi}(k) + \widetilde{\boldsymbol{C}}_k \widetilde{\boldsymbol{A}}_k^{N_p-1} \widetilde{\boldsymbol{B}}_k \Delta \boldsymbol{u}(k) + \cdots + \widetilde{\boldsymbol{C}}_k \widetilde{\boldsymbol{B}}_k \Delta \boldsymbol{u}(k+N_p-1) \end{aligned} \tag{4.11}$$

To make the overall relation to be clearer, the output of the system in the prediction horizon can be expressed in matrix form as follow [156]:

$$\boldsymbol{Y} = \boldsymbol{\Psi} \boldsymbol{\xi}(k) + \boldsymbol{\Theta} \Delta \boldsymbol{U} \tag{4.12}$$

where,

$$\boldsymbol{Y} = \begin{bmatrix} \boldsymbol{\eta}(k+1) \\ \boldsymbol{\eta}(k+2) \\ \cdots \\ \boldsymbol{\eta}(k+N_e) \\ \cdots \\ \boldsymbol{\eta}(k+N_p) \end{bmatrix}, \boldsymbol{\Psi} = \begin{bmatrix} \widetilde{\boldsymbol{C}}_k \widetilde{\boldsymbol{A}}_k \\ \widetilde{\boldsymbol{C}}_k \widetilde{\boldsymbol{A}}_k^2 \\ \cdots \\ \widetilde{\boldsymbol{C}}_k \widetilde{\boldsymbol{A}}_k^{N_e} \\ \cdots \\ \widetilde{\boldsymbol{C}}_k \widetilde{\boldsymbol{A}}_k^{N_p} \end{bmatrix}, \boldsymbol{\Theta} = \begin{bmatrix} \widetilde{\boldsymbol{C}}_k \widetilde{\boldsymbol{B}}_k & \boldsymbol{0} & \boldsymbol{0} & \boldsymbol{0} \\ \widetilde{\boldsymbol{C}}_k \widetilde{\boldsymbol{A}}_k \widetilde{\boldsymbol{B}}_k & \widetilde{\boldsymbol{C}}_k \widetilde{\boldsymbol{B}}_k & \boldsymbol{0} & \boldsymbol{0} \\ \cdots & \cdots & \ddots & \cdots \\ \widetilde{\boldsymbol{C}}_k \widetilde{\boldsymbol{A}}_k^{N_e-1} \widetilde{\boldsymbol{B}}_k & \widetilde{\boldsymbol{C}}_k \widetilde{\boldsymbol{A}}_k^{N_e-2} \widetilde{\boldsymbol{B}}_k & \cdots & \widetilde{\boldsymbol{C}}_k \widetilde{\boldsymbol{B}}_k \\ \widetilde{\boldsymbol{C}}_k \widetilde{\boldsymbol{A}}_k^{N_e} \widetilde{\boldsymbol{B}}_k & \widetilde{\boldsymbol{C}}_k \widetilde{\boldsymbol{A}}_k^{N_e-1} \widetilde{\boldsymbol{B}}_k & \cdots & \widetilde{\boldsymbol{C}}_k \widetilde{\boldsymbol{A}}_k \widetilde{\boldsymbol{B}}_k \\ \vdots & \vdots & \ddots & \vdots \\ \widetilde{\boldsymbol{C}}_k \widetilde{\boldsymbol{A}}_k^{N_p-1} \widetilde{\boldsymbol{B}}_k & \widetilde{\boldsymbol{C}}_k \widetilde{\boldsymbol{A}}_k^{N_p-2} \widetilde{\boldsymbol{B}}_k & \cdots & \widetilde{\boldsymbol{C}}_k \widetilde{\boldsymbol{A}}_k^{N_p-N_e-1} \widetilde{\boldsymbol{B}}_k \end{bmatrix},$$

$$\Delta \boldsymbol{U} = [\Delta \boldsymbol{u}(k) \quad \Delta \boldsymbol{u}(k+1) \quad \cdots \quad \Delta \boldsymbol{u}(k+N_e)]^T.$$

From equation 4.12, it is intuitive that both the system state and output value within the prediction horizon can be obtained using current system state $\boldsymbol{\xi}(k)$ and control increment $\Delta \boldsymbol{U}$ within the control horizon, which is the realization of "prediction" of model predictive control.

Now the reference output vector is defined as $\boldsymbol{Y}_{ref}(k) = [\boldsymbol{\eta}_{ref}(k+1) \quad \cdots \quad \boldsymbol{\eta}_{ref}(k+N_p)]^T$, let $\boldsymbol{E} = \boldsymbol{\Psi} \boldsymbol{\xi}(k)$, and substitute equation 4.12 into equation 4.5. The following equation can be obtained [155]:

$$\begin{aligned}\boldsymbol{\mathcal{J}} &= \left(\boldsymbol{Y}-\boldsymbol{Y}_{ref}\right)^T\boldsymbol{Q}_Q\left(\boldsymbol{Y}-\boldsymbol{Y}_{ref}\right)+\Delta\boldsymbol{U}^T\boldsymbol{R}_R\Delta\boldsymbol{U}\\ &= \left[\boldsymbol{\Psi}\boldsymbol{\xi}(k)+\boldsymbol{\Theta}_t\Delta\boldsymbol{U}(t)-\boldsymbol{Y}_{ref}\right]^T\boldsymbol{Q}_Q\left[\boldsymbol{\Psi}\boldsymbol{\xi}(k)+\boldsymbol{\Theta}_t\Delta\boldsymbol{U}(t)-\boldsymbol{Y}_{ref}\right]+\Delta\boldsymbol{U}^T\boldsymbol{R}_R\Delta\boldsymbol{U}\\ &= \Delta\boldsymbol{U}^T\left(\boldsymbol{\Theta}^T\boldsymbol{Q}_Q\boldsymbol{\Theta}+\boldsymbol{R}_R\right)\Delta\boldsymbol{U}+2\left(\boldsymbol{E}^T\boldsymbol{Q}_Q\boldsymbol{\Theta}-\boldsymbol{Y}_{ref}^T\boldsymbol{Q}_Q\boldsymbol{\Theta}\right)\Delta\boldsymbol{U}+\boxed{\boldsymbol{E}^T\boldsymbol{Q}_Q\boldsymbol{E}+\boldsymbol{Y}_{ref}^T\boldsymbol{Q}_Q\boldsymbol{Y}_{ref}-2\boldsymbol{Y}_{ref}^T\boldsymbol{Q}\boldsymbol{E}}\end{aligned} \tag{4.13}$$

where $\boldsymbol{Q}_Q=\boldsymbol{I}_{N_P}\otimes\boldsymbol{Q}$, $\boldsymbol{R}_R=\boldsymbol{I}_{N_p}\otimes\boldsymbol{R}$, $\otimes$ denotes the Kroneck product.

The terms within $\square$ are constants, which can be ignored during optimization. Thus, the cost function can be rewritten as [155]~[156]:

$$\boldsymbol{\mathcal{J}}=2\left(\frac{1}{2}\Delta\boldsymbol{U}^T\boldsymbol{H}\Delta\boldsymbol{U}+\boldsymbol{g}^T\Delta\boldsymbol{U}\right) \tag{4.14}$$

During the process of optimization, the equation 4.14 is equivalent to:

$$\boldsymbol{\mathcal{J}}=\frac{1}{2}\Delta\boldsymbol{U}^T\boldsymbol{H}\Delta\boldsymbol{U}+\boldsymbol{g}^T\Delta\boldsymbol{U} \tag{4.15}$$

Considering there exists the following relation between control value and control increment value:

$$\boldsymbol{u}(k+i)=\boldsymbol{u}(k+i-1)+\Delta\boldsymbol{u}(k) \tag{4.16}$$

Note that the system constraints in equation 4.6 and 4.7 are about control value and control increment value, respectively. Therefore, the variables within constraints needs to be unified before optimization. Thus, the constraints 4.6 and 4.7 can be rewritten as:

$$\boldsymbol{U}_{min}\le\boldsymbol{A}_k\Delta\boldsymbol{U}+\boldsymbol{U}_t\le\boldsymbol{U}_{max} \tag{4.17}$$

$$\Delta\boldsymbol{U}_{min}\le\Delta\boldsymbol{U}_t\le\Delta\boldsymbol{U}_{max} \tag{4.18}$$

where $\boldsymbol{U}_t=\boldsymbol{1}_{N_e}\otimes\boldsymbol{u}(k-1)$, $\boldsymbol{1}_{N_e}$ is a column vector with the N_e rows, $\boldsymbol{u}(k-1)$ is the actual control value of last time instant, $\boldsymbol{U}_{min}$ and $\boldsymbol{U}_{max}$ are the sets of minimum and maximum control value within control horizon, $\Delta\boldsymbol{U}_{min}$ and $\Delta\boldsymbol{U}_{max}$ are the sets of minimum and maximum control increment values respectively within the control horizon.

$$\boldsymbol{A}_k=\begin{bmatrix}1&0&\cdots&\cdots&0\\1&1&0&\cdots&0\\1&1&1&\ddots&0\\\vdots&\vdots&\ddots&\ddots&0\\1&1&\cdots&1&1\end{bmatrix}_{N_e\times N_e}$$

At this point, the MPC problem in equation 4.8 is transformed into a standard quadratic QP problem:

$$\min_{\Delta\boldsymbol{U}}\frac{1}{2}\Delta\boldsymbol{U}^T\boldsymbol{H}\Delta\boldsymbol{U}+\boldsymbol{g}^T\Delta\boldsymbol{U} \tag{4.19}$$

$s.t.$

$$\begin{aligned}\Delta\boldsymbol{U}_{min}\le\Delta\boldsymbol{U}\le\Delta\boldsymbol{U}_{max}\\ \boldsymbol{U}_{min}\le\boldsymbol{A}_k\Delta\boldsymbol{U}+\boldsymbol{U}_t\le\boldsymbol{U}_{max}\end{aligned}$$

The problem described by equation 4.19 can be solved by the QP solver "**quadprog**" within MATLAB. And a sequence of control increment values can be obtained:

$$\Delta\boldsymbol{U}^*=[\Delta\boldsymbol{u}^*(k),\Delta\boldsymbol{u}^*(k+1),\cdots,\Delta\boldsymbol{u}^*(N_c-1)]^T \tag{4.20}$$

According to the principle of MPC, the first element of the above control sequence will be applied to the system:

$$\boldsymbol{u}(k) = \boldsymbol{u}(k-1) + \Delta\boldsymbol{u}^*(k) \tag{4.21}$$

Taking as the input to the system, it will be executed until the next time instant. At the next new instant, the system will re-predict the output in the next prediction horizon based on the system state. A new sequence of control value will be obtained by solving an optimization problem. With such an iteratively process, the system completes the control process.

Simulation realization:

Based on the above theoretical analysis and derivation, the co-simulation built based on Simulink/CarSim in this section realizes the vehicle speed tracking based on MPC. The overall MPC algorithm will be achieved within the Simulink environment, while an integrated vehicle dynamics model is provided by CarSim. The co-simulation environment is shown in Figure 4.4

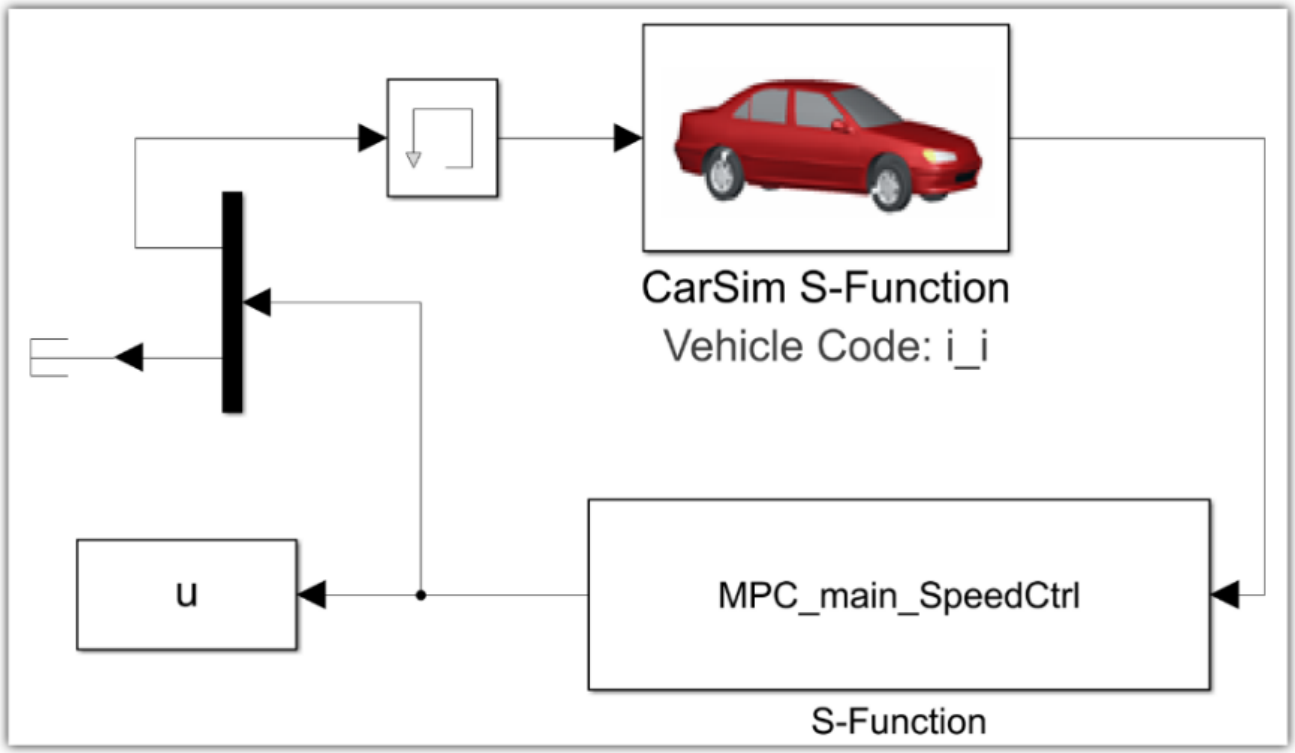

Fig. 4.4 Co-simulation Platform for Vehicle Speed Tracking Based on MPC Algorithm

The MPC-based vehicle speed tracking controller is designed through an S-Function block within Simulink. The main function of the MPC algorithm is shown in Figure 4.5.

Given a step-signal as the reference speed trajectory, the speed tracking performance of the proposed MPC controller is shown in Figure 4.6. The proposed MPC-based vehicle longitudinal speed tracking system shows good performance. It can rapidly respond to the step-signal and track without any overshooting.

This complete example shows how to design a model predictive controller from mathematical derivation to code implementation. The concept of mathematical derivation is similar for the following section of this research. The most critical part is the optimization problem formulation. Different from a conventional control law, MPC is more of an idea that determine the control input to the system by solving an optimization problem

at each sampling time. Because of this, online computation complexity becomes the major disadvantage of MPC algorithm. Therefore, it is worthwhile to discuss about the problem of practical application of MPC in the following sections.

```
function sys = mdlOutputs(t,x,u) %Calculate output subfunction

global InitialGapflag;
global MPCParameters;
global WarmStart;
Vx    = 0;
a_x   = 0;
a_des = 0;

t_Start = tic; % Time start

if InitialGapflag < 2      % Neglect first two inputs
    InitialGapflag = InitialGapflag + 1;
else
    InitialGapflag = InitialGapflag + 1;
    % 1.Input
    Vx    = u(1)/3.6;  %vehicle longitudinal velocity unit: km/h-->m/s
    a_x   = u(2)*9.8;  %vehicle longitudinal acceleration unit: g's-->m/s2
    kesi = [Vx;  a_x]; %update the vehicle state vector
    % 2.reference velocity
    switch MPCParameters.refspeedT,
        case 0 % step speed curve
            SpeedProfile = func_ConstantSpeed(InitialGapflag, MPCParameters);
        case 1 % sine speed curve
            SpeedProfile = func_SineSpeed(InitialGapflag,MPCParameters);
        otherwise
            error(['unexpected speed-profile:',num2str(MPCParameters.refspeedT)]);
    end
    % 3.model
    Ts = MPCParameters.Ts;
    StateSpaceModel.A =  [1      Ts;
                          0      1];
    StateSpaceModel.B =  [0;     1];
    StateSpaceModel.C =  [1,    0];
    % 4.prediction
    [PHI, THETA] = func_Update_PHI_THETA(StateSpaceModel, MPCParameters);
    % 5.objective function
    [H, f, g] = func_Update_H_f(kesi, SpeedProfile, PHI, THETA, MPCParameters);
    % 6.optimization solution with different solver
    switch MPCParameters.qp_solver,
        case 0 % quadprog
            [A, b, Aeq, beq, lb, ub] = func_Constraints_du_quadprog(MPCParameters, a_x);
            options = optimset('Display','off', ...
                               'TolFun', 1e-8, ...
                               'MaxIter', 2000, ...
                               'Algorithm', 'interior-point-convex', ...
                               'FinDiffType', 'forward', ...
                               'RelLineSrchBnd', [], ...
                               'RelLineSrchBndDuration', 1, ...
                               'TolConSQP', 1e-8);
            warning off all
            U0 = WarmStart;
            [U, FVAL, EXITFLAG] = quadprog(H, g, A, b, Aeq, beq, lb, ub, U0, options);
            WarmStart = shiftHorizon(U);
            if (1 ~= EXITFLAG)
                U(1) = 0.0;
                fprintf('MPC solver not converged!\n');
            end
            a_des =  U(1);

        case 1 % qpOASES
            [A, lb, ub, lbA, ubA] = func_Constraints_du_qpOASES(MPCParameters, a_x);
            options = qpOASES_options('default', ...
                                      'printLevel', 0);
            [U, FVAL, EXITFLAG, iter, lambda] = qpOASES(H, g, A, lb, ub, lbA, ubA, options);
            if (0 ~= EXITFLAG)
                U(1) = 0.0;
                fprintf('MPC solver: qpOASES not converged!\n');
            end
            a_des =  U(1);

    end %  end of switch

end % end of if Initialflag

    [Throttle, Brake] = func_AccelerationTrackingController(a_des);

t_Elapsed = toc( t_Start ); % time calculation

sys = [Throttle; Brake;t_Elapsed; Vx; a_x; a_des];
% end % End of mdlOutputs
```

Fig. 4.5 Main Function of MPC Algorithm

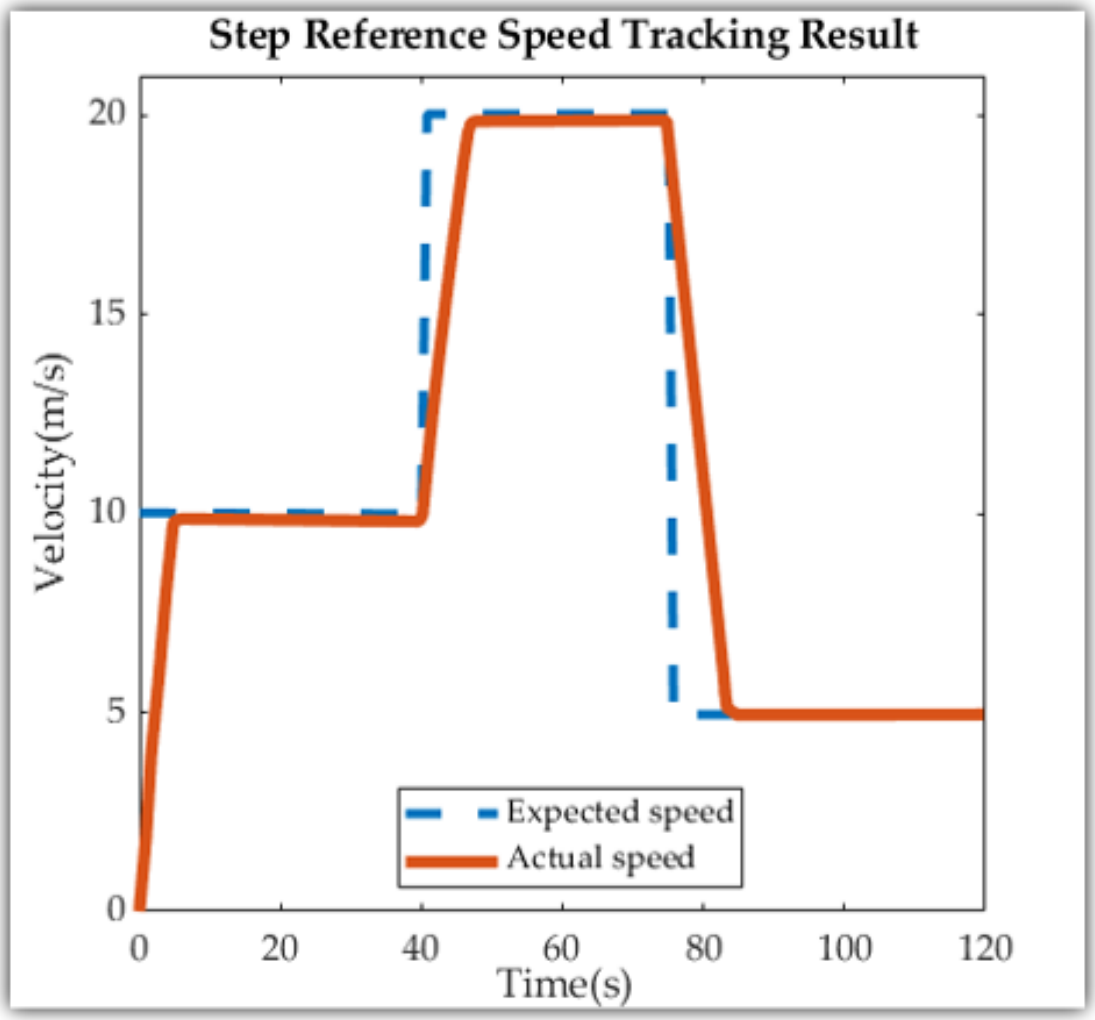

Fig. 4.6 Result of Vehicle Speed Tracking based on MPC Algorithm

4.1.3. Multi-Objective Optimization Considering Preceding Vehicle Based on LMPC

As the key component of the entire predictive cruise control system, car following driving scenario is the most frequent and typical driving condition. During following the preceding vehicle, driving comfortability and energy economy are also required to be considered. Hence, in this section, the predictive cruise control system for EV's eco-driving is designed based on MPC, taking the inter-vehicle longitudinal dynamics model as the control plant. By integrating the driving state of preceding vehicle and the safety distance model, the motion of the host and preceding vehicle can be predicted within the prediction horizon. Based on ensuring the car-following safety, the energy economy is maximized. The cost function is established considering both driving safety and comfortability. By means of using rolling horizon optimization algorithm, the optimal control value, i.e. the desired longitudinal acceleration, can be obtained, which is further fed into the vehicle longitudinal dynamics model. The controller structure of car following scenario is shown in Figure 4.7.

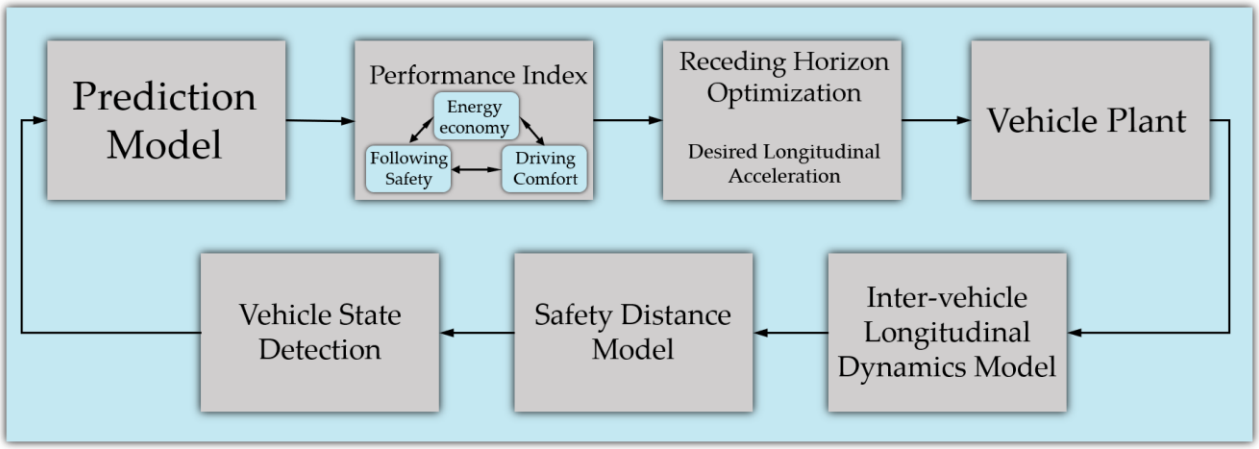

Fig. 4.7 Controller Structure of Car Following Scenario

Taking the inter-vehicle longitudinal dynamics model proposed in Chapter 2 as the controller plant of MPC, the state variables of the system are inter-vehicle distance error Δd, the relative velocity between the host and preceding vehicle v_{rel}, and acceleration of host vehicle a_{host}:

$$\boldsymbol{x} = [\Delta d, v_{rel}, a_{host}]^T \tag{4.22}$$

According to the derivation in Chapter 2 – 2.2.5, the system state-space equation is expressed as follow:

$$\dot{\boldsymbol{x}} = \boldsymbol{A}x + \boldsymbol{B}u + \boldsymbol{G}w \tag{4.23}$$

where desired acceleration is the control input u, the acceleration of preceding is regarded as system disturbance w.

With $\mathcal{H} = 2\tau_1 v_{host} + 3\tau_2 v_{host}^2 - 2\tau_3 v_{rel} v_{host} + \tau_3 v_{host}^2 - d_{min}$, then the system matrices are derived as:

$$\boldsymbol{A} = \begin{bmatrix} 0 & 1 & -\mathcal{H} \\ 0 & 0 & -1 \\ 0 & 0 & -\frac{1}{T_g} \end{bmatrix}, \boldsymbol{B} = \begin{bmatrix} 0 \\ 0 \\ \frac{K_g}{T_g} \end{bmatrix}, \boldsymbol{G} = \begin{bmatrix} \tau_3 v_{host}^2 \\ 1 \\ 0 \end{bmatrix}, u = a_{desired}, w = a_{pre}.$$

i.e.

$$\begin{bmatrix} \dot{\Delta d} \\ \dot{v_{rel}} \\ \dot{a_{host}} \end{bmatrix} = \begin{bmatrix} 0 & 1 & -\mathcal{H} \\ 0 & 0 & -1 \\ 0 & 0 & -\frac{1}{T_g} \end{bmatrix} \begin{bmatrix} \Delta d \\ v_{rel} \\ a_{host} \end{bmatrix} + \begin{bmatrix} 0 \\ 0 \\ \frac{K_g}{T_g} \end{bmatrix} a_{desired} + \begin{bmatrix} \tau_3 v_{host}^2 \\ 1 \\ 0 \end{bmatrix} a_{pre} \tag{4.24}$$

where T_g is the time constant, K_g is the system gain.

The discrete inter-vehicle longitudinal dynamics model can be derived as follow:

$$\begin{aligned} \boldsymbol{x}(k+1) &= \bar{\boldsymbol{A}}\boldsymbol{x}(k) + \bar{\boldsymbol{B}}u(k) + \bar{\boldsymbol{G}}w(k) \\ \boldsymbol{y}(k) &= \boldsymbol{C}\boldsymbol{x}(k) \end{aligned} \tag{4.25}$$

where k refers to the kth sampling time step, $\bar{\boldsymbol{A}}$, $\bar{\boldsymbol{B}}$, and $\bar{\boldsymbol{G}}$ are discretized system coefficient matrices, $\boldsymbol{y}$ represents the system output, $\boldsymbol{C}$ is an identity matrix. The detailed derivation is referred to the Chapter 2-2.2.5.

As the bond between control objectives and control algorithm, control performance index in the car following scenario is important in that, firstly, it is the foundation of coordinated control for energy economy, driving safety and driving comfortability; secondly, its cost function and constraints together constitute the predictive

optimization problem, which is the core of the MPC algorithm. Accordingly, the design of the performance index should follow the rules: (1) accurately quantify the multiple control objectives, including energy economy, driving safety and comfortability; (2) the cost function and constraints should be as simple as possible so as to ensure the real-time solving capability of the MPC algorithm.

Energy economy:

During the car following process, energy consumption is closely related to the longitudinal acceleration. Hence, by smoothing the acceleration and jerk to reduce the hard acceleration and deceleration, the energy economy can be efficiently improved. The derivative of vehicle acceleration can be defined as jerk:

$$j(t) = \frac{a(t) - a(t-1)}{T_s} \tag{4.26}$$

The control objective can be mathematically expressed as:

$$objective \begin{cases} \min|a_{host}(k)| \\ \min|j_{host}(k)| \end{cases} \tag{4.27}$$

where $a_{host}(k)$ is the transient acceleration of the host vehicle, $j_{host}(k)$ is the transient jerk of the host vehicle.

According to the analysis by Li [133], an approximate linear relation between energy consumption and vehicle acceleration can be found. So, here the energy economy can be quantified using Euclidean norm of desired acceleration and desired jerk of the host vehicle:

$$\mathcal{J}_E = w_u a_{desired}^2 + w_{du} j_{desired}^2 \tag{4.28}$$

where $\mathcal{J}_E$ is the performance index of the energy economy, w_u is the weight coefficient of desired acceleration, and w_{du} is the weight coefficient of the desired jerk. For the former term, by minimizing the $\mathcal{J}_E$, the acceleration amplitude can be lowered so that the energy economy can be improved. For latter term, it limits the frequent acceleration or deceleration of the electric motor so as to further improve the energy economy. Besides, lowering the jerk can efficiently reduce the longitudinal driving impact so that the driving comfortability can be improved.

Driving safety:

During the car following process, driving safety is always the top priority. In the previous chapter, the desired car following model has been proposed based on a customized safety distance model. The control system regulates the vehicle to reach the desired car-following distance by manipulating its acceleration based on the V2V state information. Apart from the desired car-following distance calculated by the safety distance model as the ultimate control objective, another real-time safe distance d_{safe} before reaching the final desired value is required to constrain the actual inter-vehicle distance. To ensure the driving safety and keep the host vehicle from a collision with the preceding vehicle, the actual car-following distance should be always greater than safety distance d_{safe}. This real-time safe distance d_{safe} can be defined by a Time-to-Collision (TTC) Strategy, which is used to describe the car-following safety during braking, e.g., when the host vehicle velocity is much greater than the preceding vehicle, it is still risky to collide with the preceding vehicle even there's a long inter-vehicle distance. Therefore, the safety constraints can be defined as follow:

$$D_{actual}(k) \geq d_{safe}(k)$$
$$d_{safe}(k) = \max(t_{TTC} \cdot v_{rel}(k) + d_{min}) \tag{4.29}$$

Where D_{actual} is the actual real-time inter-vehicle distance, t_{TTC} is the time to collision.

When preceding vehicle running at a steady state, the control objective is forcing the actual inter-vehicle distance approaching the desired safety distance calculated by the safety distance model, i.e., the error Δd between D_{actual} and D_{safe} approaching zero. Simultaneously, to keep the traffic flow to be as stable as possible, another control objective is to let the host vehicle velocity approaching the preceding vehicle velocity by adjusting the acceleration of the host vehicle, i.e., v_{rel} approaching zero.

$$objective \begin{cases} \Delta d(k) \to 0 \\ v_{rel}(k) \to 0 \end{cases}, k \to \infty \tag{4.30}$$

To quantitatively describe the car-following capability, the Euclidean norm of Δd and v_{rel} is used to define the cost function of driving safety:

$$\mathcal{J}_S = w_{\Delta d} \Delta d^2 + w_{v_{rel}} v_{rel}^2 \tag{4.31}$$

Where $\mathcal{J}_S$ is the performance index of driving safety, $w_{\Delta d}$ is the weight coefficient of the tracking distance error, $w_{v_{rel}}$ is the weight coefficient of the relative velocity.

However, corresponding to the unstable driving condition of the preceding vehicle, the host vehicle tends to reflect as hard acceleration or deceleration, which is against the energy economy. If the weight of fuel economy is greater than driving safety in the final cost function, there's possible to compromise the vehicle dynamics in the pursuit of the energy economy. Therefore, the variable Δd and v_{rel} are constrained by the following boundary conditions:

$$\Delta d_{min} \cdot S_{DE}^{-1} \leq \Delta d(k) \leq \Delta d_{max} \cdot S_{DE}^{-1}$$
$$v_{rel,min} \cdot S_{VE}^{-1} \leq v_{rel}(k) \leq v_{rel,max} \cdot S_{VE}^{-1} \tag{4.32}$$

where Δd_{min} and Δd_{max} are the lower and upper boundary of inter-distance error, $v_{rel,min}$ and $v_{rel,max}$ are the extreme value of relative velocity, S_{DE} and S_{VE} are the driver's sensitivity to the Δd and v_{rel}, which can be calculated by [137]:

$$S_{DE}^{-1} = k_{SDE} \cdot v_{host} + d_{SDE}$$
$$S_{VE}^{-1} = k_{SVE} \cdot v_{host} + d_{SVE} \tag{4.33}$$

where k_{SDE} and k_{SVE} are the coefficients of first-order terms, d_{SDE} and d_{SVE} are the constant terms.

Driving Comfortability:

Driving comfortability is presented in two aspects: (1) desired acceleration calculated by the upper-level controller should be align with the driver's expectation; (2) try to drive at a constant speed and avoid frequent acceleration or deceleration. Therefore, the following control objective can be defined:

$$a_{desired,min} \leq a_{desired}(k) \leq a_{desired,max}$$
$$j_{desired,min} \leq j_{desired}(k) \leq j_{desired,max} \tag{4.34}$$

where $a_{desired,min}$ and $a_{desired,max}$ are the desired acceleration boundary condition, $j_{desire,min}$ and $j_{desire,max}$ are the desired jerk boundary condition, respectively.

Moreover, considering the physical limitation of vehicle velocity and acceleration, the control inputs into the host vehicle should be constrained by:

$$\begin{matrix} v_{min} \le v_{host}(k) \le v_{max} \\ a_{min} \le a_{host}(k) \le a_{max} \end{matrix} \tag{4.35}$$

where v_{min}, v_{max}, a_{min}, and a_{max} are all decided by the braking and acceleration capability of the vehicle itself.

Consequently, in this research, driving comfortability is realized by constraining the host vehicle acceleration as follow:

$$\mathcal{J}_C = w_a a_{host}^2 \tag{4.36}$$

where $\mathcal{J}_C$ is the performance index of driving comfortability, w_a is the weight coefficient of the host vehicle longitudinal acceleration.

In the car following scenario, the energy economy, driving safety and comfortability are mutually restricted and affected. To obtain the optimal control value, each performance index is required to be considered cooperatively. Therefore, under the car following scenario, the optimization problem of MPC in each sampling period can be integrated as:

$$\mathcal{J}_{car-following} = \mathcal{J}_E + \mathcal{J}_S + \mathcal{J}_C = w_u a_{desired}^2 + w_{du} j_{desired}^2 + w_{\Delta d} \Delta d^2 + w_{v_{rel}} v_{rel}^2 + w_a a_{host}^2 \tag{4.37}$$

where $\mathcal{J}_{car-following}$ is the system cost function under car following scenario.

Replacing the $[\Delta d, v_{rel}, a_{host}]^T$ and $a_{desired}$ with $\boldsymbol{y}$ and u, respectively, the following equation can be obtained:

$$\mathcal{J}_{car-following} = \boldsymbol{y}^T \boldsymbol{w}_y \boldsymbol{y} + w_u u^2 + w_{du} \dot{u}^2 \tag{4.38}$$

where $\boldsymbol{w}_y$ is the weight matrix of the output vector:

$$\boldsymbol{w}_y = \begin{bmatrix} w_{\Delta d} & 0 & 0 \\ 0 & w_{v_{rel}} & 0 \\ 0 & 0 & w_a \end{bmatrix}.$$

The next step is to transform the constraints of the performance indexes above into system input-and-output constraints.

As the input to the inter-vehicle longitudinal dynamics model, the comfortability constraints can be directly transformed into constraints of system inputs, as follow:

$$\begin{matrix} a_{host,min} \le u \le a_{host,max} \\ j_{host,min} = \dot{a_{host,min}} \le \dot{u} \le \dot{a_{host,max}} = j_{host,max} \end{matrix} \tag{4.39}$$

Transform the driving safety constraints into system output constraints:

$$\begin{matrix} \Delta d + D_{safe} \ge t_{TTC} \cdot v_{rel} \\ \Delta d + D_{safe} \ge d_{min} \end{matrix} \tag{4.40}$$

Substitute D_{safe}, and rewrite it as:

$$\begin{bmatrix} 1 & -t_{TCC} - VTH \\ 1 & -VTH \end{bmatrix} \begin{bmatrix} \Delta d \\ v_{rel} \end{bmatrix} \geq \begin{bmatrix} VTH \cdot v_{pre} - d_{min} \\ -VTH \cdot v_{pre} \end{bmatrix} \tag{4.41}$$

For boundary condition 4.32, it can be transformed into system output constraints:

$$\begin{bmatrix} \Delta d_{min} \cdot S_{DE}^{-1} \\ v_{rel,min} \cdot S_{VE}^{-1} \\ a_{host,min} \end{bmatrix} \leq \boldsymbol{y} \leq \begin{bmatrix} \Delta d_{max} \cdot S_{DE}^{-1} \\ v_{rel,max} \cdot S_{VE}^{-1} \\ a_{host,max} \end{bmatrix} \tag{4.42}$$

Until here, the multi-objective optimization for the car following scenario is well-designed. The next step is to merge the overall optimization problem, including cost function and various constraints, into the framework of the MPC algorithm to realize closed-loop control.

4.1.4. Energy Consumption Minimization Considering SPaT Information and Preceding Vehicle Based on NLMPC

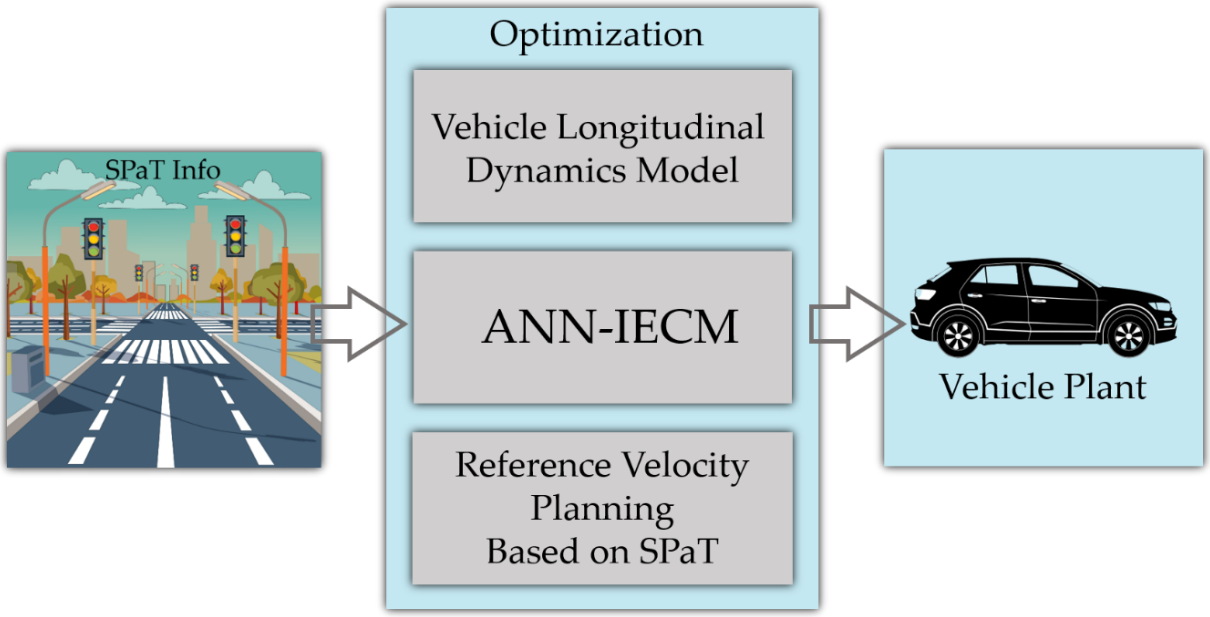

Fig. 4.8 Fundamental Concept of Signal Anticipation Scenario

When the host vehicle is driving in the signal anticipation scenario based on the driving scenario switching logic (DSSL) defined in Chapter 2 – 2.1.2, the predictive cruise control system enters the optimization problem defined in equation 4.54. within the nonlinear equality constrains 4.56-4.57, linear inequality constraints 4.58 – 4.62. At each sampling time t, a reference velocity is obtained based on the reference velocity planning algorithm using real-time SPaT information, which is a velocity that can pass the upcoming signalized intersection without any stop, i.e., always capture the green timing of traffic lights crossing the intersection. The cost function in equation 4.54 takes the obtained reference velocity to execute the optimization. The first term of equation 4.54 is to minimize the energy consumption of the vehicle during the signal anticipation. If the first term is only existing, the vehicle would have no moving motivation because the first term forces the vehicle to consume as little energy as possible. Therefore, the second term is required to penalize the error between actual driving velocity and reference velocity so that the host vehicle can track the reference velocity at each moment in the signal anticipation scenario to realize passing signalized intersection without any stop and further minimize the energy consumption. The third term is introduced with the slack factor ε to minimize the variation

rate of acceleration – jerk, so that the driving comfortability during signal anticipation scenario is guaranteed. The velocity is bounded with the road section speed limitation in equation 4.58. The vehicle acceleration, motor torque, and motor speed are all limited by the technical characteristics of the vehicle itself in equations 4.59, 4.61, and 4.62, respectively. After solving the nonlinear optimization problem with nonlinear constraints in each time step, an optimal control sequence can be obtained, and use the first control in the sequence as the vehicle's input. Such an nonlinear online optimization is rolling forward with the moving of the prediction horizon to achieve real-time reference velocity tracking to minimize energy consumption. The Controller Structure of the signal anticipation scenario is shown as Figure 4.8.

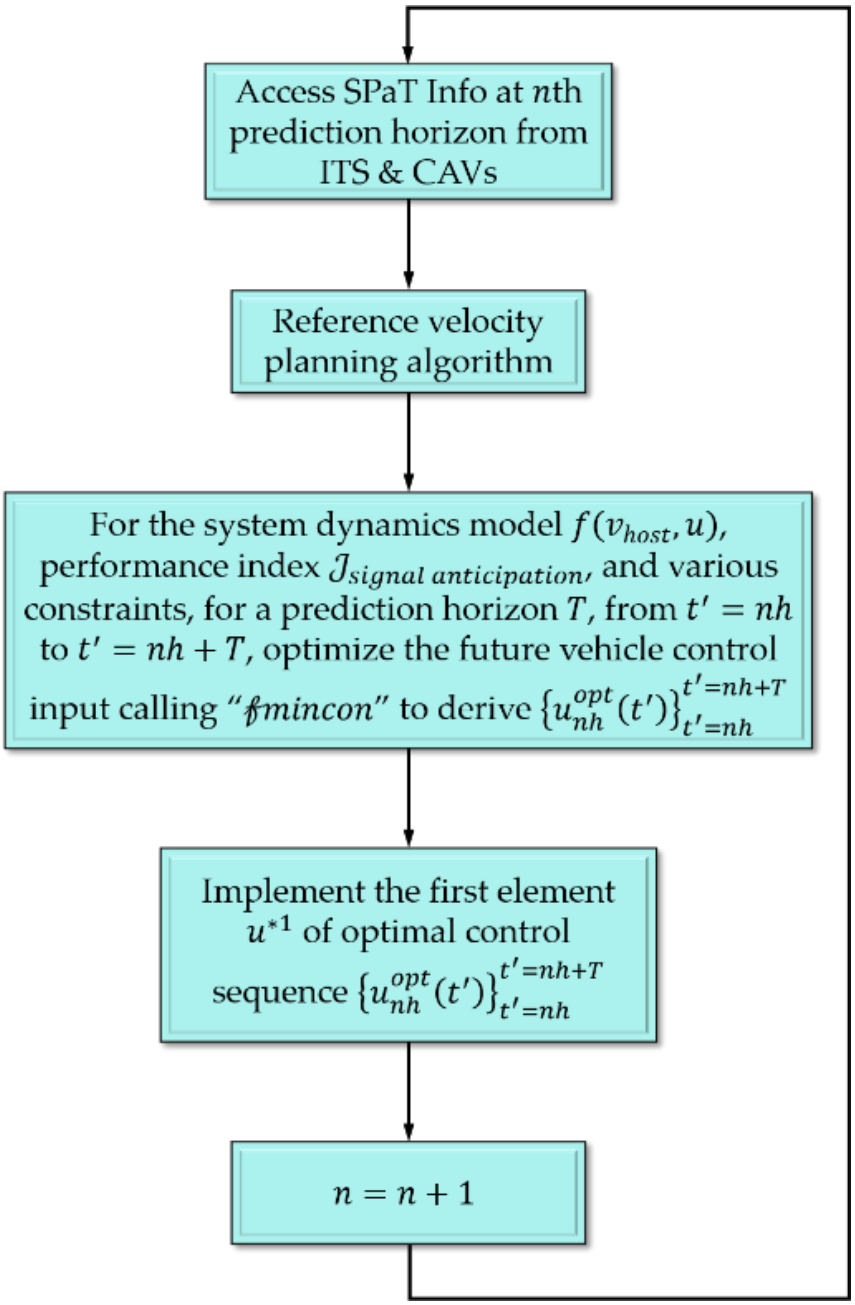

Fig. 4.9 Workflow of The MPC Problem for Signal Anticipation Scenario

Rewrite the vehicle longitudinal dynamics model in Chapter 2 – 2.2.1 into a state equation:

$$f(v_{host},u)=\begin{bmatrix} v_{host} \\ (-\frac{1}{2m_{eq}}\rho_a A_f C_D v_{host}^2 - c_r g\cos\theta - g\sin\theta)+u \end{bmatrix} \tag{4.43}$$

$$\mathcal{L}=w_{E_{ins}}[E_{ins}(v_{host},a_{host},T_m,\omega_m)]+w_{v_e}\left(v_{host}-v_{ref}\right)^2+w_\varepsilon\varepsilon^2 \tag{4.44}$$

$$\underset{u}{\text{Min}}\,\mathcal{J}_{signal\ anticipation}=\int_t^{t+T}\mathcal{L}[v_{host}(t'),u(t')]\,dt' \tag{4.45}$$

$s.t.$

$$a_{host}=\frac{1}{m_{eq}}\left[-c_r m_{eq} g\cos\theta - m_{eq} g\sin\theta-\frac{1}{2}\rho_a A_f C_D v_{host}^2\right]+u \tag{4.46}$$

$$E_{ins}=IECM\left(v_{host},a_{host},T_{m,host},\omega_{m,host}\right) \tag{4.47}$$

$$v_{min}\le v_{host}\le v_{max} \tag{4.48}$$

$$a_{min}\le a_{host}\le a_{max} \tag{4.49}$$

$$\dot{a_{min}}-\varepsilon\le\dot{a_{host}}\le\dot{a_{max}}+\varepsilon \tag{4.50}$$

$$0\le T_m\le T_{m,max} \tag{4.51}$$

$$0\le\omega_m\le\omega_{m,max} \tag{4.52}$$

During the prediction horizon T, the weights here $w_{E_{ins}}$, w_{v_e}, and w_ε are chosen with the criterion that normal magnitudes of cost terms are balanced. Finally, the weights can be tuned through the observation of simulation results to maximize the energy economy. To solve the above nonlinear optimization problem and derive the optimal control sequence, the encapsulated function "$fmincon$" with sequential quadratic programming (SQP) algorithm from MATLAB is called. The workflow of the MPC problem for the signal anticipation scenario is shown in Figure 4.9.

4.1.5. Energy Consumption Minimization Considering Road Grade Based on NLMPC

When the driving scenario switching logic (DSSL) selects the free driving mode, the vehicle starts eco-driving in scenario accessing the upcoming road gradients information. The basic concept is that predictive cruise control system utilizes the vehicle longitudinal dynamics model combined with ANN-IECM to calculate the optimal control input based on the information of specific road altitude of the driving position to improve the energy economy over free travel distance. In the real implementation, the information of real-time road altitude is provided by ITS. The basic concept of the free driving scenario is demonstrated in Figure 4.10.

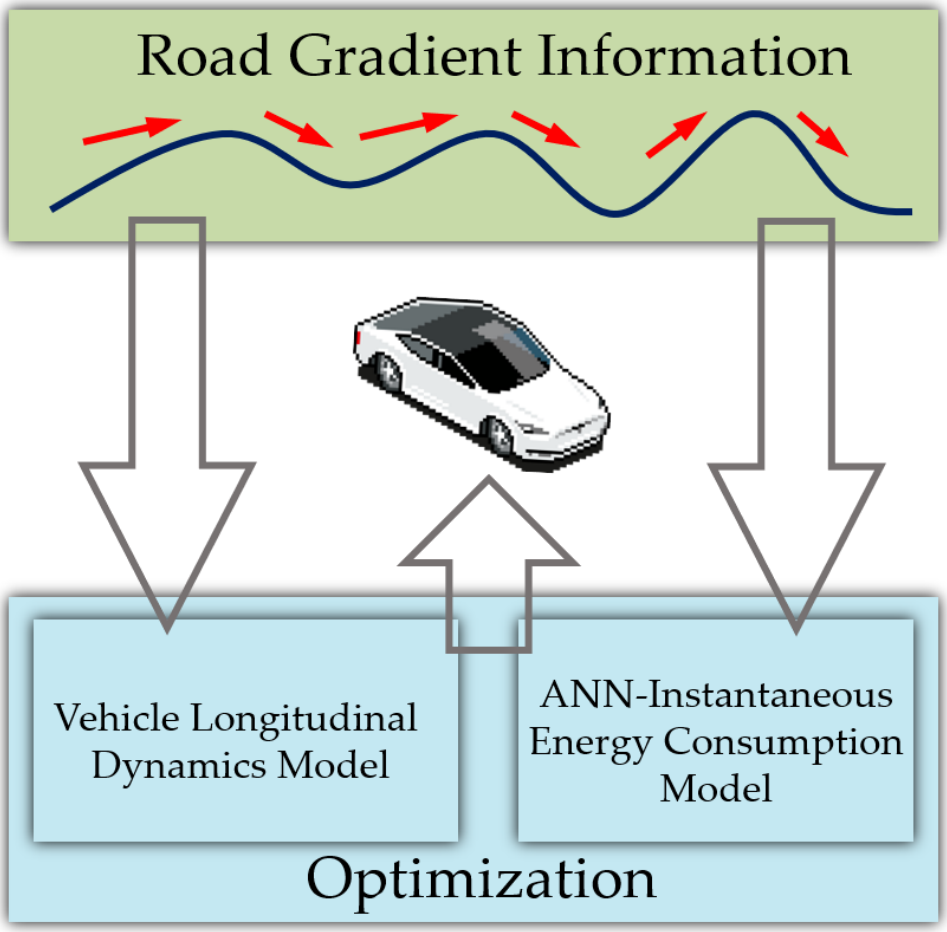

Fig. 4.10 Basic Concept of Free Driving Scenario

Based on the vehicle longitudinal dynamics model proposed in Chapter 2 – 2.2.1, the state-space equation of the vehicle in the free driving scenario can be expressed as:

$$f(v_{host}, u) = \begin{bmatrix} v \\ (-\frac{1}{2m_{eq}}\rho_a A_f C_D v_{host}^2 - c_r g\cos\theta(x) - g\sin\theta(x)) + u \end{bmatrix} \tag{4.53}$$

The road gradient $\theta(x)$ can be calculated using the real-time road altitude information $\hbar(x)$ as [87]:

$$\theta(x) = \tan^{-1}\left[\frac{\hbar(x+\Delta x) - \hbar(x-\Delta x)}{2\Delta x}\right] \tag{4.54}$$

The cost function in the free driving scenario is defined as:

$$\mathcal{L}(u) = w_{E_{ins}} E_{ins}(v_{host}, a_{host}, T_m, \omega_m) + w_v(v_{host} - v_{desired})^2 + w_u u^2 \tag{4.55}$$

The performance index thereby can be written as:

$$\min_u \mathcal{J}_{free\ driving} = \int_t^{t+T} \mathcal{L}(u)dt \tag{4.56}$$

$s.t.$

$$a_{host} = (-\frac{1}{2m_{eq}}\rho_a A_f C_D v_{host}^2 - c_r g\, cos\, \theta(x) - g\, sin\, \theta(x)) + u \tag{4.57}$$

$$E_{ins} = IECM\left(v_{host}, a_{host}, T_{m,host}, \omega_{m,host}\right) \tag{4.58}$$

$$u_{min} \leq u(t) \leq u_{max} \tag{4.59}$$

$$v_{min} \leq v(t) \leq v_{max} \tag{4.60}$$

where, the most important parameter is the $v_{desired}$. Basically, the efficiency of the electric motor is relatively stable, which features the broad high efficiency range and energy conversion efficiency. However, the power in the high rotation speed will decline; and the aerodynamics resistance will be the main source of energy consumption when the vehicle velocity is faster than $60km/h$. Therefore, the most energy-efficient driving velocity for electric vehicle will be $50{\sim}60km/s$. Hence, the $v_{dedired}$ for the free driving scenario is set by $15.28m/s$ ($55km/h$).

T is the prediction horizon of the MPC algorithm, during which the optimal control inputs are calculated, u is the optimal acceleration command. Given the performance index 4.66, T is discretized into N steps with size h. For each prediction horizon, the future vehicle control sequence $\{u_{nh}(t)\}_{t=nh}^{t=nh+T}$ are obtained. Then, the first element of the sequence is input into the vehicle plant. The first term in the cost function is to minimize the overall energy consumption during the prediction horizon T. The second term is to penalize the deviation of the actual vehicle velocity v_{host} from the desired energy-efficient velocity $v_{desired}$. The third term is the cost for acceleration command to avoid hard input because of tracking the desired velocity. $w_{E_{ins}}$, w_v and w_u are the weight factors for each term, respectively.

Similarly, the encapsulated function "$fmincon$" with sequential quadratic programming (SQP) algorithm from MATLAB is called, to solve this nonlinear optimization problem. The workflow of the MPC problem for the free driving scenario is demonstrated in Figure 4.11.

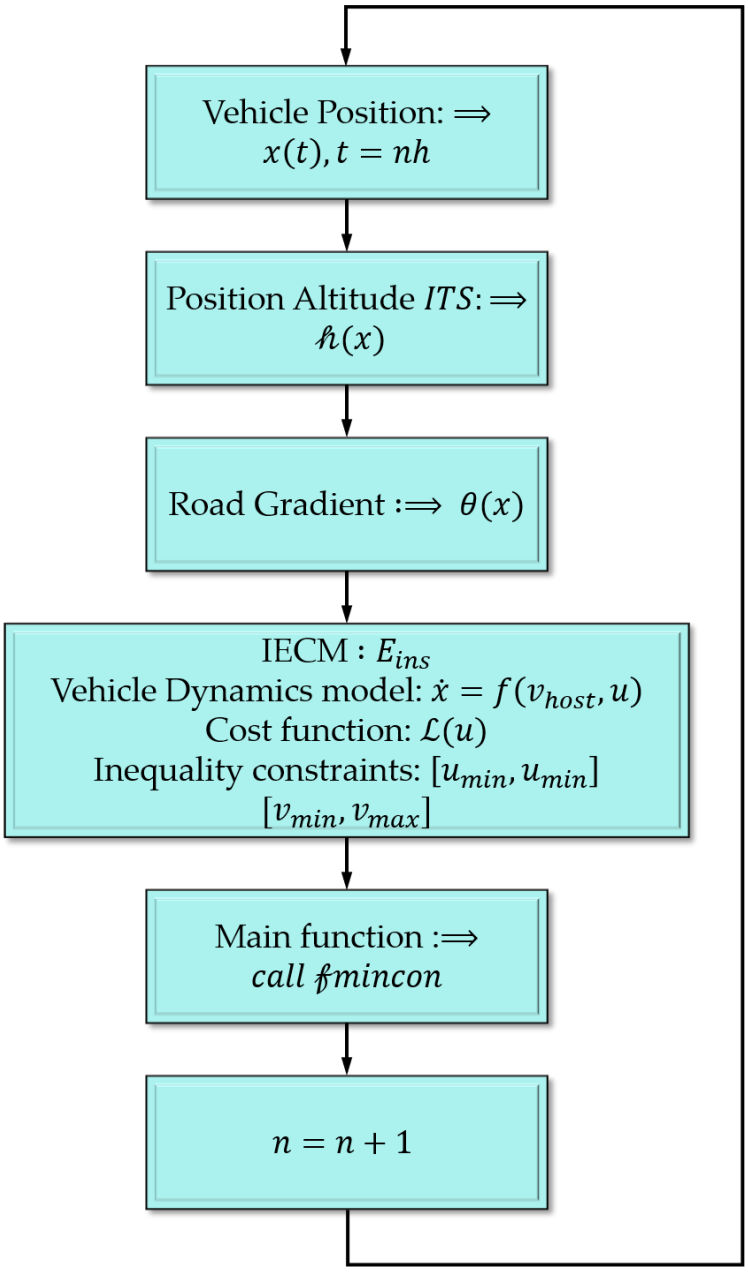

Fig. 4.11 Workflow of MPC Problem for Free Driving Scenario

4.2. Derivation of Predictive Optimization Problem

The basic principle of MPC is to predict the system future state variable based on the current system state. Then, based on the predicted state and control input, an optimization problem is presented and solved using the numerical method during the prediction horizon. For the linear MPC problem for the car following scenario, the mathematical derivations of the predictive optimization problem are discussed in this section based on the system state equation, cost function and corresponding constraints proposed in the previous section.

4.2.1. Predictive Model Transformation of Inter-Vehicle Longitudinal Dynamics Model

The discrete inter-vehicle longitudinal dynamics model was derived previously as follow:

$$\begin{aligned} \boldsymbol{x}(k+1) &= \bar{\boldsymbol{A}}\boldsymbol{x}(k) + \bar{\boldsymbol{B}}u(k) + \bar{\boldsymbol{G}}w(k) \\ \boldsymbol{y}(k) &= \boldsymbol{C}\boldsymbol{x}(k) \end{aligned} \tag{4.61}$$

Assume current time instant is k, prediction horizon is p, then inter-vehicle longitudinal dynamics model during the prediction horizon p can be written as:

$$\boldsymbol{X}(k+p|k) = \boldsymbol{A}_x\boldsymbol{x}(k) + \boldsymbol{B}_x\boldsymbol{U}(k+m) + \boldsymbol{G}_x\boldsymbol{W}(k+p) \tag{4.62}$$

where p and m are the prediction horizon and control horizon of MPC, respectively, and $m \leq p$.

The coefficient matrices can be derived as:

$$\boldsymbol{X}(k+p|k) = \begin{bmatrix} x(k+1|k) \\ x(k+2|k) \\ \vdots \\ x(k+p|k) \end{bmatrix}, \boldsymbol{A}_x = \begin{bmatrix} \overline{\boldsymbol{A}} \\ \overline{\boldsymbol{A}}^2 \\ \vdots \\ \overline{\boldsymbol{A}}^p \end{bmatrix}, \boldsymbol{U}(k+m) = \begin{bmatrix} u(k) \\ u(k+1) \\ \vdots \\ u(k+m-1) \end{bmatrix}, \boldsymbol{W}(k+p) = \begin{bmatrix} \boldsymbol{w}(k) \\ \boldsymbol{w}(k+1) \\ \vdots \\ \boldsymbol{w}(k+p-1) \end{bmatrix},$$

$$\boldsymbol{B}_x = \begin{bmatrix} \overline{\boldsymbol{B}} & \boldsymbol{0} & \cdots & \boldsymbol{0} \\ \overline{\boldsymbol{A}}\overline{\boldsymbol{B}} & \overline{\boldsymbol{B}} & \cdots & \boldsymbol{0} \\ \vdots & \vdots & \ddots & \vdots \\ \overline{\boldsymbol{A}}^{p-1}\overline{\boldsymbol{B}} & \overline{\boldsymbol{A}}^{p-2}\overline{\boldsymbol{B}} & \cdots & \sum_{z=0}^{p-m}\overline{\boldsymbol{A}}^z\,\overline{\boldsymbol{B}} \end{bmatrix}, \boldsymbol{G}_x = \begin{bmatrix} \overline{\boldsymbol{G}} & \boldsymbol{0} & \cdots & \boldsymbol{0} \\ \overline{\boldsymbol{A}}\overline{\boldsymbol{G}} & \overline{\boldsymbol{G}} & \cdots & \boldsymbol{0} \\ \vdots & \vdots & \ddots & \vdots \\ \overline{\boldsymbol{A}}^{p-1}\overline{\boldsymbol{G}} & \overline{\boldsymbol{A}}^{p-2}\overline{\boldsymbol{G}} & \cdots & \sum_{z=0}^{p-m}\overline{\boldsymbol{A}}^z\,\overline{\boldsymbol{G}} \end{bmatrix}.$$

Correspondingly, the system output for the future $k+1, \cdots, k+p$ time instant can be predicted as:

$$\boldsymbol{Y}(k+p|k) = \boldsymbol{A}_y\boldsymbol{x}(k) + \boldsymbol{B}_y\boldsymbol{U}(k+m) + \boldsymbol{G}_y\boldsymbol{W}(k+p) \tag{4.63}$$

where,

$$\boldsymbol{Y}(k+p|k) = \begin{bmatrix} \boldsymbol{y}(k+1|k) \\ \boldsymbol{y}(k+2|k) \\ \vdots \\ \boldsymbol{y}(k+p|k) \end{bmatrix}, \boldsymbol{A}_x = \begin{bmatrix} \boldsymbol{C}\overline{\boldsymbol{A}} \\ \boldsymbol{C}\overline{\boldsymbol{A}}^2 \\ \vdots \\ \boldsymbol{C}\overline{\boldsymbol{A}}^p \end{bmatrix},$$

$$\boldsymbol{B}_y = \begin{bmatrix} \boldsymbol{C}\overline{\boldsymbol{B}} & \boldsymbol{0} & \cdots & \boldsymbol{0} \\ \boldsymbol{C}\overline{\boldsymbol{A}}\overline{\boldsymbol{B}} & \boldsymbol{C}\overline{\boldsymbol{B}} & \cdots & \boldsymbol{0} \\ \vdots & \vdots & \ddots & \vdots \\ \boldsymbol{C}\overline{\boldsymbol{A}}^{p-1}\overline{\boldsymbol{B}} & \boldsymbol{C}\overline{\boldsymbol{A}}^{p-2}\overline{\boldsymbol{B}} & \cdots & \sum_{z=0}^{p-m}\boldsymbol{C}\overline{\boldsymbol{A}}^z\,\overline{\boldsymbol{B}} \end{bmatrix}, \boldsymbol{G}_x = \begin{bmatrix} \boldsymbol{C}\overline{\boldsymbol{G}} & \boldsymbol{0} & \cdots & \boldsymbol{0} \\ \boldsymbol{C}\overline{\boldsymbol{A}}\overline{\boldsymbol{G}} & \boldsymbol{C}\overline{\boldsymbol{G}} & \cdots & \boldsymbol{0} \\ \vdots & \vdots & \ddots & \vdots \\ \boldsymbol{C}\overline{\boldsymbol{A}}^{p-1}\overline{\boldsymbol{G}} & \boldsymbol{C}\overline{\boldsymbol{A}}^{p-2}\overline{\boldsymbol{G}} & \cdots & \sum_{z=0}^{p-m}\boldsymbol{C}\overline{\boldsymbol{A}}^z\,\overline{\boldsymbol{G}} \end{bmatrix}.$$

4.2.2. Predictive Model Transformation of Constraints and Cost Function

The cost function for car following scenario was defined as follow:

$$\mathcal{J}_{car-following} = \boldsymbol{y}^T\boldsymbol{w}_y\boldsymbol{y} + w_u u^2 + w_{du}\dot{u}^2 \tag{4.64}$$

where,

$$\boldsymbol{w}_y = \begin{bmatrix} w_{\Delta d} & 0 & 0 \\ 0 & w_{v_{rel}} & 0 \\ 0 & 0 & w_a \end{bmatrix}.$$

The predictive form transformation can be written as follow [152]~[156]:

$$\boldsymbol{\mathcal{J}}_{car-following} = \sum_{i=1}^{p} \|\boldsymbol{y}(k+i|k)\|^2_{w_y(k+i|k)} + \|\boldsymbol{u}(k+i|k)\|^2_{w_u} + \|\Delta\boldsymbol{u}(k+i|k)\|^2_{w_{\Delta u}} \tag{4.65}$$

where,

$$w_y(k+i|k) = \begin{bmatrix} w_{\Delta d}(k+i|k) & 0 & 0 \\ 0 & w_{v_{rel}}(k+i|k) & 0 \\ 0 & 0 & w_a(k+i|k) \end{bmatrix}$$

where, $\boldsymbol{\mathcal{J}}_{car-follwing}$ is the cost function in the prediction horizon, $(k+i|k)$ means that the system predicts the state information of $k+i$ time instant at k instant. $\Delta\boldsymbol{u}$, the control increment, is written as follow:

$$\Delta\boldsymbol{u}(k+i|k) = \boldsymbol{u}(k+i|k) - \boldsymbol{u}(k+i-1|k) \tag{4.66}$$

Note that the Δu is the discretized difference, which is correlated with $\dot{u}$ by following relation:

$$\dot{u} = \frac{\Delta u}{T_s} \tag{4.67}$$

where T_s is the sampling period.

Hence, the $w_{\Delta u}$ of the Δu is different from w_{du} of $\dot{u}$ as:

$$w_{\Delta u} = \frac{w_{du}}{T_s^2} \tag{4.68}$$

The constraint for driving safety was proposed previously as follow:

$$\begin{bmatrix} 1 & -t_{TCC} - VTH \\ 1 & -VTH \end{bmatrix} \begin{bmatrix} \Delta d \\ v_{rel} \end{bmatrix} \geq \begin{bmatrix} VTH \cdot v_{pre} - d_{min} \\ -VTH \cdot v_{pre} \end{bmatrix} \tag{4.69}$$

The prediction form of it can be written as:

$$\begin{bmatrix} 1 & -t_{TCC} - VTH & 0 \\ 1 & -VTH & 0 \\ 0 & 0 & 0 \end{bmatrix} \boldsymbol{y}(k+i|k) \geq \begin{bmatrix} TH \cdot v_{pre} \\ -VTH \cdot v_{pre} \\ 0 \end{bmatrix} v_{pre}(k+i|k) + \begin{bmatrix} -d_{min} \\ 0 \\ 0 \end{bmatrix} \tag{4.70}$$

The car following constraints can be written into prediction form as:

$$\boldsymbol{y}_{min} \leq \boldsymbol{y}(k+i|k) \leq \boldsymbol{y}_{max} \tag{4.71}$$

$$\boldsymbol{y}_{min} = \begin{bmatrix} \Delta d_{min} \cdot S_{DE}^{-1} \\ v_{rel,min} \cdot S_{VE}^{-1} \\ a_{host,min} \end{bmatrix}, \boldsymbol{y}_{max} = \begin{bmatrix} \Delta d_{max} \cdot S_{DE}^{-1} \\ v_{rel,max} \cdot S_{VE}^{-1} \\ a_{host,max} \end{bmatrix}$$

where $\boldsymbol{y}_{min}$ and $\boldsymbol{y}_{max}$ are the system output lower and lower boundary, respectively.

The constraints of driving comfortability can be rewritten in predictive form as:

$$\begin{aligned} u_{min} \leq u(k+i|k) \leq u_{max} \\ \Delta u_{min} \leq \Delta u(k+i|k) \leq \Delta u_{max} \end{aligned} \tag{4.72}$$

4.2.3. Predictive Optimization Problem Construction

To sum up, the predictive optimization problem of MPC for car following scenario can be integrated as follow:

$$\min \boldsymbol{J}(\boldsymbol{y}, u, \Delta u) \tag{4.73}$$

$s.t.$

discretized inter-vehicle longitudinal dynamics state-space equation (4.62, 4.63)

driving safety constraints (4.69)
car following constraints (4.71)
driving comfortability (4.72)

4.3. System Robustness Enhancement Based on Feedback Correction

Despite the superiority of MPC that can handle the optimization with multiple objectives, it still has its limitations that can be concluded as follow:

Due to the modeling error, uncertainty and time-variability of modeling parameters, and external disturbance, there are some errors between the inter-vehicle longitudinal dynamics prediction model and real states, which make the model cannot accurately reflect the characteristics of car following. The poor robustness of the system will not only lower the capability of car following but also has an impact on the energy economy of the vehicle cruise. Garcia [157] once also pointed out that linear MPC does not have good robustness under the circumstance of without constraints. Therefore, in order to improve the robustness of the proposed predictive cruise control system based on the MPC algorithm, it is indispensable to find a solution to make up this shortcoming.

Basically, there are three methods to overcome the low robustness of MPC, including feedback correction method[158], hybrid control method[159], Min-Max method [160]. The principle of feedback correction is to

take the error between prediction value from the model and actual measurement as the feedback correction term to improve the prediction accuracy. The concept of the hybrid control method is to control the certainty using MPC and uncertainty using other control method, dealing with them separately. The principle of the third method is to transform the prediction problem in the infinite time domain of MPC into a Min-Max Value problem. Although the hybrid control method is capable of improving the robustness of system, it may also compromise the optimality of the control algorithm. The issue of the Min-Max method is that it may cause low computation efficiency and decrease the feasible region range. Therefore, in this research, the feedback correction method is used to improve the system robustness. The block diagram of MPC with feedback correction is shown in Figure 4.12.

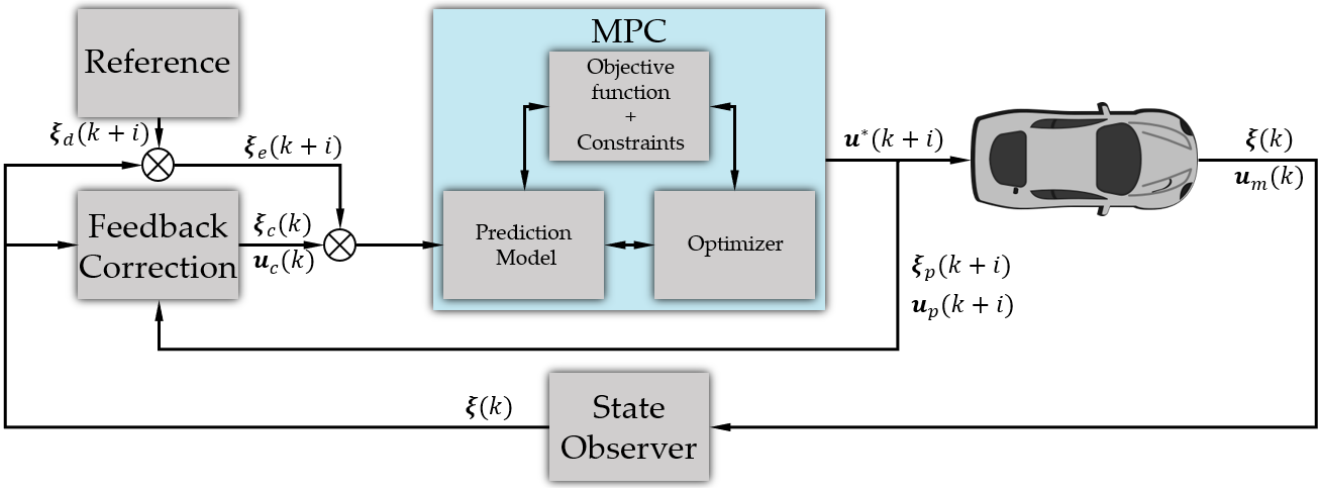

Fig. 4.12 Block Diagram of MPC with Feedback Correction

Now define the error at time instant k between prediction state from inter-vehicle dynamics model and actual state from state observer is ξ_e, which can be expressed as follow:

$$\boldsymbol{\xi}_e = \boldsymbol{x}(k) - \boldsymbol{x}(k|k-1) \tag{4.74}$$

where $x(k)$ is the actual state between host and preceding vehicle at time instant k, $x(k|k-1)$ is the state at k being predicted at $k-1$.

According to the prediction form of the inter-vehicle longitudinal dynamics model, the following equation can be obtained:

$$\boldsymbol{x}(k|k-1) = \bar{\boldsymbol{A}}\boldsymbol{x}(k-1) + \bar{\boldsymbol{B}}u(k-1) + \bar{\boldsymbol{G}}w(k-1) \tag{4.75}$$

where $\boldsymbol{x}(k|k-1)$ is the system state at time instant $k-1$, $u(k-1)$ is the control input at the $k-1$ time instant, $w(k-1)$ is the external disturbance at time instant $k-1$.

To improve the prediction accuracy at instant k, the following equation can be obtained using error $\boldsymbol{\xi}_e(k)$ and actual measurement $\boldsymbol{x}(k+1|k)$:

$$\boldsymbol{x}(k+1|k) = \bar{\boldsymbol{A}}\boldsymbol{x}(k) + \bar{\boldsymbol{B}}u(k-1) + \bar{\boldsymbol{B}}\Delta u(k+0|k) + \bar{\boldsymbol{G}}w(k) + \boldsymbol{H}\boldsymbol{\xi}_e(k) \tag{4.76}$$

where $\Delta u(k+0|k)$ is the control increment at time instant $k+0|k$, $\boldsymbol{H}$ is the correction matrix as follow:

$$\boldsymbol{H} = \begin{bmatrix} h_1 & \cdots & 0 \\ \vdots & \ddots & \vdots \\ 0 & \cdots & h_n \end{bmatrix}, h_i \in (0,1) \tag{4.77}$$

According to the equation 7.83 and 7.84, it is known that $\xi_e(k)$ describes the error between prediction and actual measurement value at time instant k. Thus, the $\xi_e(k)$ can be used at instant $k+1$ to compensate the error of prediction, so as to improve the prediction accuracy.

The prediction form of robust inter-vehicle longitudinal dynamics model can thereby be derived as follow [155]:

$$\boldsymbol{Y} = [\boldsymbol{R}_x + \boldsymbol{R}_e\boldsymbol{H}]x(k) + \boldsymbol{R}_u\boldsymbol{u}(k-1) + \boldsymbol{R}_{\Delta u}\Delta\boldsymbol{U} - \boldsymbol{R}_e\boldsymbol{H}\boldsymbol{x}(k|k-1) + \boldsymbol{H}_w\boldsymbol{W} \tag{4.78}$$

where system output within prediction horizon $\boldsymbol{Y}$, system control input $\boldsymbol{U}$, control increment $\Delta\boldsymbol{U}$, and system disturbance $\boldsymbol{W}$ is derived as [155]:

$$\boldsymbol{Y} = \begin{bmatrix} \boldsymbol{y}(k+1|k) \\ \boldsymbol{y}(k+2|k) \\ \vdots \\ \boldsymbol{y}(k+p|k) \end{bmatrix}, \boldsymbol{U} = \begin{bmatrix} u(k+0|k) \\ u(k+1|k \\ \vdots \\ u(k+p-1|k \end{bmatrix}, \Delta\boldsymbol{U} = \begin{bmatrix} \Delta u(k+0|k) \\ \Delta u(k+1|k) \\ \vdots \\ \Delta u(k+p-1|k) \end{bmatrix}, \boldsymbol{W} = \begin{bmatrix} w(k+0|k) \\ w(k+1|k \\ \vdots \\ w(k+p-1|k \end{bmatrix}$$

$$\boldsymbol{R}_x = \begin{bmatrix} \boldsymbol{C}\overline{\boldsymbol{A}} \\ \boldsymbol{C}\overline{\boldsymbol{A}}^2 \\ \vdots \\ \boldsymbol{C}\overline{\boldsymbol{A}}^p \end{bmatrix}, \boldsymbol{R}_e = \begin{bmatrix} \boldsymbol{C}\overline{\boldsymbol{A}} \\ \boldsymbol{C}\overline{\boldsymbol{A}}^2 \\ \vdots \\ \boldsymbol{C}\overline{\boldsymbol{A}}^{p-1} \end{bmatrix}, \boldsymbol{R}_u = \begin{bmatrix} \boldsymbol{C}\overline{\boldsymbol{B}} \\ \boldsymbol{C}(\overline{\boldsymbol{A}}\overline{\boldsymbol{B}} + \overline{\boldsymbol{B}}) \\ \vdots \\ \boldsymbol{C}\sum_{m=0}^{p-1} C\overline{\boldsymbol{A}}^m\overline{\boldsymbol{B}} \end{bmatrix},$$

$$\boldsymbol{R}_{\Delta u} = \begin{bmatrix} \boldsymbol{C}\overline{\boldsymbol{B}} & 0 & \cdots & 0 \\ \boldsymbol{C}(\overline{\boldsymbol{A}}\overline{\boldsymbol{B}} + \overline{\boldsymbol{B}}) & \boldsymbol{C}\overline{\boldsymbol{B}} & \cdots & 0 \\ \vdots & \vdots & \vdots & \vdots \\ \boldsymbol{C}\sum_{m=0}^{p-1} C\overline{\boldsymbol{A}}^m\overline{\boldsymbol{B}} & \boldsymbol{C}\sum_{m=0}^{p-2} C\overline{\boldsymbol{A}}^m\overline{\boldsymbol{B}} & \cdots & \boldsymbol{C}\overline{\boldsymbol{B}} \end{bmatrix}, \boldsymbol{H}_w = \begin{bmatrix} \boldsymbol{C}\overline{\boldsymbol{G}} & 0 & \cdots & 0 \\ \boldsymbol{C}\overline{\boldsymbol{A}}\overline{\boldsymbol{G}} & \boldsymbol{C}\overline{\boldsymbol{G}} & \cdots & 0 \\ \vdots & \vdots & \vdots & \vdots \\ \boldsymbol{C}\overline{\boldsymbol{A}}^{p-1}\overline{\boldsymbol{G}} & \boldsymbol{C}\overline{\boldsymbol{A}}^{p-2}\overline{\boldsymbol{G}} & \cdots & \boldsymbol{C}\overline{\boldsymbol{G}} \end{bmatrix}.$$

4.4. Summary of Chapter 4

This chapter presented the core methodology used to develop the predictive cruise control system for eco-driving ---- model predictive control (MPC) algorithm. The basic concept of MPC theory the essential understanding to the MPC was introduced. What follows was a complete demonstration using MPC to realize vehicle velocity tracking, from mathematical derivation to simulation realization. After that, three representative predictive optimization problems for driving scenarios, including car following scenario, signal anticipation scenario, and free driving scenario, were discussed in detail based on rigorous mathematical derivation. For signal anticipation scenario and free driving scenario, nonlinear MPC problems were formulated with corresponding algorithm workflows. For the car following scenario, the derivations of predictive model transformation were presented for linear MPC, which can be transformed into a quadratic programming (QP) problem. Finally, the MPC-based system robustness was especially proposed and solved using the feedback correction method.

Chapter 5. Simulation Experiments of Predictive Cruise Control for Eco-Driving

According to the artificial neural network-based instantaneous energy consumption model (ANN-IECM) developed in Chapter 3, and the model predictive control (MPC) algorithm based predictive cruise control system for eco-driving proposed in Chapter 4, this chapter is intended to conduct the simulation experiments to validate the concept and models based on the idea of comparative analysis. At first, the co-simulation platform is established based on the CarSim and MATLAB/Simulink, laying the foundation for the subsequent case studies. Then, respective case study for each typical driving scenario is conducted to test the effectiveness of energy-saving. Finally, a comprehensive simulation test is designed for a mixed driving scenario to verify the capability of handling the integrated day-to-day traffic situation and energy economy improvement of the proposed PCC system.

5.1. Establishment of Simulation Platform Based on CarSim and MATLAB/Simulink

CarSim® is a software that precisely predicts the performance of the vehicle in response to driver controls in a user-defined environment. It provides integrated vehicle dynamics simulation for conventional ICE vehicles, hybrid vehicles, and electric vehicles. MATLAB/Simulink is more focused on the development of the control system. The connection port provided within CarSim makes it possible to link with MATLAB/Simulink. Therefore, the co-simulation based on these two platforms realizes the integrated analysis of mechatronics.

To begin with, the simulation platforms for three representative driving scenarios (car following scenario, signal anticipation scenario, free driving scenario) are established, respectively. The first step is conducting parametric modeling within CarSim according to the configuration Table 5.1, and set the inputs and outputs of the vehicle dynamics model, shown in Figure 5.1.

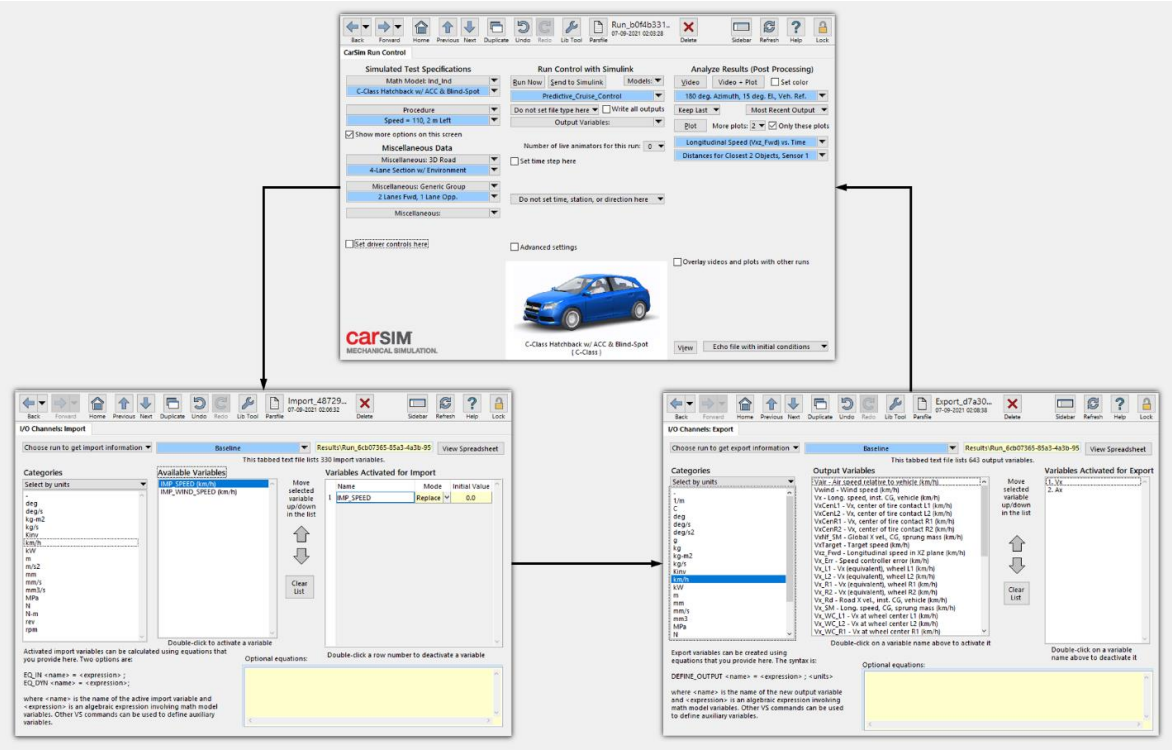

Fig. 5.1 Parametric Modeling of Vehicle Dynamics within CarSim

Once completing the settings within CarSim, “Send to Simulink” button can connect the CarSim with the MATLAB/Simulink. Then, the detailed predictive cruise control system can be developed within the Simulink environment. The respective simulation environments are shown in Figure 5.2.

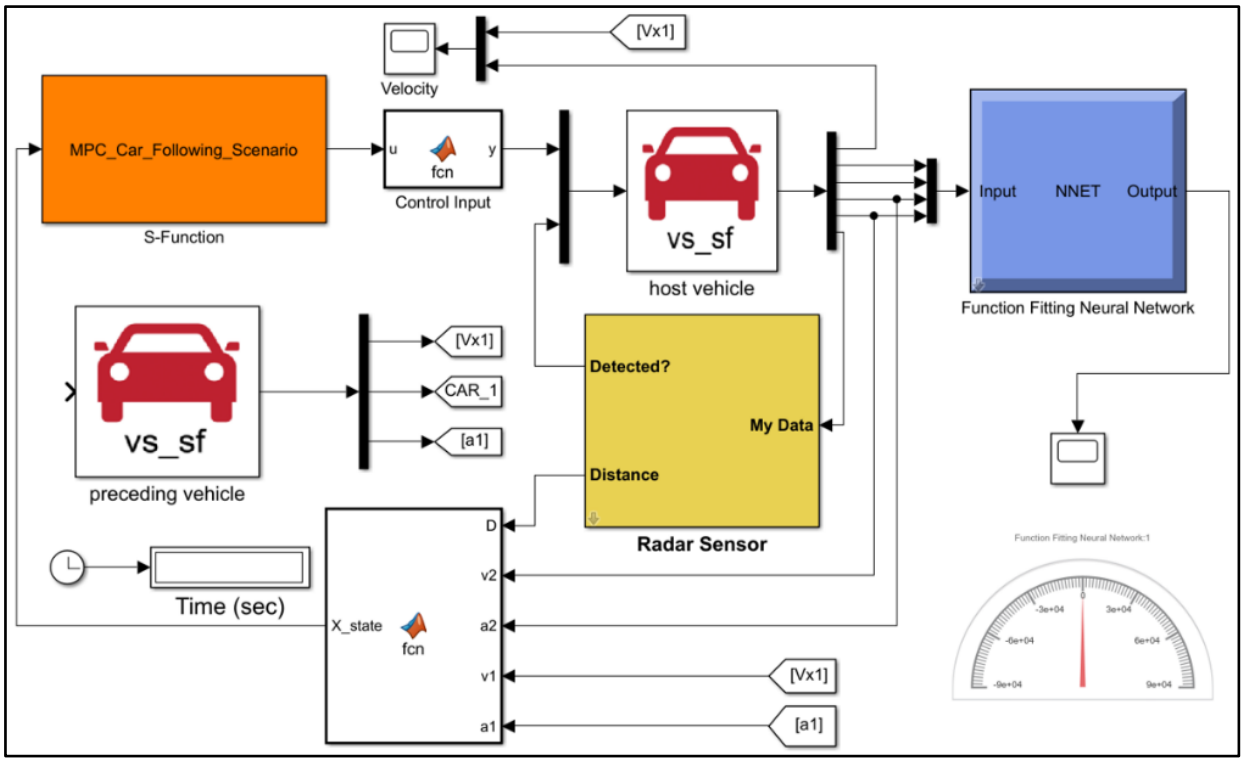

Fig. 5.2.1 Simulation Platform of Car Following Scenario

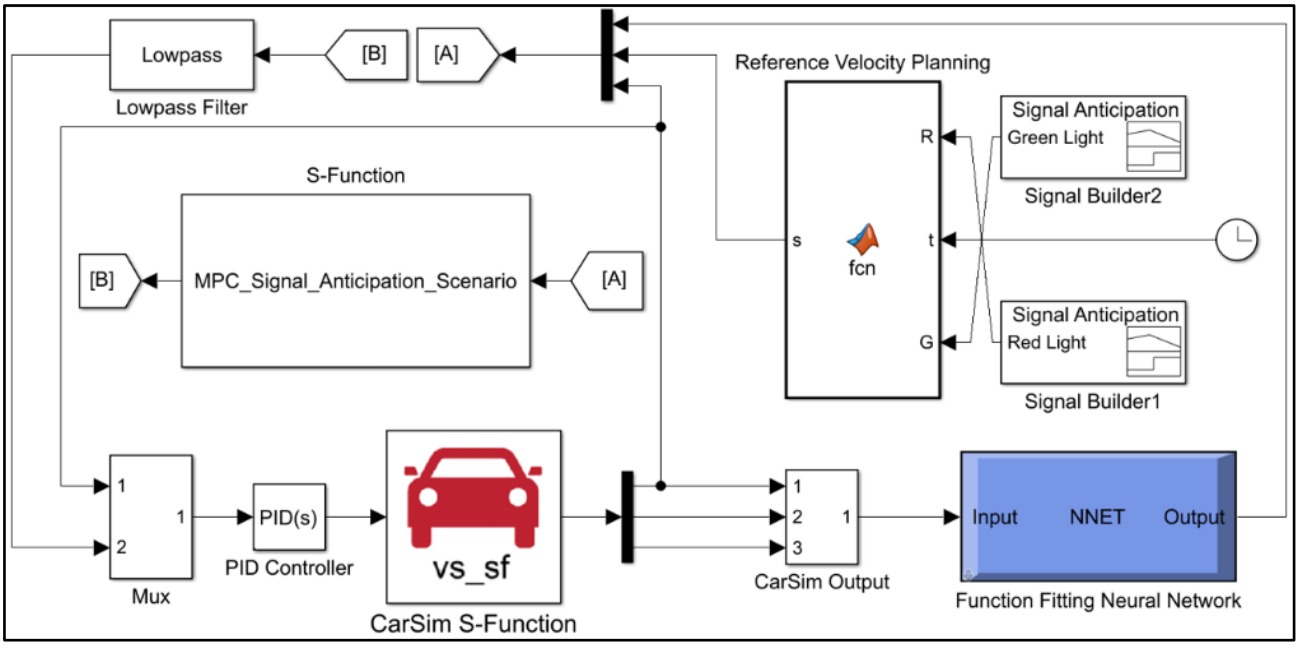

Fig. 5.2.2 Simulation Platform of Signal Anticipation Scenario

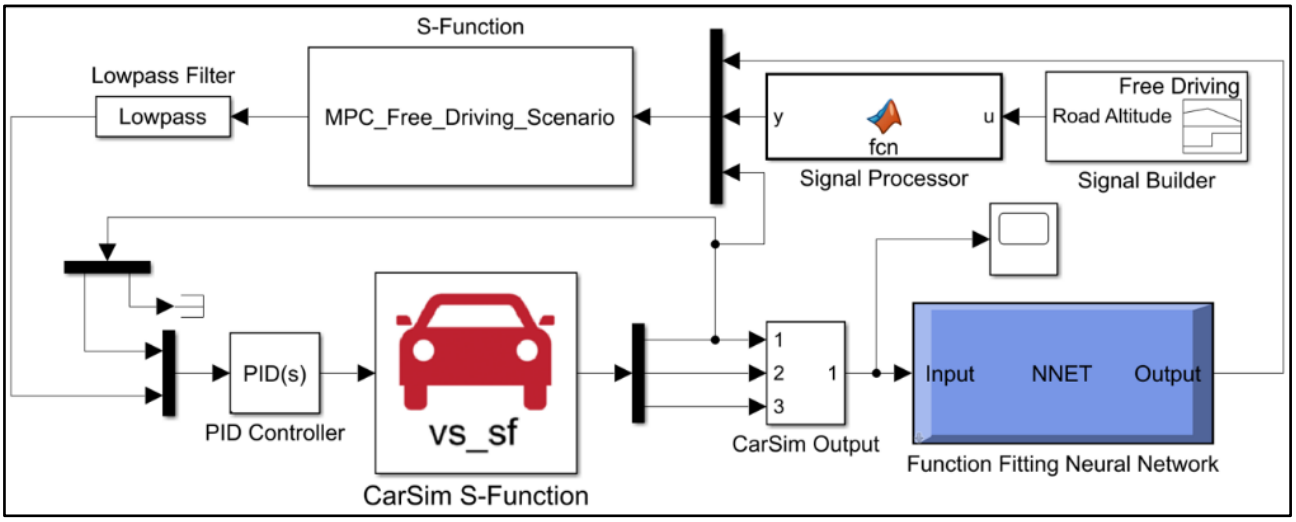

Fig. 5.2.3 Simulation Platform of Free Driving Scenario

The core MPC algorithms were written as S-Functions, so that the required optimization problem solver "quadprog" and "fmincon" can be successfully called. The lower level controllers which accepts the optimal acceleration command are designed using a PID controller. The ANN-IECM are both embedded in the MPC algorithm as a callable function and also deployed as a portable Simulink block to explicitly show the instantaneous energy consumption. The external data, such as the SPaT information and the road altitude information can be imported using Signal Builder Block.

Another advantage of the Co-simulation based on CarSim and MATLAB/Simulink is that the CarSim is capable of visualizing the simulation scenario so that the developer can intuitively check the performance of the overall system. The visualization of mentioned three typical driving scenarios is shown in Figure 5.3.

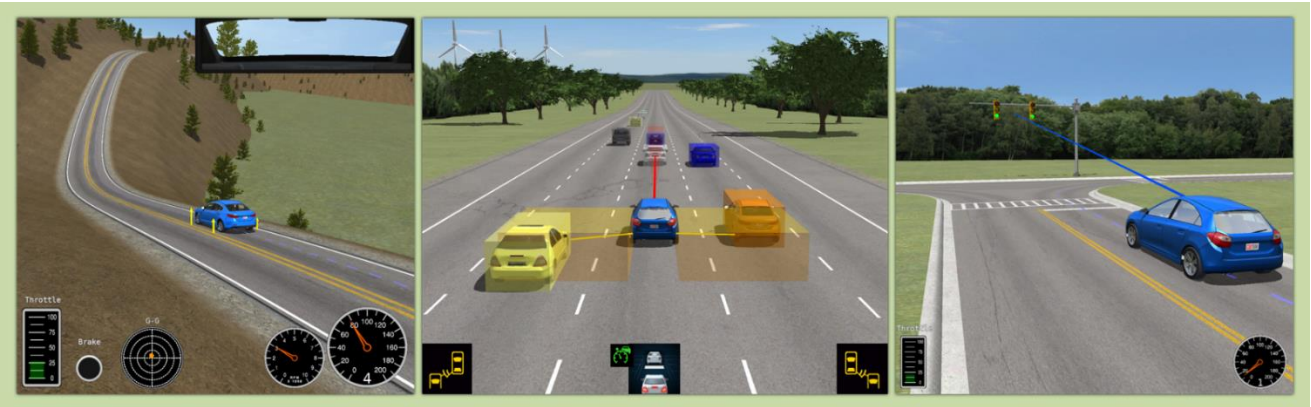

Fig. 5.3 Visualization of Free Driving Scenario (Left), Car Following Scenario (Middle),

Signal Anticipation Scenario (Right)

The simulated parameters are shown in Table 5.1.

TABLE 5.1 Simulation Parameters

Parameter	Symbol	Values & Unit
System gain	K_g	1.05
Time constant	τ_d	0.40s
Minimal stop distance	d_{min}	5m
Sampling period	T_s	0.1s
Prediction horizon	T	30
Time-to-Collision	TTC	-2.5s
Sensitivity first-order term coefficient	k_{SDE}	0.06
Sensitivity first-order term coefficient	k_{SVE}	0.005
Constant term of Sensitivity	d_{SDE}	-0.13
Constant term of Sensitivity	d_{SVE}	0.92
Upper bound of acceleration	$a_{host,max}$	$1.5 m/s^2$
Lower bound of acceleration	$a_{host,min}$	$-2 m/s^2$
Upper bound of jerk	$\dot{a}_{host,max}(jerk)$	$1.5 m/s^3$
Lower bound of jerk	$\dot{a}_{host,min}(jerk)$	$2 m/s^3$

5.2. Typical Case Study for Car-following Driving Scenario

For car-following driving scenario, two sub-scenarios are specially discussed, including steady following scene and lane-changing cut-in scene.

Steady following scene:

During the driving of host vehicle, if the preceding vehicle is within the radar detection range, then the PCC system will automatically control the velocity of host vehicle to follow the preceding vehicle. The real-time driving scenario is visualized in Figure 5.4. The initial velocity of preceding and host vehicles are $25.7\ m/s$ and $26.4\ m/s$, respectively. The initial inter-vehicle distance is $43\ m$, which is larger than the desired inter-vehicle distance. The corresponding velocity comparison, relative position, battery state-of-charge (SOC), instantaneous energy consumption, and preceding vehicle detection state are shown in Figure 5.5.

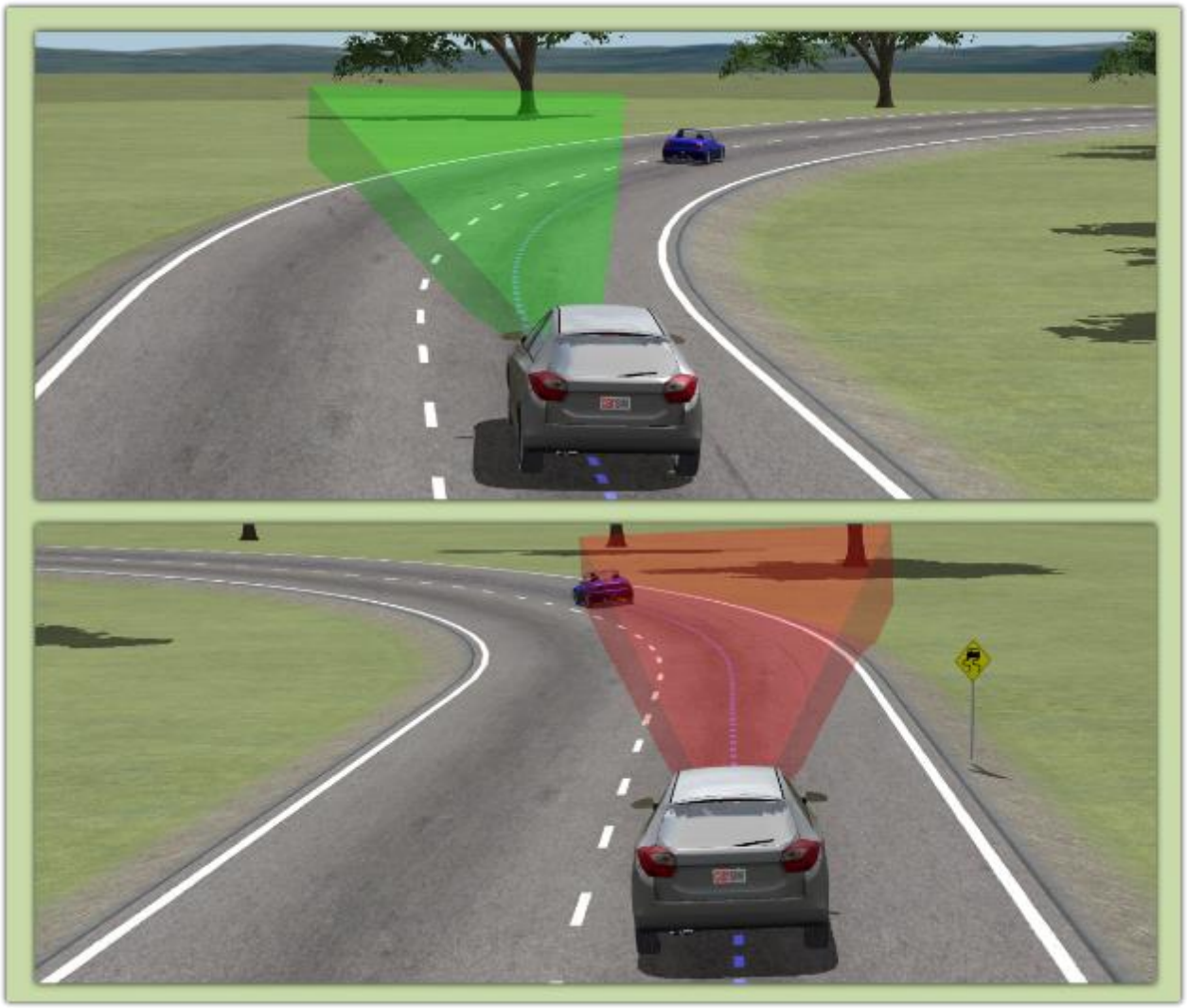

Fig. 5.4 Simulation Visualization of Steady Following Scene

From the first plot of figure 5.5, with the velocity decrease of preceding vehicle from 2s to 7s, the host vehicle reacted by slowing down the velocity as well. As shown in the fifth plot, from 11s to 39s, the preceding vehicle was not detected by the host vehicle PCC system. Therefore, the host vehicle cruised with the driver set velocity 25.8 m/s. Starting from 39s, with the braking of the preceding vehicle, the preceding vehicle was again detected by the host vehicle, which triggered the car following function of PCC system. Therefore, the host vehicle also decreased its velocity. From the third plot, the battery state of the preceding vehicle finally settled at 78.4%, while the SOC of host vehicle finalized at 78.8%. Therefore, it can be concluded that during this specific driving scenario, the energy consumption reduction was realized by 16.7% from the cumulative energy consumption.

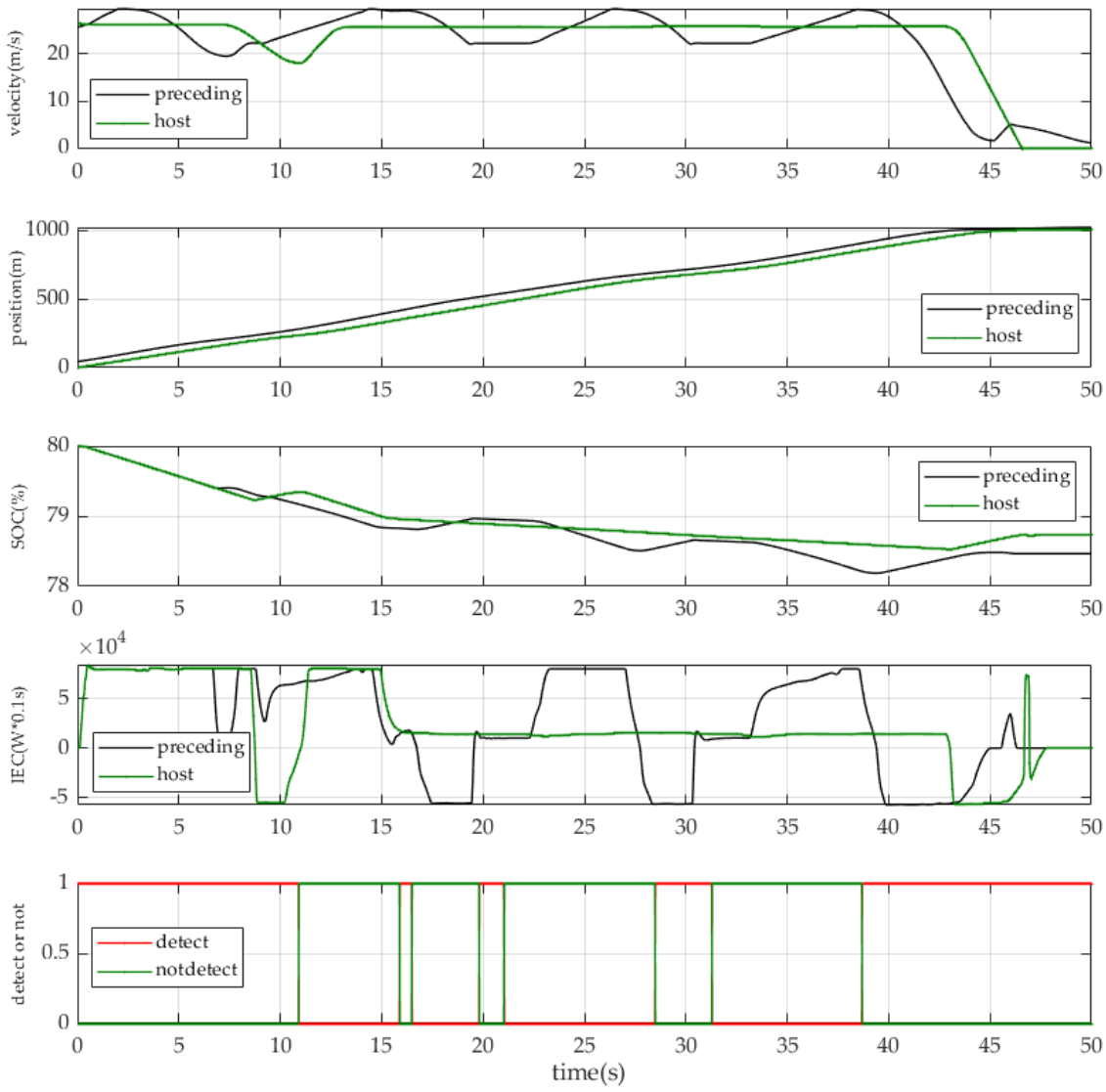

Fig. 5.5 Simulation Results of Steady Following Scene

lane-changing cut-in scene:

For the car-following scenario, the host vehicle is required to determine which vehicle is the “preceding vehicle” in front of the host vehicle in the same lane. A typical scenario from the viewpoint of the host vehicle can be illustrated in Figure 5.6.

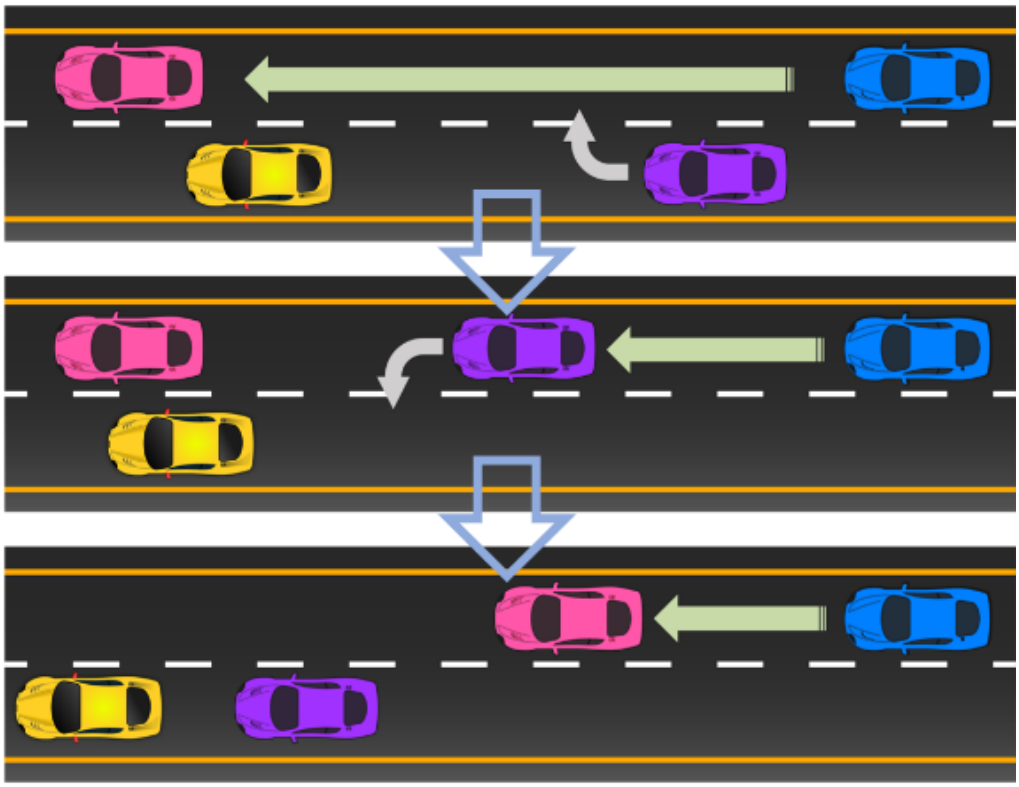

Fig. 5.6 Lane-Changing Cut-in Scene

The host vehicle (blue) drives on the right lane. In the beginning, the preceding vehicle is the pink one. Then the purple vehicle cuts into the lane of the host vehicle and becomes the preceding vehicle. After a while, the purple changes to another lane, and the pink vehicle becomes the preceding vehicle again. The PCC system must react to the change in the preceding vehicle on the road. The real-time vehicle coordinates view and world coordinates view are shown in Figure 5.7.

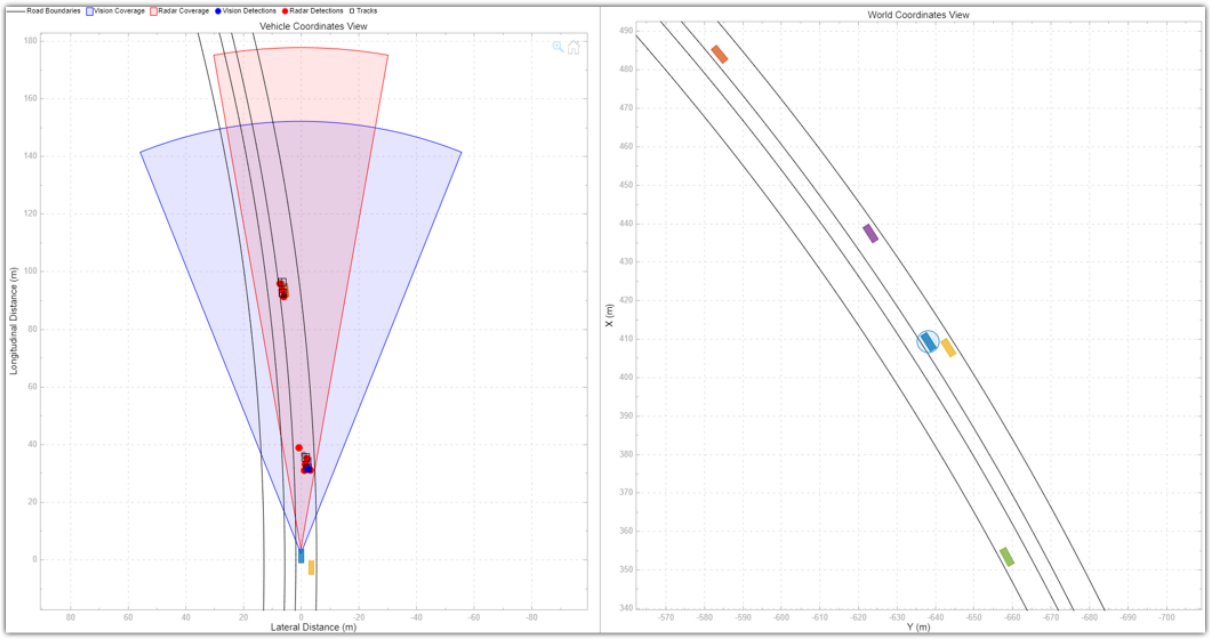

Fig. 5.7 Coordinates View of Lane-changing Cut-in Scene

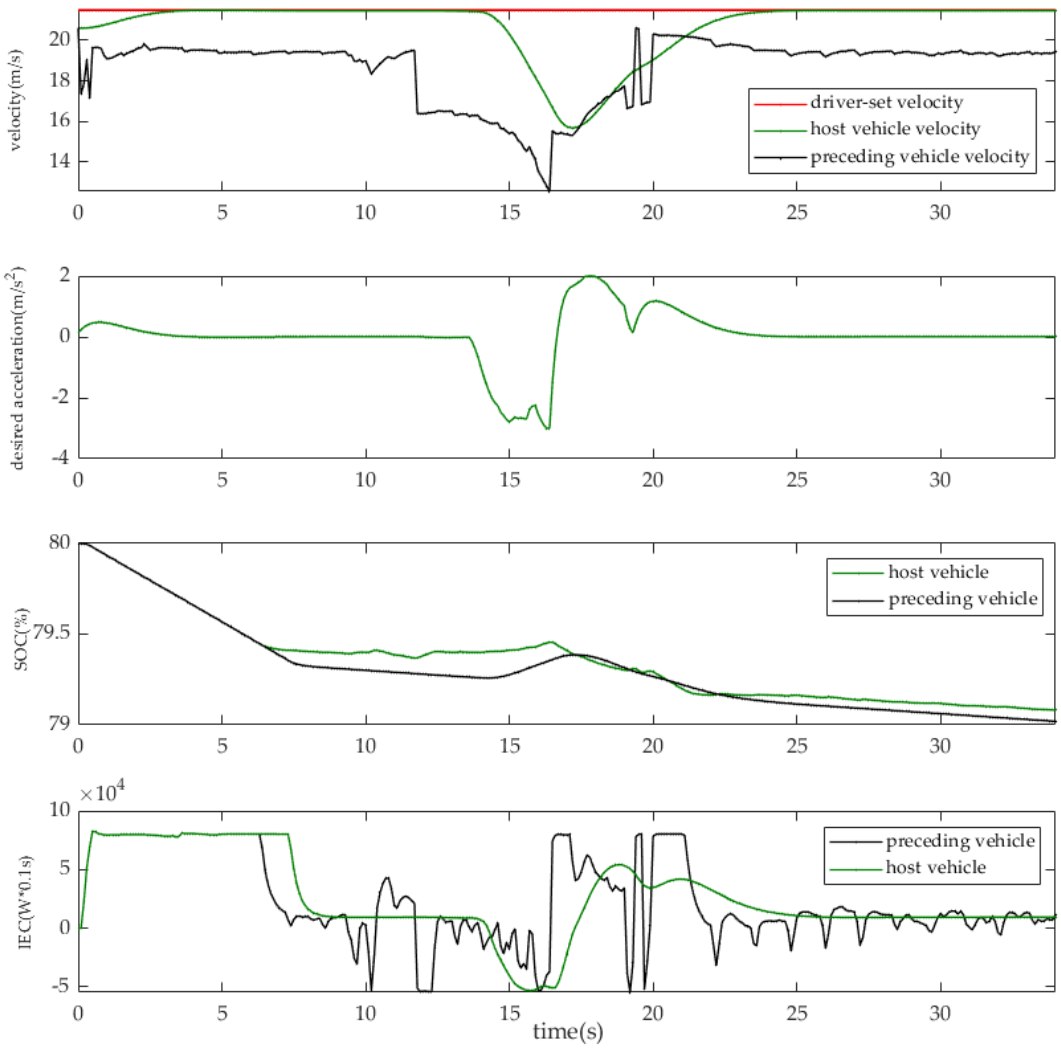

Fig. 5.8 Simulation Results of Lane-changing Cut-in Scene

The simulation results of the lane-changing cut-in scene are shown in Figure 5.8. As shown in the first plot, although the detected preceding vehicle was changing, a speed curve of "preceding vehicle" can still be calculated as the black line based on the relative velocity. When the calculated preceding vehicle velocity slowed down from 12s, the velocity of host vehicle also started to decrease the velocity from 14s, responding and following the motion of the preceding vehicle. The battery state-of-charge of preceding vehicle and host vehicle were 79.11% and 79.02%, respectively. From the cumulative energy consumption results, 6.3% energy-savings was realized by the PCC system.

5.3. Typical Case Study for Signal Anticipation Driving Scenario

The case study for the signal anticipation scenario was conducted for the real road sections in the area located in the core commercial district, which is shown in Figure 5.9.The selected location is characterized by an average traffic flow movement of 30 to 50km/h, during off-peak hours, here called Daytime, and 35km/h

rush hour. The situation of different times directly influences the running condition of the preceding vehicle. Seven traffic signal lights were considered in the SPaT data collection process. Assuming that only the host and preceding vehicles were operating during simulation, without considering the constraints of other vehicles, the host vehicle maintained a safe distance from the preceding vehicle using the function of car following of the PCC system.

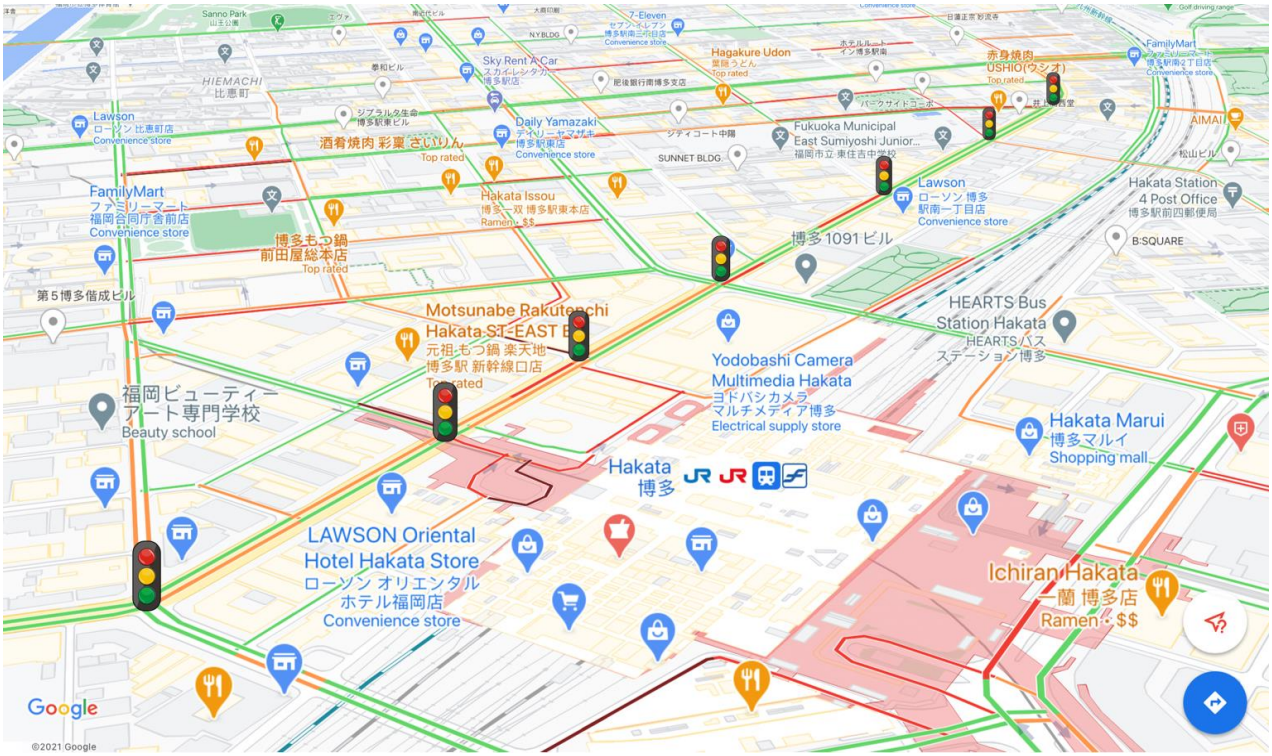

Fig. 5.9 Map of The Road Section for Signal Anticipation Scenario

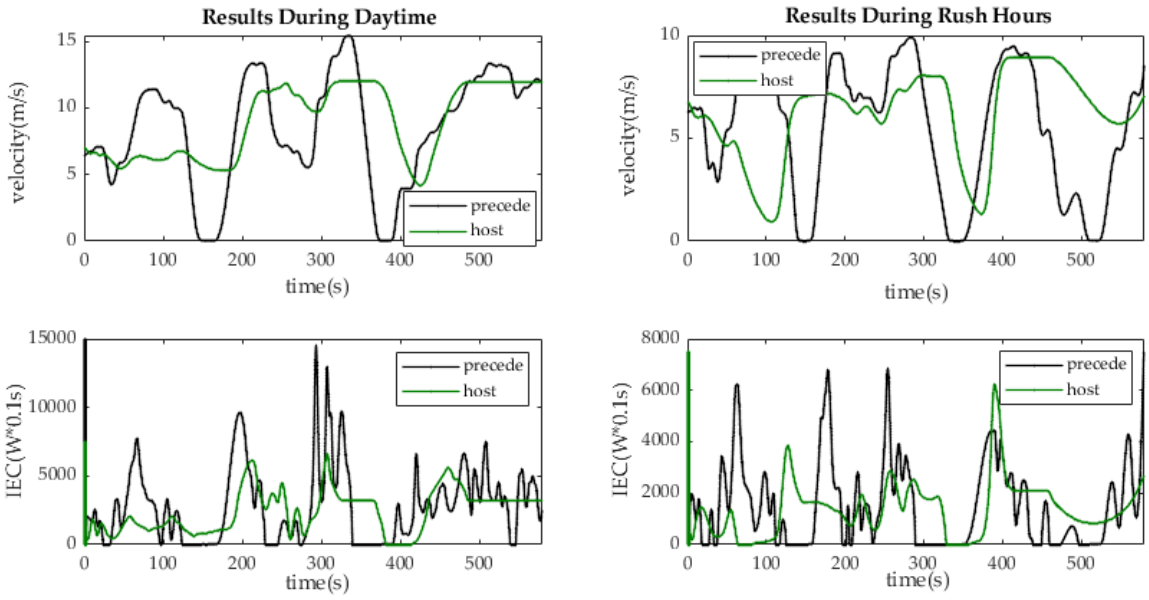

Fig. 5.10 Results of Signal Anticipation Scenario During Both Daytime (Left) and Rush Hours (Right)

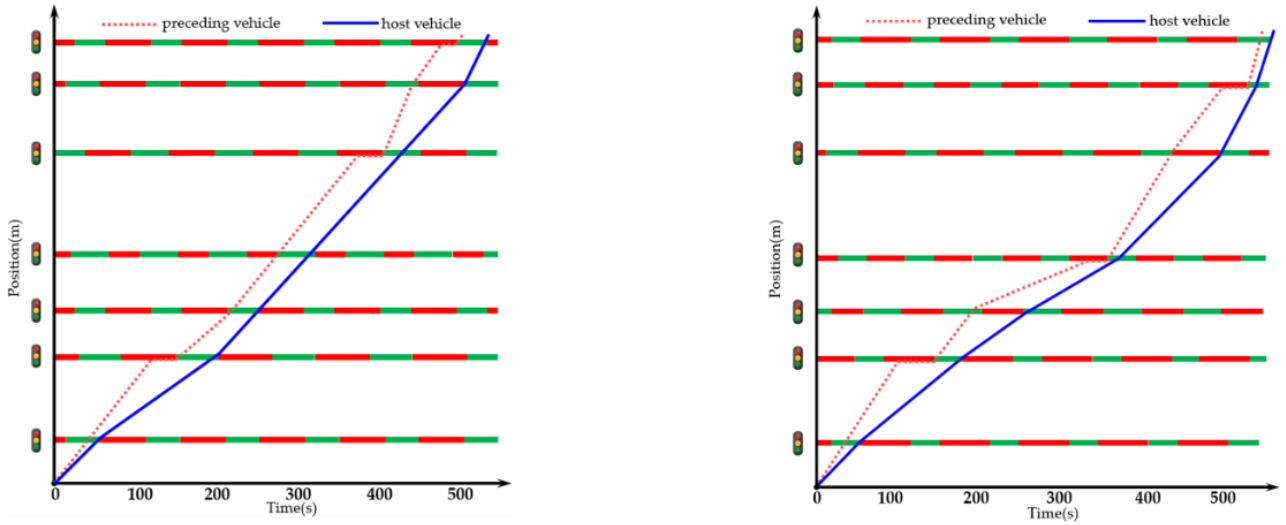

Fig. 5.11 Space-time Diagram with SPaT Information Comparing Preceding and Host Vehicle with PCC system During Both Daytime (Left) and Rush Hours (Right)

During the daytime, the host vehicle maintained a safe distance from the preceding vehicle by 60s. After that, the preceding vehicle kept accelerating, which entailed an increase of inter-distance between two vehicles. It follows that the PCC system switched to the signal anticipation scenario to track the reference velocity optimized by upcoming traffic SPaT information to avoid coming to a red interval. After 320s, the preceding vehicle implemented a sharp deceleration. However, by managing the velocity of the host vehicle by the proposed PCC system, it avoided the arrival at the signalized intersection during the red interval. Figure 5.11 left diagram demonstrates the space-time diagram comparing preceding and PCC-equipped host vehicles. The solid blue line represented the optimized trajectory passing each traffic signal light sequence through green intervals. By contrast, the preceding vehicle trajectory illustrated by the dotted pink line encountered two stops during red intervals. The amount of energy savings by the proposed PCC system is estimated at9.7%.

During rush hours, at the very beginning, the car-following scenario lasted for 60s. Afterwards, relative distance kept increasing due to the acceleration of the preceding vehicle, during which the host vehicle tracked the reference velocity optimized by upcoming traffic SPaT information. After a stop in front of the red interval from 140 to 155s, the preceding vehicle started to accelerate. However, the host vehicle deployed by the proposed PCC system crossed the signalized intersection without any stop through managing the driving velocity. A sharp deceleration was implemented by the preceding vehicle because of the upcoming red interval from 290 to 310s, during which the host vehicle was controlled by the PCC system to avoid encountering the red interval. Starting from 420s, the signal anticipation scenario began again to track the reference speed and successfully past the signalized intersection without any stop. However, the preceding vehicle without any velocity optimization had to experience a stop at around 510s. Figure 5.11 right diagram visualized the behavior of both host and preceding vehicles in a space-time schematic. The energy savings during rush hour reached a remarkable value of 15.6% based on the cumulative energy consumption.

5.4. Typical Case Study for Free Driving Scenario

The test for free driving scenario is conducted on a simulated hilly road section covered $2900m$ in total. The simulated scenario is visualized in Figure 5.12. The global coordinate of this simulated hilly road section is shown as Figure 5.13. The comparative analysis was conducted between the driving pattern controlled by the proposed PCC system and the automatic speed control drive (ASCD). The initial velocity was same for both

driving patterns set as 22.1m/s. The altitude, gradient of the road section, velocity comparison of both driving patterns, acceleration comparison, instantaneous motor speed and motor torque comparison, battery SOC, and instantaneous energy consumption are shown in Figure 5.14.

Fig. 5.12 Simulation Visualization for Case Study of Free Driving Scenario

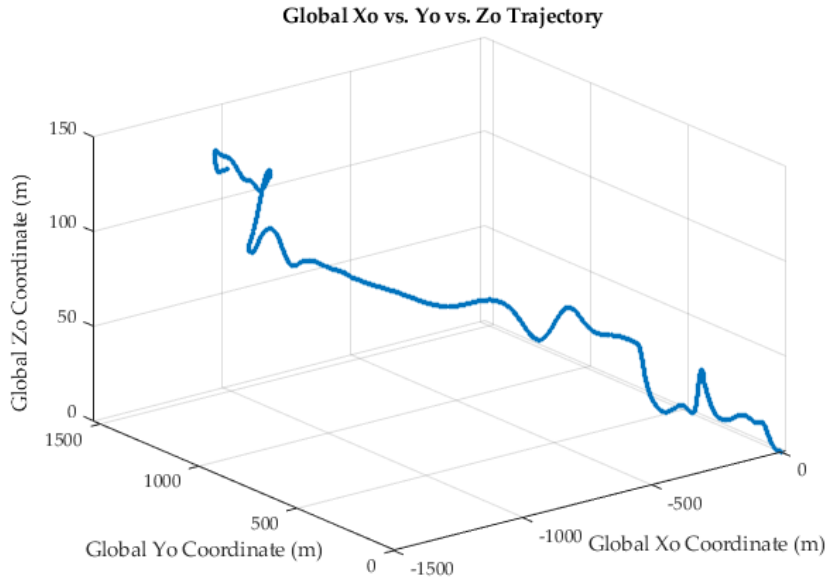

Fig. 5.13 Global Coordinate of Simulated Hilly Road Section

The overall simulation results are shown in Figure 5.14. From the first plot, it is known that the overall elevation exhibited an upward trend. The corresponding road gradient information can be obtained as the second plot, with the gradient range of $-26^{\circ}\sim23^{\circ}$. Because of the PCC system, the velocity of the PCC-vehicle varied around desired velocity 15m/s. The optimized acceleration of PCC-vehicle presented smoother variation trend. The basic rules can be concluded based on the gradient plot and acceleration plot that the PCC-vehicle always

accelerated just before the upslope, instead of accelerating during climbing the slope. When driving on the downslope section, the PCC-vehicle tends to rely on the inertia of the vehicle to drive, which was in line with the principle of eco-driving behavior. From the results of battery state-of-charge, it can be calculated that the baseline ASCD vehicle finalized at 77.2%, while the PCC-vehicle settled at 78.3%. The cumulative energy consumption for the baseline ASCD vehicle can be obtained as 94593009 $W \cdot 0.1s$, while the PCC-vehicle consumed 65918481.56 $W \cdot 0.1s$ in total. The energy savings was realized by 30.3%. Here in this case study, both the base line ASCD vehicle and PCC-vehicle are electric vehicles with the regenerative braking system, which means that during the braking process, the vehicles can be charged instantaneous. The instantaneous energy consumption plot 8 also shows the negative values. Therefore, the 30.3% energy-savings rate was already considered into the charging process.

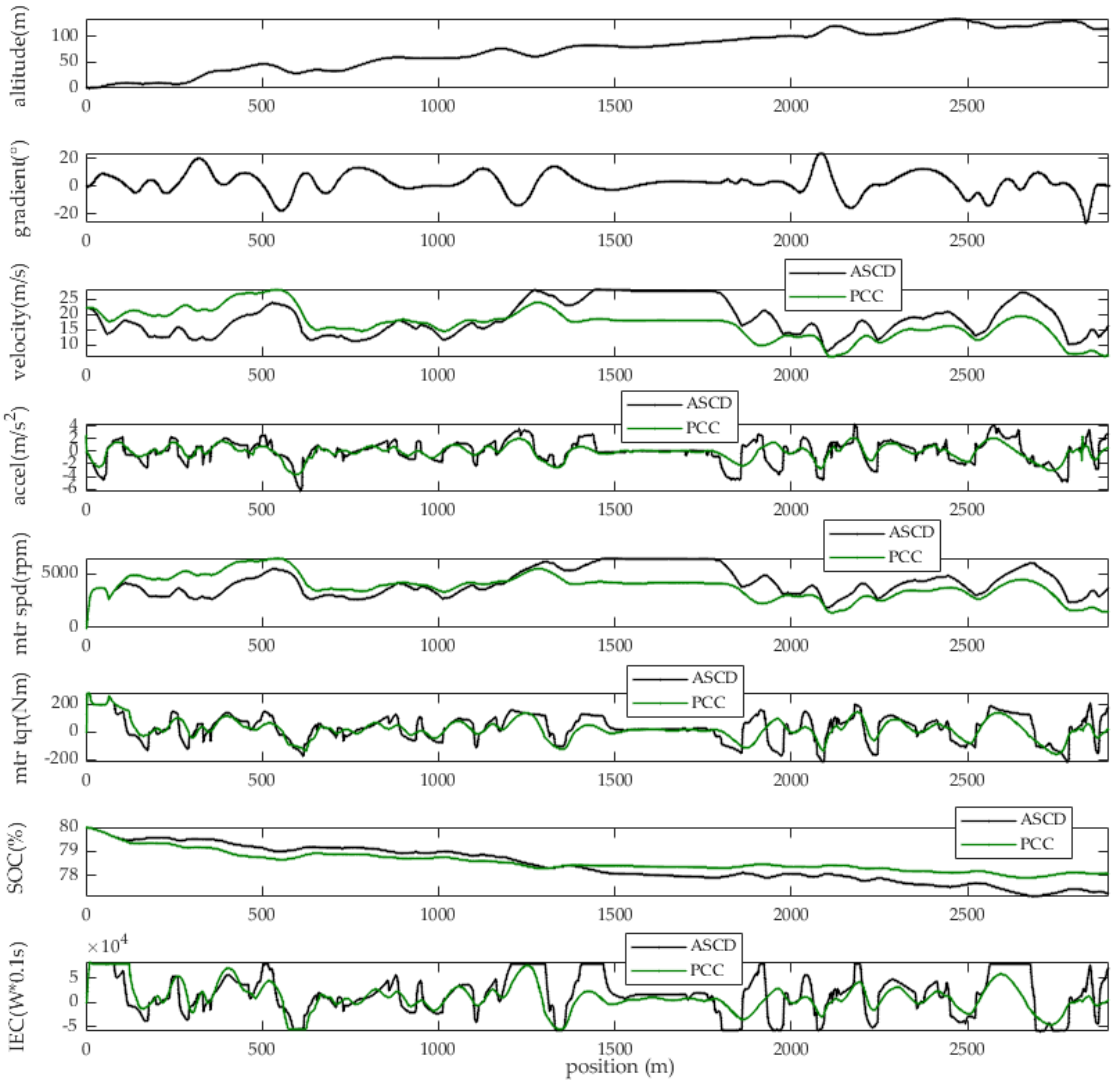

Fig. 5.14 Simulation Results of Free Driving Scenario

5.5. A Comprehensive Simulation Test of PCC system in Synthetic Driving Scenario

To test the capability of handling the synthetic daily driving scenarios which includes all the above three typical driving scenarios, a specific area near Kyushu University Chikushi Campus was selected to conduct the comprehensive simulation. The concerned traffic signal lights SPaT information were recorded for each involved signalized intersection. The road gradient information was collected using the built-in GPS sensors on MATLAB Mobile Version. The initial velocity of the PCC-vehicle was set as 8.9 m/s. The baseline vehicle was simulated by the automatic speed control drive (ASCD) with Gipps model for car following. Except for initial velocity, other initial conditions for baseline vehicle are the same with PCC-vehicle. Given different control style, the PCC-vehicle and ASCD-Gipps vehicle faced different traffic situations. The proposed PCC system controlled the vehicle based on the designed eco-driving algorithm, which leads to a relatively conservative driving style while dealing with the car following scenario, signal anticipation scenario and free driving scenario. However, the ASCD-Gipps vehicle was controlled by aggressive control actions, imitating the style of a human driver. The detailed description of the Gipps model can be referred to book *Traffic Flow Dynamics – Data, Models, and Simulation* by Martin Treiber and Arne Kesting [161]. The roadmap for the selected area and the simulated synthetic driving scenario is shown in Figure 5.15.

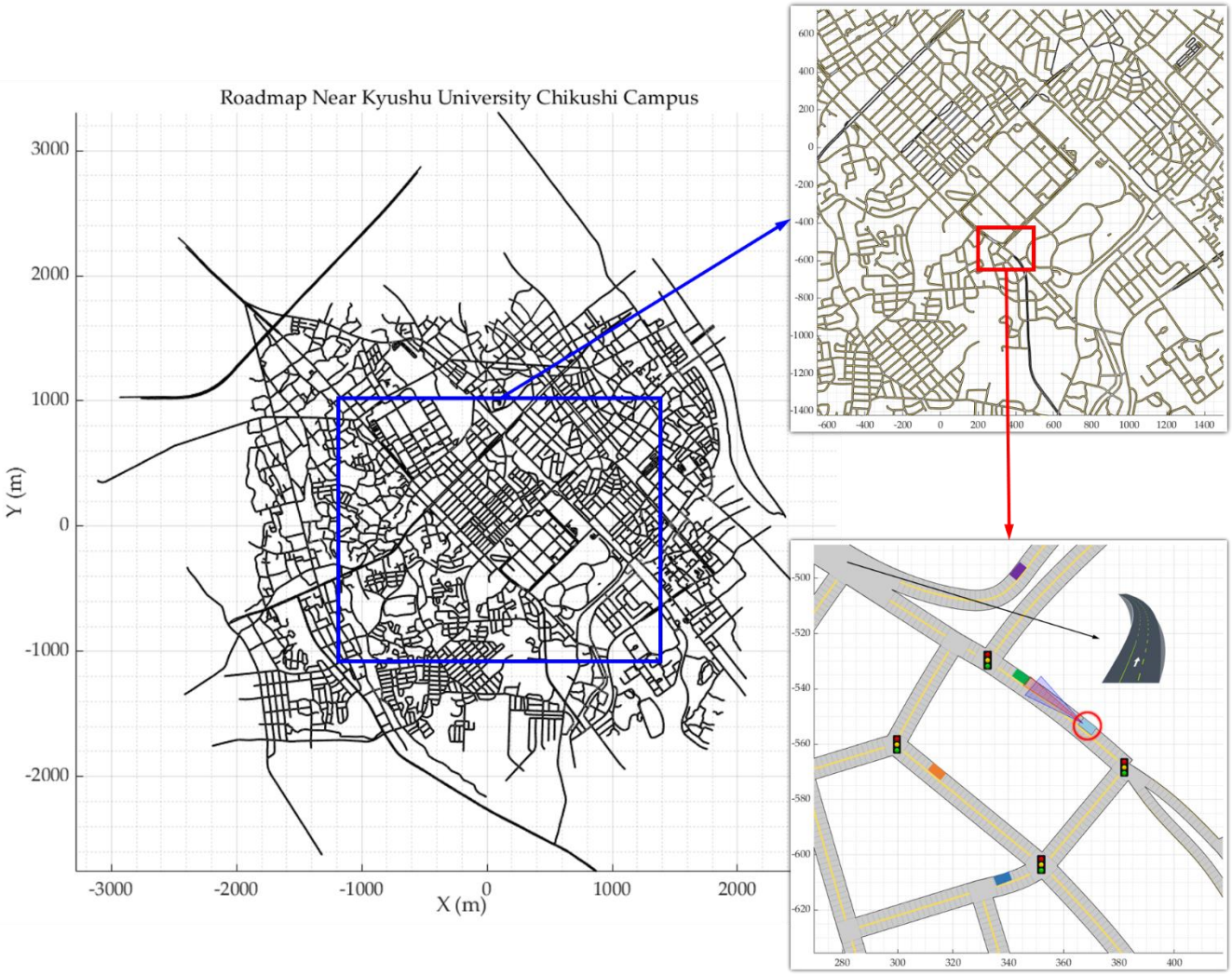

Fig. 5.15 Roadmap for Selected Area and Simulated Synthetic Driving Scenario

As shown in Figure 5.16, the first plot shows the velocity comparison between PCC-vehicle and baseline

ASCD+Gipps-vehicle. The region with different color represents that the PCC system dynamically switched into driving scenarios, red for signal anticipation scenario, green for the free driving scenario, and blue for the car following scenario. Within the beginning 50s, the baseline vehicle first accelerated under the control of ASCD. Then, under the manipulation of Gipps model, it sharply decelerated to follow the preceding vehicle. While, the PCC-vehicle can steadily follow the preceding vehicle without aggressive maneuvers. In the first free driving period, the PCC-vehicle was capable of adjust its velocity to the desired velocity $15m/s$ based on the road slope information. In the first signal anticipation period, the PCC-vehicle started automatically following the optimal reference velocity with the purpose of avoiding stop in the upcoming traffic signalized intersection. By contrast, the baseline vehicle was still under acceleration. It turned out that during 260 to 310s, the PCC-vehicle can pass the intersection without any stop, but the baseline vehicle implemented a stop during the red interval. The same results happened during 406s to 430s. The battery SOC percentages for baseline and PCC vehicle are 77.4% and 78.0%, respective. The cumulative 19.97% energy-savings can be achieved.

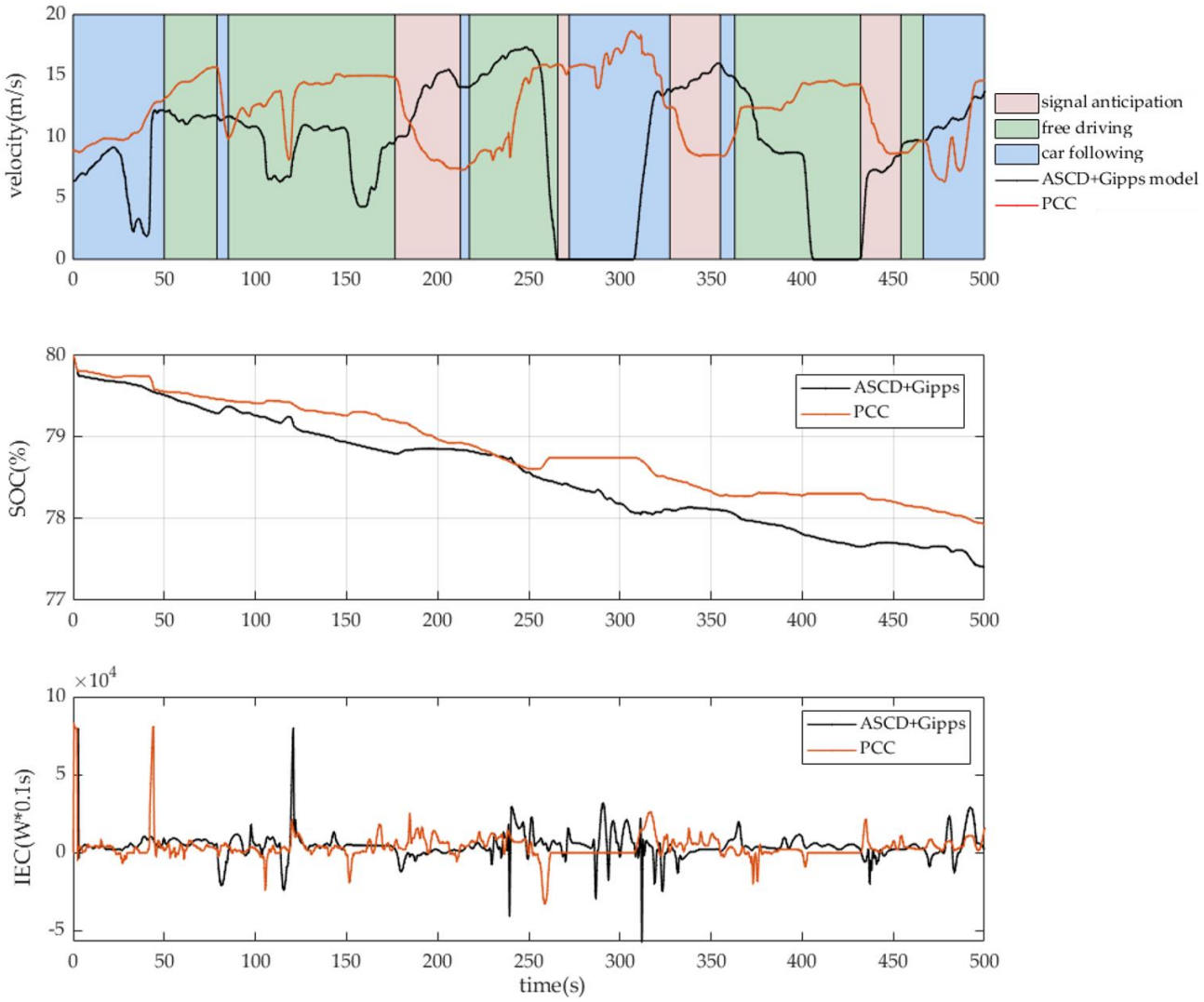

Fig. 5.16 Simulation Results of Synthetic Driving Scenario

5.6. Summary of Chapter 5

This chapter presented the simulated case studies to test the proposed dynamic predictive cruise control system in the previous chapters. At first, the simulation platform based on the CarSim and MATLAB/Simulink was established. Then, three case studies were conducted respectively for the car-following driving scenario, signal anticipation scenario, and free driving scenario. The respective simulated results showed that the three MPC algorithm worked well and showed the effects of energy saving. Finally, a synthetic driving scenario was designed to verify the entire PCC system handling the integrated day-to-day traffic situation, with the results that the proposed PCC system enabled the vehicle to realize the eco-driving by significant energy savings rate.

Chapter 6. Conclusion and Prospects

6.1. Conclusion

To improve the energy economy of the electric vehicle and alleviate the energy and environmental burden from the road transportation system, and to extend the driving range of the current electric vehicle, a comprehensive predictive cruise control system for eco-driving based on the electric vehicle has been designed for three representative driving scenarios, including car following scenario, signal anticipation scenario, and free driving scenario. With the premise of driving safety and comfortability, the energy economy of the electric vehicle was maximized by the proposed PCC system in daily synthetic traffic situation. The main research works, and corresponding conclusions can be summarized as follow:

(1). Architecture design of a comprehensive predictive cruise control system and system dynamics modeling:
Most of the current research are focused on eco-driving in limited driving scenarios. With the purpose of filling the existing research gap, a comprehensive predictive cruise control system was designed using a real-time dynamic driving scenario switching logic (DSSL) to handle the synthetic driving scenarios, including car following scenario, signal anticipation scenario, and free driving scenario. An electric vehicle longitudinal dynamics model and an inter-vehicle longitudinal dynamics model based on a customized VTH strategy were proposed. Through the theoretical analysis, the model convergence was verified. In order to obtain an optimal velocity for the signal anticipation scenario, a reference velocity planning model was studied based on the upcoming traffic signal phase and timing (SPaT) information.

(2). Modeling of an instantaneous energy consumption calculation based on the artificial neural network:
After summarizing the existing vehicle fuel/energy consumption model, the idea of developing an artificial neural network-based instantaneous energy consumption model for the electric vehicle was proposed. By processing and analyzing the real measurements dataset of electric vehicle dynamometer chassis experiments, the neural network model structure was designed. Using the Levenberg-Marquardt algorithm, a feedforward neural network training algorithm, the neural network was well trained. Model validation results showed that the proposed ANN-based instantaneous energy consumption model has more accurate estimation precision than existing EV-MFECM, more suitable for the application of developing eco-driving system for EV.

(3). Development of predictive cruise control system based on model predictive control algorithm:
Based on the model predictive control algorithm, taking the vehicle dynamics model and inter-vehicle dynamics model, different cruise objectives were analyzed and quantified for each typical driving scenario. Taking the minimization of energy consumption as the main optimization objective, three different MPC problems, including the linear and nonlinear MPC, were formulated. For linear MPC, detailed mathematical derivation and transformation from MPC problem to QP problem were conducted. For nonlinear MPCs, a suitable solver was found and utilized to solve the optimization problem online. In order to make up for the predictive error caused by model mismatch, and improve the system robustness, the feedback correction was introduced.

(4). Establishment of a simulation test bench for the validation of the PCC system:
In order to testify the effectiveness of the proposed PCC system, a co-simulation platform based on MATLAB/Simulink and CarSim was established. Through the comparative simulation experiments, for the car following scenario, the proposed PCC system not only ensured the driving safety and comfortability but also realized 6.3% ~ 16.7% energy saving rates. Under the signal anticipation scenario, the proposed

PCC system achieved 9.7% ~ 15.6% energy savings rates compared with the preceding vehicle without a PCC system. For the free driving scenario, by utilizing the road gradient information to optimize the velocity, 30.3% energy consumption reduction was accomplished by PCC-vehicle compared with ASCD-vehicle. Finally, a synthetic driving scenario was simulated to test the comprehensive performance of handling the mixed driving scenarios of the proposed PCC system, the simulation results indicated that 19.97% cumulative energy savings was obtained by using the proposed PCC system compared with the conventional human-driver-like Gipps model.

Mainly originality can be listed as follow:

(1). Based on the analysis of existing safety distance model, a customized variable time headway strategy was designed considering the relative velocity and the velocity trend of the preceding vehicle. Through the stability analysis of the designed safety distance model based on the customized VTH strategy, not only the driving safety can be ensured but also the road utilization can be improved.

(2). According to the problem of estimation error for the existing fuel consumption model and the lack of energy consumption model for electric vehicles, an instantaneous energy consumption model for EV was developed and well trained by an artificial neural network training algorithm. The model validation results showed an unprecedented instantaneous energy consumption estimation precision.

(3). An integrated predictive cruise control system was innovatively proposed based on the model predictive control algorithm, which is capable of handling daily typical driving scenarios automatically by a designed Driving Scenario Switching Logic (DSSL). The respective eco-driving problem taking into account either preceding vehicle, traffic signal lights, or road terrain information can be considered simultaneously by proposed PCC system so that the higher energy economy can be realized. Besides, to implement the proposed PCC system in a real application, the system robustness was discussed and enhanced by using the feedback correction method.

6.2. Research Prospects

For this research, three prospects of future research can be pointed out:

(1). The model predictive control algorithm, as an advanced optimization-based control method, is hard to implement into the fast system in the real application, e.g., automobile or robotics, due to its real-time computational complexity. MPC utilizes a numerical optimization algorithm to solve a predictive optimization problem to obtain the optimal control value. For vehicles, the control period is usually set as seconds-level or milliseconds-level, which highly requires the real-time performance of the control law. Therefore, the online optimization problem-solving algorithm is required to be studied further.

(2). The proposed predictive cruise control system currently was just tested based on the co-simulation platform using MATLAB/Simulink and CarSim. Next step, a hardware-in-loop test can be implemented to further test the feasibility of the proposed algorithm and models.

(3). The driving scenarios covered by the proposed PCC system are limited. The corner cases during real driving process is more difficult to handle by solely using model-based methodology due to the limitation of mathematical modeling in terms of various driving situations. Therefore, the learning-based method such as reinforcement learning or imitating learning can be introduced and combined with optimal control, so that the eco-driving problem for much more complex traffic systems can be extensively handled.

Reference

[1] Alshehry, A. S., & Belloumi, M. (2017). Study of the environmental Kuznets curve for transport carbon dioxide emissions in Saudi Arabia. *Renewable and Sustainable Energy Reviews*, *75*, 1339-1347. https://doi.org/10.1016/j.rser.2016.11.122

[2] Shahbaz, M., Khraief, N., & Jemaa, M. M. (2015). On the causal nexus of road transport CO2 emissions and macroeconomic variables in Tunisia: Evidence from combined cointegration tests. *Renewable and Sustainable Energy Reviews*, *51*, 89-100. https://doi.org/10.1016/j.rser.2015.06.014

[3] United Nations. Sustainable Development Goal 11: Make Cities Inclusive, Safe, Resilient and Sustainable. https://sdgs.un.org/topics/sustainable-transport

[4] Guo, L., Gao, B., Gao, Y., & Chen, H. (2017). Optimal energy management for HEVs in eco-driving applications using Bi-level MPC. *IEEE Transactions on Intelligent Transportation Systems*, *18*(8), 2153-2162. https://doi.org/10.1109/tits.2016.2634019

[5] Hu, J., Shao, Y., Sun, Z., Wang, M., Bared, J., & Huang, P. (2016). Integrated optimal eco-driving on rolling terrain for hybrid electric vehicle with vehicle-infrastructure communication. *Transportation Research Part C: Emerging Technologies*, *68*, 228-244. https://doi.org/10.1016/j.trc.2016.04.009

[6] Lai, W. (2015). The effects of eco-driving motivation, knowledge and reward intervention on fuel efficiency. *Transportation Research Part D: Transport and Environment*, *34*, 155-160. https://doi.org/10.1016/j.trd.2014.10.003

[7] Li, M., Wu, X., He, X., Yu, G., & Wang, Y. (2018). An eco-driving system for electric vehicles with signal control under V2X environment. *Transportation Research Part C: Emerging Technologies*, *93*, 335-350. https://doi.org/10.1016/j.trc.2018.06.002

[8] Maamria, D., Gillet, K., Colin, G., Chamaillard, Y., & Nouillant, C. (2019). Optimal predictive eco-driving cycles for conventional, electric, and hybrid electric cars. *IEEE Transactions on Vehicular Technology*, *68*(7), 6320-6330. https://doi.org/10.1109/tvt.2019.2914256

[9] Mensing, F., Bideaux, E., Trigui, R., & Tattegrain, H. (2013). Trajectory optimization for eco-driving taking into account traffic constraints. *Transportation Research Part D: Transport and Environment*, *18*, 55-61. https://doi.org/10.1016/j.trd.2012.10.003

[10] Mensing, F., Trigui, R., & Bideaux, E. (2011). Vehicle trajectory optimization for application in ECO-driving. *2011 IEEE Vehicle Power and Propulsion Conference*. https://doi.org/10.1109/vppc.2011.6042993

[11] Park, S., Rakha, H., Ahn, K., & Moran, K. (2013). Fuel economy impacts of manual, conventional cruise control, and predictive eco-cruise control driving. *International Journal of Transportation Science and Technology*, *2*(3), 227-242. https://doi.org/10.1260/2046-0430.2.3.227

[12] Saboohi, Y., & Farzaneh, H. (2008). Model for optimizing energy efficiency through controlling speed and gear ratio. *Energy Efficiency*, *1*(1), 65-76. https://doi.org/10.1007/s12053-008-9005-y

[13] Thibault, L., De Nunzio, G., & Sciarretta, A. (2018). A unified approach for electric vehicles range maximization via eco-routing, eco-driving, and energy consumption prediction. *IEEE Transactions on Intelligent Vehicles*, *3*(4), 463-475. https://doi.org/10.1109/tiv.2018.2873922

[14] Intelligent Transportation Systems Joint Program Office. (2015). *Intelligent Transportation Systems (ITS) Program Overview*. Intelligent Transportation Systems - Joint Program Office. https://www.its.dot.gov/about/its_jpo.htm

[15] Yonezawa, M. (2011). Energy Saving ITS“ Eco-driving support” Estimation and Results. *IEEE Forum on Integrated and Sustainable Transportation System*.

[16] Barić, D., Zovak, G., & Periša, M. (2013). Effects of eco-drive education on the reduction of fuel consumption and CO2 emissions. *PROMET - Traffic&Transportation*, *25*(3), 265-272. https://doi.org/10.7307/ptt.v25i3.1260

[17] Sciarretta, A., De Nunzio, G., & Ojeda, L. L. (2015). Optimal Ecodriving control: Energy-efficient driving of road vehicles as an optimal control problem. *IEEE Control Systems*, *35*(5), 71-90. https://doi.org/10.1109/mcs.2015.2449688

[18] Swaroop, D., & Rajagopal, K. (n.d.). A review of constant time headway policy for automatic vehicle following. *ITSC 2001. 2001 IEEE Intelligent Transportation Systems. Proceedings (Cat. No.01TH8585)*. https://doi.org/10.1109/itsc.2001.948631

[19] SWAROOP, D., HEDRICK, J., CHIEN, C. C., & IOANNOU, P. (1994). A Comparision of spacing and headway control laws for automatically controlled Vehicles. *Vehicle System Dynamics*, *23*(1), 597-625. https://doi.org/10.1080/00423119408969077

[20] Feng, G., Wang, W., Feng, J., Tan, H., & Li, F. (2010). Modelling and simulation for safe following distance based on vehicle braking process. *2010 IEEE 7th International Conference on E-Business Engineering*. https://doi.org/10.1109/icebe.2010.66

[21] Qiang Luo, Lunhui Xun, Zhihui Cao, & Yanguo Huang. (2011). Simulation analysis and study on car-following safety distance model based on braking process of leading vehicle. *2011 9th World Congress on Intelligent Control and Automation*. https://doi.org/10.1109/wcica.2011.5970612

[22] Wang, L., & Liu, G. (2019). Vehicle Braking Distance Estimation Model and Safe Distance Control Algorithm. *Agricultural Equipment & Vehicle Engineering*, *57*(12), 23-28. https://doi.org/10.3969/j.issn.1673-3142.2019.12.005

[23] Hou, D. (2004). *Study on Vehicle Forward Collision Avoidance System* [Doctoral dissertation]. https://kns.cnki.net/KCMS/detail/detail.aspx?dbname=CDFD9908&filename=2005035330.nh

[24] Yanakiev, D., & Kanellakopoulos, I. (1995). Variable time headway for string stability of automated heavy-duty vehicles. *Proceedings of 1995 34th IEEE Conference on Decision and Control*, 4077-4081. https://doi.org/10.1109/cdc.1995.479245

[25] Zhou, J., & Peng, H. (2005). Range policy of adaptive cruise control vehicles for improved flow stability and string stability. *IEEE Transactions on Intelligent Transportation Systems*, *6*(2), 229-237. https://doi.org/10.1109/tits.2005.848359

[26] Loannou, P. A., & Chien, C. C. (1993). Autonomous intelligent cruise control. *IEEE Transactions on Vehicular Technology*, *42*(4), 657-672. https://doi.org/ 10.1109/25.260745

[27] Lin, T., Hwang, S., & Green, P. A. (2009). Effects of time-gap settings of adaptive cruise control (ACC) on driving performance and subjective acceptance in a bus driving simulator. *Safety Science*, *47*(5), 620-625. https://doi.org/10.1016/j.ssci.2008.08.004

[28] Broqua, F., Lerner, G., Mauro, V., & Morello, E. (1991). Cooperative Driving: Basic Concepts and A First Assessment of "Intelligent Cruise Control" Strategies. *Advanced Telematics in Road Transport, Proceedings of the DRIVE Conference*, *2*, 908-929.

[29] Yanakiev, D., & Kanellakopoulos, I. (1998). Nonlinear spacing policies for automated heavy-duty vehicles. *IEEE Transactions on Vehicular Technology*, *47*(4), 1365-1377. https://doi.org/10.1109/25.728529

[30] Darbha, S., & Rajagopal, K. (1999). Intelligent cruise control systems and traffic flow stability. *Transportation Research Part C: Emerging Technologies*, *7*(6), 329-

352. https://doi.org/10.1016/s0968-090x(99)00024-8

[31] Rajamani, R., Levinson, D. M., Michalopoulos, P., Wang, J., Santhanakrishnan, K., & Zhu, X. (2005). Adaptive Cruise Control System Design And Its Impact on Traffic Flow. *Retrieved from the University of Minnesota Digital Conservancy*. https://hdl.handle.net/11299/1233

[32] Greenshields, B. D., Bibbins, J. R., Channing, W. S., & Miller, H. H. (1935). A Study of Traffic Capacity. *Proceedings of the Fourteenth Annual Meeting of the Highway Research Board Held at Washington, D.C. December 6-7, 1934. Part I*, *14*(1), 448-477.

[33] Moon, S., & Yi, K. (2008). Human driving data-based design of a vehicle adaptive cruise control algorithm. *Vehicle System Dynamics*, *46*(8), 661-690. https://doi.org/10.1080/00423110701576130

[34] Yanakiev, D., & Kanellakopoulos, I. (n.d.). Longitudinal control of heavy-duty vehicles for automated highway systems. *Proceedings of 1995 American Control Conference - ACC'95*. https://doi.org/10.1109/acc.1995.532086

[35] Li, S., Li, K., Rajamani, R., & Wang, J. (2009). Multi-objective coordinated control for advanced adaptive cruise control system. *Proceedings of the 48h IEEE Conference on Decision and Control (CDC) held jointly with 2009 28th Chinese Control Conference*. https://doi.org/10.1109/cdc.2009.5400863

[36] Ahn, K., Rakha, H., Trani, A., & Van Aerde, M. (2002). Estimating vehicle fuel consumption and emissions based on instantaneous speed and acceleration levels. *Journal of Transportation Engineering*, *128*(2), 182-190. https://doi.org/10.1061/(asce)0733-947x(2002)128:2(182)

[37] Zhou, M., Jin, H., & Wang, W. (2016). A review of vehicle fuel consumption models to evaluate eco-driving and eco-routing. *Transportation Research Part D: Transport and Environment*, *49*, 203-218. https://doi.org/10.1016/j.trd.2016.09.008

[38] Ahn, K., & Rakha, H. (2008). The effects of route choice decisions on vehicle energy consumption and emissions. *Transportation Research Part D: Transport and Environment*, *13*(3), 151-167. https://doi.org/10.1016/j.trd.2008.01.005

[39] Barth, M., Boriboonsomsin, K., & Vu, A. (2007). Environmentally friendly navigation. *2007 IEEE Intelligent Transportation Systems Conference*. https://doi.org/10.1109/itsc.2007.4357672

[40] Boriboonsomsin, K., & Barth, M. (2009). Impacts of road grade on fuel consumption and carbon dioxide emissions evidenced by use of advanced navigation systems. *Transportation Research Record: Journal of the Transportation Research Board*, *2139*(1), 21-30. https://doi.org/10.3141/2139-03

[41] Frey, H. C., Zhang, K., & Rouphail, N. M. (2008). Fuel use and emissions comparisons for alternative routes, time of day, road grade, and vehicles based on in-use measurements. *Environmental Science & Technology*, *42*(7), 2483-2489. https://doi.org/10.1021/es702493v

[42] *Where the energy goes: Gasoline vehicles*. (n.d.). U.S. Environmental Protection Agency. https://www.fueleconomy.gov/feg/atv.shtml

[43] Wang, J., Yu, Q., Li, S., & Li, K. (2014). Eco-Speed Optimization Based on Real-Time Information of Road Gradient. *Journal of Automotive Safety and Energy*, *5*(03), 257-262. https://kns.cnki.net/kcms/detail/detail.aspx?FileName=QCAN201403006&DbName=CJFQ2014

[44] Ding, F., & Jin, H. (2018). On the optimal speed profile for eco-driving on curved roads. *IEEE Transactions on Intelligent Transportation Systems*, *19*(12), 4000-4010. https://doi.org/10.1109/tits.2018.2795602

[45] Emir, D. (2019). *Eco-driving potentiality of road infrastructures according to the adequacy between infrastructure geometrical characteristics and vehicles speed* [Doctoral dissertation]. https://hal.archives-ouvertes.fr/tel-02311794v2

[46] Asadi, B., & Vahidi, A. (2011). Predictive cruise control: Utilizing upcoming traffic signal information for improving fuel economy and reducing trip time. *IEEE Transactions on Control Systems Technology*, *19*(3), 707-714. https://doi.org/10.1109/tcst.2010.2047860

[47] Sanchez, M., Cano, J., & Kim, D. (2006). Predicting traffic lights to improve urban traffic fuel consumption. *2006 6th International Conference on ITS Telecommunications*. https://doi.org/10.1109/itst.2006.288906

[48] Tielert, T., Killat, M., Hartenstein, H., Luz, R., Hausberger, S., & Benz, T. (2010). The impact of traffic-light-to-vehicle communication on fuel consumption and emissions. *2010 Internet of Things (IOT)*. https://doi.org/10.1109/iot.2010.5678454

[49] Berry, I. R. (2010). *The effects of driving style and vehicle performance on the real-world fuel consumption of US light-duty vehicles* [Master's thesis]. https://web.mit.edu/sloan-auto-lab/research/beforeh2/files/IreneBerry_Thesis_February2010.pdf

[50] Beusen, B., Broekx, S., Denys, T., Beckx, C., Degraeuwe, B., Gijsbers, M., Scheepers, K., Govaerts, L., Torfs, R., & Panis, L. I. (2009). Using on-board logging devices to study the longer-term impact of an eco-driving course. *Transportation Research Part D: Transport and Environment*, *14*(7), 514-520. https://doi.org/10.1016/j.trd.2009.05.009

[51] Ericsson, E. (2001). Independent driving pattern factors and their influence on fuel-use and exhaust emission factors. *Transportation Research Part D: Transport and Environment*, *6*(5), 325-345. https://doi.org/10.1016/s1361-9209(01)00003-7

[52] EVANS, L. (1979). Driver behavior effects on fuel consumption in urban driving. *Human Factors: The Journal of the Human Factors and Ergonomics Society*, *21*(4), 389-398. https://doi.org/10.1177/001872087902100401

[53] Taniguchi, M. (2008). Eco-driving and Fuel Economy of Passenger Cars. *Proc. of Annual Meeting of IEE Japan*, *21*, 5-8.

[54] Van Mierlo, J., Maggetto, G., Van de Burgwal, E., & Gense, R. (2004). Driving style and traffic measures-influence on vehicle emissions and fuel consumption. *Proceedings of the Institution of Mechanical Engineers, Part D: Journal of Automobile Engineering*, *218*(1), 43-50. https://doi.org/10.1243/095440704322829155

[55] Zarkadoula, M., Zoidis, G., & Tritopoulou, E. (2007). Training urban bus drivers to promote smart driving: A note on a Greek eco-driving pilot program. *Transportation Research Part D: Transport and Environment*, *12*(6), 449-451. https://doi.org/10.1016/j.trd.2007.05.002

[56] Post, K., Kent, J., Tomlin, J., & Carruthers, N. (1984). Fuel consumption and emission modelling by power demand and a comparison with other models. *Transportation Research Part A: General*, *18*(3), 191-213. https://doi.org/10.1016/0191-2607(84)90126-2

[57] Akcelik, R. (1989). Efficiency and drag in the power-based model of fuel consumption. *Transportation Research Part B: Methodological*, *23*(5), 376-385. https://doi.org/10.1016/0191-2615(89)90014-3

[58] Leung, D. Y., & Williams, D. J. (2000). Modelling of motor vehicle fuel consumption and emissions using a power-based model. *Urban Air Quality: Measurement, Modelling and Management*, 21-29. https://doi.org/10.1007/978-94-010-0932-4_3

[59] Piccoli, B., Ke Han, Friesz, T. L., & Tao Yao. (2013). Estimating fuel consumption and emissions via traffic data from mobile sensors. *2013 51st Annual Allerton Conference on Communication, Control, and Computing (Allerton)*. https://doi.org/10.1109/allerton.2013.6736562

[60] Chang, D. J., & Morlok, E. K. (2005). Vehicle speed profiles to minimize work and fuel

consumption. *Journal of Transportation Engineering*, *131*(3), 173-182. https://doi.org/10.1061/(asce)0733-947x(2005)131:3(173)

[61] Ahn, K., Rakha, H. A., & Moran, K. (2010). A simple fuel consumption model based on instantaneous vehicle power. *Proc. of the Transportation Research Board 89th Annual Meeting*, 10-14.

[62] Rakha, H. A., Ahn, K., Moran, K., Saerens, B., & Bulck, E. V. (2011). Virginia Tech comprehensive power-based fuel consumption model: Model development and testing. *Transportation Research Part D: Transport and Environment*, *16*(7), 492-503. https://doi.org/10.1016/j.trd.2011.05.008

[63] Saerens, B., Rakha, H., Ahn, K., & Van Den Bulck, E. (2013). Assessment of alternative polynomial fuel consumption models for use in intelligent transportation systems applications. *Journal of Intelligent Transportation Systems*, *17*(4), 294-303. https://doi.org/10.1080/15472450.2013.764801

[64] Passenberg, B., Kock, P., & Stursberg, O. (2009). Combined time and fuel optimal driving of trucks based on a hybrid model. *2009 European Control Conference (ECC)*. https://doi.org/10.23919/ecc.2009.7075185

[65] Rakha, H., & Ahn, K. (2003). Closure to "Estimating vehicle fuel consumption and emissions based on instantaneous speed and acceleration levels" by Kyoung Ahn, Hesham Rakha, Antonio Trani, and michel van Aerde. *Journal of Transportation Engineering*, *129*(5), 579-581. https://doi.org/10.1061/(asce)0733-947x(2003)129:5(579)

[66] Lei, W., Chen, H., & Lu, L. (2010). Microscopic Emission and Fuel Consumption Modeling for Light-duty Vehicles Using Portable Emission Measurement System Data. *World Academy of Science, Engineering and Technology*, *66*, 918-925. https://doi.org/10.5281/zenodo.1085936

[67] Akcelik, R. (1982). Derivation and calibration of fuel consumption models. *Australian Road Research Board. Internal Report*, AIR 367-3.

[68] Hung, W., Tong, H., & Cheung, C. (2005). A modal approach to vehicular emissions and fuel consumption model development. *Journal of the Air & Waste Management Association*, *55*(10), 1431-1440. https://doi.org/10.1080/10473289.2005.10464747

[69] Kamal, M., Mukai, M., Murata, J., & Kawabe, T. (2010). On board eco-driving system for varying road-traffic environments using model predictive control. *2010 IEEE International Conference on Control Applications*. https://doi.org/10.1109/cca.2010.5611196

[70] Humphrey, N. (1996). Expanding Metropolitan Highways: Implications for Air Quality and Energy Use MOBILE. *Transportation Research Board*, *56*, 38-39. https://trid.trb.org/view/462578

[71] Lattemann, F., Neiss, K., Terwen, S., & Connolly, T. (2004). The predictive cruise control – A system to reduce fuel consumption of heavy-duty trucks. *SAE Technical Paper Series*. https://doi.org/10.4271/2004-01-2616

[72] Hellström, E., Ivarsson, M., Åslund, J., & Nielsen, L. (2009). Look-ahead control for heavy trucks to minimize trip time and fuel consumption. *Control Engineering Practice*, *17*(2), 245-254. https://doi.org/10.1016/j.conengprac.2008.07.005

[73] Schwarzkopf, A., & Leipnik, R. (1977). Control of highway vehicles for minimum fuel consumption over varying terrain. *Transportation Research*, *11*(4), 279-286. https://doi.org/10.1016/0041-1647(77)90093-4

[74] Chang, D. J., & Morlok, E. K. (2005). Vehicle speed profiles to minimize work and fuel consumption. *Journal of Transportation Engineering*, *131*(3), 173-182. https://doi.org/10.1061/(asce)0733-947x(2005)131:3(173)

[75] Hellström, E. (2005). *Explicit use of road topography for model predictive cruise control in heavy trucks* [Master's thesis]. http://www.vehicular.isy.liu.se/Publications/MSc/05_EX_3660_EH.pdf

[76] Hellström, E. (2007). *Look-ahead control of heavy trucks utilizing road topography* [Doctoral dissertation]. https://www.diva-portal.org/smash/get/diva2:23829/fulltext01.pdf

[77] Hellström, E., Fröberg, A., & Nielsen, L. (2006). A real-time fuel-optimal cruise controller for heavy trucks using road topography information. *SAE Technical Paper Series*. https://doi.org/10.4271/2006-01-0008

[78] Hellström, E., Åslund, J., & Nielsen, L. (2010). Design of an efficient algorithm for fuel-optimal look-ahead control. *Control Engineering Practice*, *18*(11), 1318-1327. https://doi.org/10.1016/j.conengprac.2009.12.008

[79] Söderstedt, F. (2014). *Fuel Consumption Estimation for Vehicle Configuration Optimization* [Master's thesis]. http://liu.diva-portal.org/smash/get/diva2:764652/FULLTEXT01.pdf

[80] Nicholas, K. (2009). Integrating traffic data and model predictive control to improve fuel economy. *12th IFAC Symposium on Control in Transportation Systems*. https://doi.org/10.3182/20090902-3-us-2007.00025

[81] Tu Luu, H., Nouvelière, L., & Mammar, S. (2010). Dynamic programming for fuel consumption optimization on light vehicle. *IFAC Proceedings Volumes*, *43*(7), 372-377. https://doi.org/10.3182/20100712-3-de-2013.00097

[82] Kamal, M. A., Mukai, M., Murata, J., & Kawabe, T. (2011). Ecological vehicle control on roads with up-down slopes. *IEEE Transactions on Intelligent Transportation Systems*, *12*(3), 783-794. https://doi.org/10.1109/tits.2011.2112648

[83] Yu, Q. (2014). *Vehicular Speed Control of Eco-Driving Systems Based on Connected Vehicles* (TP273;TP391.44;TN929.5) [Master's thesis]. www.cnki.com. https://oversea.cnki.net/kns/detail/detail.aspx?FileName=1015039017.nh&DbName=CMFD2015

[84] Themann, P., Bock, J., & Eckstein, L. (2015). Optimization of energy efficiency based on average driving behavior and driver's preferences for automated driving. *IET Intelligent Transport Systems*, *9*(1), 50-58. https://doi.org/10.1049/iet-its.2013.0121

[85] Markschläger, P., Wahl, H., Weberbauer, F., & Lederer, M. (2012). Assistance system for higher fuel efficiency. *ATZ worldwide*, *114*(11), 8-13. https://doi.org/10.1007/s38311-012-0241-6

[86] Asadi, B., & Vahidi, A. (2011). Predictive cruise control: Utilizing upcoming traffic signal information for improving fuel economy and reducing trip time. *IEEE Transactions on Control Systems Technology*, *19*(3), 707-714. https://doi.org/10.1109/tcst.2010.2047860

[87] Kamal, M. A., Mukai, M., Murata, J., & Kawabe, T. (2013). Model predictive control of vehicles on urban roads for improved fuel economy. *IEEE Transactions on Control Systems Technology*, *21*(3), 831-841. https://doi.org/10.1109/tcst.2012.2198478

[88] Mahler, G., & Vahidi, A. (2014). An optimal velocity-planning scheme for vehicle energy efficiency through probabilistic prediction of traffic-signal timing. *IEEE Transactions on Intelligent Transportation Systems*, *15*(6), 2516-2523. https://doi.org/10.1109/tits.2014.2319306

[89] De Nunzio, G., De Wit, C. C., Moulin, P., & Di Domenico, D. (2015). Eco-driving in urban traffic networks using traffic signals information. *International Journal of Robust and Nonlinear Control*, *26*(6), 1307-1324. https://doi.org/10.1002/rnc.3469

[90] Meng, X., & Cassandras, C. G. (2019). A real-time optimal eco-driving approach for autonomous vehicles crossing multiple signalized intersections. *2019 American Control Conference (ACC)*. https://doi.org/10.23919/acc.2019.8814864

[91] Bae, S., Kim, Y., Guanetti, J., Borrelli, F., & Moura, S. (2019). Design and implementation of ecological

adaptive cruise control for autonomous driving with communication to traffic lights. *2019 American Control Conference (ACC)*. https://doi.org/10.23919/acc.2019.8814905

[92] Zhang, J., & Ioannou, P. (2006). Longitudinal control of heavy trucks in mixed traffic: Environmental and fuel economy considerations. *IEEE Transactions on Intelligent Transportation Systems*, *7*(1), 92-104. https://doi.org/10.1109/tits.2006.869597

[93] Shengbo Li, Keqiang Li, Jianqiang Wang, Lei Zhang, Xiaomin Lian, Hiroshi Ukawa, & Dongsheng Bai. (2008). MPC based vehicular following control considering both fuel economy and tracking capability. *2008 IEEE Vehicle Power and Propulsion Conference*. https://doi.org/10.1109/vppc.2008.4677689

[94] Wu, C., Zhao, G., & Ou, B. (2011). A fuel economy optimization system with applications in vehicles with human drivers and autonomous vehicles. *Transportation Research Part D: Transport and Environment*, *16*(7), 515-524. https://doi.org/10.1016/j.trd.2011.06.002

[95] Kamal, M. A., Mukai, M., Murata, J., & Kawabe, T. (2013). Model predictive control of vehicles on urban roads for improved fuel economy. *IEEE Transactions on Control Systems Technology*, *21*(3), 831-841. https://doi.org/10.1109/tcst.2012.2198478

[96] Luo, Y., Chen, T., Zhang, S., & Li, K. (2015). Intelligent hybrid electric vehicle ACC with coordinated control of tracking ability, fuel economy, and ride comfort. *IEEE Transactions on Intelligent Transportation Systems*, *16*(4), 2303-2308. https://doi.org/10.1109/tits.2014.2387356

[97] Zhao, R. C., Wong, P. K., Xie, Z. C., & Zhao, J. (2017). Real-time weighted multi-objective model predictive controller for adaptive cruise control systems. *International Journal of Automotive Technology*, *18*(2), 279-292. https://doi.org/10.1007/s12239-017-0028-2

[98] Manzie, C., Watson, H., & Halgamuge, S. (2007). Fuel economy improvements for urban driving: Hybrid vs. intelligent vehicles. *Transportation Research Part C: Emerging Technologies*, *15*(1), 1-16. https://doi.org/10.1016/j.trc.2006.11.003

[99] Li, S. E., Peng, H., Li, K., & Wang, J. (2012). Minimum fuel control strategy in automated car-following scenarios. *IEEE Transactions on Vehicular Technology*, *61*(3), 998-1007. https://doi.org/10.1109/tvt.2012.2183401

[100] Yang, C., Wang, M., Wang, W., Pu, Z., & Ma, M. (2021). An efficient vehicle-following predictive energy management strategy for PHEV based on improved sequential quadratic programming algorithm. Energy, 219, 119595. https://doi.org/10.1016/j.energy.2020.119595

[101] Hu, X., Zhang, X., Tang, X., & Lin, X. (2020). Model predictive control of hybrid electric vehicles for fuel economy, emission reductions, and inter-vehicle safety in car-following scenarios. Energy, 196, 117101. https://doi.org/10.1016/j.energy.2020.117101

[102] Ma, F., Yang, Y., Wang, J., Liu, Z., Li, J., Nie, J., Shen, Y., & Wu, L. (2019). Predictive energy-saving optimization based on nonlinear model predictive control for cooperative connected vehicles platoon with V2V communication. Energy, 189, 116120. https://doi.org/10.1016/j.energy.2019.116120

[103] Wu, Y., Tan, H., Peng, J., Zhang, H., & He, H. (2019). Deep reinforcement learning of energy management with continuous control strategy and traffic information for a series-parallel plug-in hybrid electric bus. *Applied Energy*, *247*, 454-466. https://doi.org/10.1016/j.apenergy.2019.04.021

[104] Shi, D., Liu, S., Cai, Y., Wang, S., Li, H., & Chen, L. (2021). Pontryagin's minimum principle based fuzzy adaptive energy management for hybrid electric vehicle using real-time traffic information. *Applied Energy*, *286*, 116467. https://doi.org/10.1016/j.apenergy.2021.116467

[105] Lin, Q., Li, S. E., Xu, S., Du, X., Yang, D., & Li, K. (2021). Eco-driving operation of connected vehicle

with V2I communication among multiple signalized intersections. *IEEE Intelligent Transportation Systems Magazine*, *13*(1), 107-119. https://doi.org/10.1109/mits.2020.3014113

[106] Jia, Y., Jibrin, R., & Gorges, D. (2020). Energy-optimal adaptive cruise control for electric vehicles based on linear and nonlinear model predictive control. *IEEE Transactions on Vehicular Technology*, *69*(12), 14173-14187. https://doi.org/10.1109/tvt.2020.3044265

[107] Wang, Z., Wu, G., & Barth, M. J. (2020). Cooperative eco-driving at signalized intersections in a partially connected and automated vehicle environment. *IEEE Transactions on Intelligent Transportation Systems*, *21*(5), 2029-2038. https://doi.org/10.1109/tits.2019.2911607

[108] Ma, F., Yang, Y., Wang, J., Li, X., Wu, G., Zhao, Y., Wu, L., Aksun-Guvenc, B., & Guvenc, L. (2021). Eco-driving-based cooperative adaptive cruise control of connected vehicles platoon at signalized intersections. *Transportation Research Part D: Transport and Environment*, *92*, 102746. https://doi.org/10.1016/j.trd.2021.102746

[109] Zhao, S., & Zhang, K. (2021). Online predictive connected and automated eco-driving on signalized arterials considering traffic control devices and road geometry constraints under uncertain traffic conditions. *Transportation Research Part B: Methodological*, *145*, 80-117. https://doi.org/10.1016/j.trb.2020.12.009

[110] Vahidi, A., & Eskandarian, A. (2003). Research advances in intelligent collision avoidance and adaptive cruise control. *IEEE Transactions on Intelligent Transportation Systems*, *4*(3), 143-153. https://doi.org/10.1109/tits.2003.821292

[111] Sei-Bum Choi, & Hedrick, J. (n.d.). Vehicle longitudinal control using an adaptive observer for automated highway systems. *Proceedings of 1995 American Control Conference - ACC'95*. https://doi.org/10.1109/acc.1995.532088

[112] Moon, S., & Yi, K. (2008). Human driving data-based design of a vehicle adaptive cruise control algorithm. *Vehicle System Dynamics*, *46*(8), 661-690. https://doi.org/10.1080/00423110701576130

[113] Fritz, A., & Schiehlen, W. (2001). Nonlinear ACC in simulation and measurement. *Vehicle System Dynamics*, *36*(2-3), 159-177. https://doi.org/10.1076/vesd.36.2.159.3556

[114] Yi, K., Hong, J., & Kwon, Y. D. (2001). A vehicle control algorithm for stop-and-go cruise control. *Proceedings of the Institution of Mechanical Engineers, Part D: Journal of Automobile Engineering*, *215*(10), 1099-1115. https://doi.org/10.1243/0954407011528653

[115] Zhang, J., & Ioannou, P. (2006). Longitudinal control of heavy trucks in mixed traffic: Environmental and fuel economy considerations. *IEEE Transactions on Intelligent Transportation Systems*, *7*(1), 92-104. https://doi.org/10.1109/tits.2006.869597

[116] Möbus, R., Baotic, M., & Morari, M. (2003). Multi-object adaptive cruise control. *Hybrid Systems: Computation and Control*, 359-374. https://doi.org/10.1007/3-540-36580-x_27

[117] Kyongsu Yi, Ilki Moon, & Young Do Kwon. (n.d.). A vehicle-to-vehicle distance control algorithm for stop-and-go cruise control. *ITSC 2001. 2001 IEEE Intelligent Transportation Systems. Proceedings (Cat. No.01TH8585)*. https://doi.org/10.1109/itsc.2001.948704

[118] Xiao-Yun Lu, Hedrick, J., & Drew, M. (2002). ACC/CACC-control design, stability and robust performance. *Proceedings of the 2002 American Control Conference (IEEE Cat. No.CH37301)*. https://doi.org/10.1109/acc.2002.1025325

[119] Yang Bin, Keqiang Li, Xiaomin Lian, Ukawa, H., Handa, M., & Idonuma, H. (n.d.). Longitudinal acceleration tracking control of vehicular stop-and-go cruise control system. *IEEE International Conference on Networking, Sensing and Control, 2004*. https://doi.org/10.1109/icnsc.2004.1297508

[120] Ganji, B., Kouzani, A. Z., Khoo, S. Y., & Shams-Zahraei, M. (2014). Adaptive cruise control of a HEV using sliding mode control. *Expert Systems with Applications*, *41*(2), 607-615. https://doi.org/10.1016/j.eswa.2013.07.085

[121] Li, S. E., Deng, K., Li, K., & Ahn, C. (2015). Terminal sliding mode control of automated car-following system without reliance on longitudinal acceleration information. *Mechatronics*, *30*, 327-337. https://doi.org/10.1016/j.mechatronics.2014.09.014

[122] Ohno, H. (2001). Analysis and modeling of human driving behaviors using adaptive cruise control. *Applied Soft Computing*, *1*(3), 237-243. https://doi.org/10.1016/s1568-4946(01)00022-9

[123] Naranjo, J., Gonzalez, C., Garcia, R., & DePedro, T. (2006). ACC+Stop&Go maneuvers with throttle and brake fuzzy control. *IEEE Transactions on Intelligent Transportation Systems*, *7*(2), 213-225. https://doi.org/10.1109/tits.2006.874723

[124] Alonso, L., Pérez-Oria, J., Fernández, M., Rodríguez, C., Arce, J., Ibarra, M., & Ordoñez, V. (2010). Genetically tuned controller of an adaptive cruise control for urban traffic based on ultrasounds. *Artificial Neural Networks – ICANN 2010*, 479-485. https://doi.org/10.1007/978-3-642-15822-3_58

[125] Khayyam, H., Nahavandi, S., & Davis, S. (2012). Adaptive cruise control look-ahead system for energy management of vehicles. *Expert Systems with Applications*, *39*(3), 3874-3885. https://doi.org/10.1016/j.eswa.2011.08.169

[126] Richalet, J., Rault, A., Testud, J., & Papon, J. (1978). Model predictive heuristic control. *Automatica*, *14*(5), 413-428. https://doi.org/10.1016/0005-1098(78)90001-8

[127] Corona, D., & De Schutter, B. (2008). Adaptive cruise control for a SMART car: A comparison benchmark for MPC-PWA control methods. *IEEE Transactions on Control Systems Technology*, *16*(2), 365-372. https://doi.org/10.1109/tcst.2007.908212

[128] Shakouri, P., Ordys, A., & Askari, M. R. (2012). Adaptive cruise control with stop&go function using the state-dependent nonlinear model predictive control approach. *ISA Transactions*, *51*(5), 622-631. https://doi.org/10.1016/j.isatra.2012.05.001

[129] Li, S., Wang, J., Li, K., & Zhang, L. (2010). Processing of MPC practical problems and its application to vehicular adaptive cruise control system. *Journal of Tsinghua University (Science and Technology)*, *5*, 645-648. https://doi.org/10.16511/j.cnki.qhdxxb.2010.05.004

[130] Li, S., Li, K., Rajamani, R., & Wang, J. (2011). Model predictive multi-objective vehicular adaptive cruise control. *IEEE Transactions on Control Systems Technology*, *19*(3), 556-566. https://doi.org/10.1109/tcst.2010.2049203

[131] Eben Li, S., Li, K., & Wang, J. (2013). Economy-oriented vehicle adaptive cruise control with coordinating multiple objectives function. *Vehicle System Dynamics*, *51*(1), 1-17. https://doi.org/10.1080/00423114.2012.708421

[132] Li, S. E., Jia, Z., Li, K., & Cheng, B. (2015). Fast online computation of a model predictive controller and its application to fuel economy–oriented adaptive cruise control. *IEEE Transactions on Intelligent Transportation Systems*, *16*(3), 1199-1209. https://doi.org/10.1109/tits.2014.2354052

[133] Li, L., Wang, X., & Song, J. (2017). Fuel consumption optimization for smart hybrid electric vehicle during a car-following process. *Mechanical Systems and Signal Processing*, *87*, 17-29. https://doi.org/10.1016/j.ymssp.2016.03.002

[134] Hu, X., Zhang, X., Tang, X., & Lin, X. (2020). Model predictive control of hybrid electric vehicles for fuel economy, emission reductions, and inter-vehicle safety in car-following scenarios. *Energy*, *196*, 117101. https://doi.org/10.1016/j.energy.2020.117101

[135] Yi, C., Epureanu, B. I., Hong, S., Ge, T., & Yang, X. G. (2016). Modeling, control, and performance of a novel architecture of hybrid electric powertrain system. *Applied Energy*, *178*, 454-467. https://doi.org/10.1016/j.apenergy.2016.06.068

[136] Chao Sun, Moura, S. J., Xiaosong Hu, Hedrick, J. K., & Fengchun Sun. (2015). Dynamic traffic feedback data enabled energy management in plug-in hybrid electric vehicles. *IEEE Transactions on Control Systems Technology*, *23*(3), 1075-1086. https://doi.org/10.1109/tcst.2014.2361294

[137] Li, S. (2009). *Vehicular Multi-Objective Coordinated Adaptive Cruise Control* [Doctoral dissertation]. https://www.researchgate.net/publication/311843554_cheliangduomubiaoxiediaoshizishiyingxunhangkongzhiboshi

[138] Chiara, F., Wang, J., Patil, C. B., Hsieh, M., & Yan, F. (2011). Development and experimental validation of a control-oriented diesel engine model for fuel consumption and brake torque predictions. *Mathematical and Computer Modelling of Dynamical Systems*, *17*(3), 261-277. https://doi.org/10.1080/13873954.2011.562902

[139] Lindgren, M. (2005). A transient fuel consumption model for non-road mobile machinery. *Biosystems Engineering*, *91*(2), 139-147. https://doi.org/10.1016/j.biosystemseng.2005.03.011

[140] Pelkmans, L., Debal, P., Hood, T., Hauser, G., & Delgado, M. (2004). Development of a simulation tool to calculate fuel consumption and emissions of vehicles operating in dynamic conditions. *SAE Technical Paper Series*. https://doi.org/10.4271/2004-01-1873

[141] Ahn, K., Rakha, H., Trani, A., & Van Aerde, M. (2002). Estimating vehicle fuel consumption and emissions based on instantaneous speed and acceleration levels. *Journal of Transportation Engineering*, *128*(2), 182-190. https://doi.org/10.1061/(asce)0733-947x(2002)128:2(182)

[142] Lei, W., Chen, H., & Lu, L. (2010). Microscopic Emission and Fuel Consumption Modeling for Light-duty Vehicles Using Portable Emission Measurement System Data. *World Academy of Science, Engineering and Technology*, *4*. citeseerx.ist.psu.edu/viewdoc/download?doi=10.1.1.1014.1073&rep=rep1&type=pdf

[143] Jin, H., Zhou, M., & Li, S. (2017). Transient Fuel Consumption Modelling Based on Transient Correction. *Transactions of Beijing Institute of Technology*, *37*(5), 473-478. http://journal.bit.edu.cn

[144] Chiara, F., Wang, J., Patil, C. B., Hsieh, M., & Yan, F. (2011). Development and experimental validation of a control-oriented diesel engine model for fuel consumption and brake torque predictions. *Mathematical and Computer Modelling of Dynamical Systems*, *17*(3), 261-277. https://doi.org/10.1080/13873954.2011.562902

[145] Downloadable dynamometer database | Argonne national laboratory. (2015, July). Retrieved April 9, 2021, from https://www.anl.gov/es/downloadable-dynamometer-database

[146] Hornik, K., Stinchcombe, M., & White, H. (1990). Universal approximation of an unknown mapping and its derivatives using multilayer feedforward networks. *Neural Networks*, *3*(5), 551-560. https://doi.org/10.1016/0893-6080(90)90005-6

[147] Goodfellow, I., Bengio, Y., & Courville, A. (2016). *Deep learning*. MIT Press.

[148] Marquardt, D. (1963). An Algorithm for Least-Squares Estimation of Nonlinear Parameters. *Journal of the Society for Industrial and Applied Mathematics*, *11*(2), 431-441. http://www.jstor.org/stable/2098941

[149] Yu, Y., Li, Y., Liang, Y., Zhang, Z., & Liao, G. (2019). Modeling of Transient Energy Consumption Model of Electric Vehicle Based on Data Mining. *Society of Automotive Engineers of Automotive Engineering Conference*, 277-283. https://oversea.cnki.net/kns/detail/detail.aspx?FileName=QCGC201910002035&DbName=CPFD2019

[150] Propoi, A. I. (1963). Application of linear programming methods for the synthesis of automatic sampled-data systems. *Avtomat. i Telemekh*, *24*(7), 912-920. http://mi.mathnet.ru/at11905

[151] Mayne, D., & Michalska, H. (1988). Receding horizon control of nonlinear systems. *Proceedings of the 27th IEEE Conference on Decision and Control*. https://doi.org/10.1109/cdc.1988.194354

[152] Rawlings, J. B., Mayne, D. Q., & Diehl, M. (2017). *Model predictive control: Theory, computation, and design*.

[153] Wang, L. (2009). *Model predictive control system design and implementation using MATLAB®*. Springer Science & Business Media.

[154] Maciejowski, J. M. (2002). *Predictive control: With constraints*. Pearson Education.

[155] Hong, C. (2013). *Model Predictive Control*. Sciencep.

[156] Xi, Y., & Li, D. (2019). *Predictive control: Fundamentals and developments*. John Wiley & Sons.

[157] García, C. E., Prett, D. M., & Morari, M. (1989). Model predictive control: Theory and practice—A survey. *Automatica*, *25*(3), 335-348. https://doi.org/10.1016/0005-1098(89)90002-2

[158] Su, L. H., LI, L., & Chu, J. (2001). Recent Advances on Predictive Control. *Mechanical & Electrical Engineering Magazine*, (5), 4-8. https://kns.cnki.net

[159] Corradini, M., & Orlando, G. (1997). A VSC algorithm based on generalized predictive control. *Automatica*, *33*(5), 927-932. https://doi.org/10.1016/s0005-1098(96)00229-4

[160] Lee, J., & Yu, Z. (1997). Worst-case formulations of model predictive control for systems with bounded parameters. *Automatica*, *33*(5), 763-781. https://doi.org/10.1016/s0005-1098(96)00255-5

[161] Treiber, M., & Kesting, A. (2012). *Traffic flow dynamics: Data, models and simulation*. Springer Science & Business Media.